DISS. ETH NO. 23411

Air quality modelling at European scale with a focus on winter organic aerosol

A thesis submitted to attain the degree of

DOCTOR OF SCIENCES of ETH ZURICH

(Dr. sc. ETH Zürich)

presented by

GIANCARLO CIARELLI

M.Sc. Environmental Engineering, Marche Polytechnic University, Italy

born on 12.02.1985

citizen of Italy

accepted on the recommendation of

Prof. Dr. Thomas Peter (examiner)
Dr. André Prévôt (co-examiner)
Dr. Sebnem Aksoyoglu (co-examiner)
Prof. Dr. Matthias Beekmann (co-examiner)

2016

Content

Summary

Atmospheric particulate matter (PM) represents one of the major environmental concerns for human health and it also affects the climate and the ecosystem. PM composition and sources are extremely variable around the globe rendering them very challenging to quantify. Moreover, one of the major and less understood fractions of the submicron (aerodynamic diameter < 1 μm) particle mass (PM_1) is represented by organic aerosol (OA). Organics in aerosols comprise thousands of different species. These can be directly emitted primary organic aerosol (POA), from anthropogenic (e.g. cooking, heating and traffic) and biogenic sources (oceans, plants and wild fires). Or they can form later in the atmosphere as secondary organic aerosol (SOA), resulting from condensation of oxidized gas-phase precursors on pre-existing particles. Gas phase precursors for SOA are known to be highly volatile organic compounds (VOCs) like terpenes, isoprene xylene and toluene as well as intermediate volatility organic compounds (IVOCs). The emission fluxes and reaction pathways in the atmosphere of the latter are still poorly understood. Moreover, under atmospheric conditions, a large fraction of POA will undergo evaporation due to dilution and its semi-volatile nature adding to the gas-phase material (SVOCs), which, after further processing in the gas phase, is also a potential contributor to SOA.

Chemical transport models (CTMs) represent an important tool, in combination with ambient and smog-chamber measurements, to identify and quantify OA sources. A detailed and promising approach to represent the formation and evolution of organic material in the atmosphere is the Volatility Basis Set (VBS) framework. In the VBS scheme, a two dimensional (2D) space is used in order to predict the composition and evolution of OA in the atmosphere: one dimension maps organic compounds according to their saturation concentration (C^*) in so called volatility bins and a second one describes the changes in the elemental oxygen to carbon (O:C) ratios as organic material undergoes functionalization or fragmentation upon reaction with various oxidants (e.g. OH, O_3, NO_3). The 2D-VBS model is computationally very demanding for common CTM applications therefore it was usually deployed with several modifications and simplifications in order to find an optimum between its complexity and its current applicability. CTMs were applied in the past at different scales (regional and global) with different schemes to represent the evolution of OA in the troposphere but, despite recent

improvements, models still tend to underestimate the observed OA fraction and findings are sometimes ambiguous. Consequently, the purpose of this thesis was:

1) to evaluate for the first time in Europe, the Air Quality Model with Extension (CAMx) including the VBS scheme against aerosol mass spectrometer (AMS) measurements and investigate the sources of OA for two specific periods representative of summer and winter conditions: June 2006 and February-March 2009,
2) to improve the previously applied VBS scheme in CAMx by means of a box model using data from the new wood burning smog chamber experiments performed at different temperatures,
3) to implement the new constrained VBS parameterization in the CAMx model and evaluate the results for POA, SOA and total OA mass with a focus on the winter period February-March 2009.

The EMEP (European Monitoring and Evaluation Programme) intensive measurement campaigns (June 2006, January-February 2007, September-October 2008 and February-March 2009) were used to evaluate CAMx-VBS model performance within the EURODELTA-III model intercomparison exercise. Detailed analysis and sensitivity tests were performed in order to investigate the effect of different POA emission inventories and volatility distributions on model performance. Nitrogen dioxide (NO_2) and carbon monoxide (CO) were found to be under-predicted for all the four periods (mean fractional bias (MFB) between -54% and -28% for NO_2 and -31% and -11% for CO) mainly due to the relatively coarse resolution of the domain, and over-estimation of daytime dilution. On the other hand, sulfur dioxide (SO_2) and ozone (O_3) were over-predicted (MFB 14%-36% for SO_2 and 2%-48% for O_3) with O_3 showing the best performance for the 2009 episode. The over-prediction in the modelled SO_2 was mainly attributed to the uncertainties in the vertical distribution of emissions since most of the SO_2 are released from high stack sources, in particular near the harbours and coastal areas where ship emissions were allocated in the second layer of the model domain (extending from ~ 20 to 50 m above ground level), whereas they can reach higher injection height in deep draft vessels. Insufficient conversion to sulfate or too low deposition processes might have also positively biased the model performance for SO_2. The under-prediction of NO_2 indirectly influenced also modelled O_3 concentration reducing its titration potential during night-time. More-over, O_3 model validation at the remote station of Mace Head, revealed a great influence of O_3 concentrations at the domain boundaries on the model performance for O_3. $PM_{2.5}$ concentrations were reproduced quite satisfactorily (mean fraction error (MFE) $\leq$ +50% and -30% < MFB < +30% most of the time). Comparison of modelled $PM_{2.5}$ concentrations with AMS measurements at 11 European sites in February-March 2009 suggested that the model could reproduce the observed particle mass with the inorganic fraction being over-predicted and the OA under-predicted (about 55% and -56%, respectively, at the rural-background site of Payerne). The sensitivity tests indicated that over-prediction of the inorganic fraction was probably due to too high ammonia (NH_3) emissions, in March. On the other hand, additional

tests with the VBS scheme suggested that underestimation of OAs was related to emissions from biomass burning, the main source of OA during February-March 2009. For this period the MFB for OA varied from -108 and -12% depending on the volatility distribution and emission inventory used. In summer, however, biogenic emissions affected OA formation significantly.

In addition, data from recent wood combustion and aging experiments performed at two different temperatures (263.15 K and 288.15 K) in a ~7 m^3 smog chamber were used to constrain and update the VBS scheme used in CAMx. Therefore, more than 30000 simulations with a box-model were performed to investigate the parameters with highest uncertainties i.e. reaction rates of usually not accounted SOA precursors in CTMs, i.e. non-traditional volatile organic compounds (NTVOCs, e.g. cresol, phenol, and naphthalene) and yields and enthalpy of evaporation for POA and SOA. The new constrained parameterization could reproduce the chamber experiments relatively well with approximately 25% and 15% error in the OA mass and on the O:C ratio, respectively.

In the last part of this work, the new VBS parameterization was implemented in the CAMx model with a focus on wood combustion emissions (SNAP2 in the Selected Nomenclature for Sources of Air Pollution Classification used in the emission inventory). Model source apportionment results were compared against positive matrix factorization (PMF) analysis on AMS OA measurements performed during the winter period February-March 2009. A considerable improvement was found in the modelled OA mass (up to 60% more OA predicted in the European domain) with respect to the previous application using the original CAMx-VBS model. In line with the AMS measurements, results based on the updated organic scheme confirmed that SOA constitutes the major fraction of the total OA mass at almost all the investigated sites, even though the absolute concentrations remained mostly under-predicted. Comparisons with the primary organic aerosol fractions i.e. hydrocarbon-like aerosol (HOA) and biomass burning-like (BBOA) resolved PMF factors, revealed that the model in general under-estimates the HOA component and slightly over-predicts the BBOA component.

Riassunto

Il particolato atmosferico, costituisce uno dei maggiori rischi per l'ambiente e la salute dell'uomo e può inoltre alterare il clima e l'ecosistema terrestre. La sua composizione chimica e le sue sorgenti sono molto variabili in diverse aree della terra il che rende molto complessa la sua caratterizzazione.

Una delle frazioni più abbondanti e ancora meno comprese della massa totale submicrometra (PM_1) è rappresentata dall' aerosol organico (OA). Tale frazione comprende migliaia di diversi composti organici i quali possono essere emessi in forma particellare, aerosol organico primario (POA), da sorgenti antropogeniche o biogeniche (emissioni da cucina, processi di combustione, oceani, piante e incendi) ma anche generata in atmosfera a seguito della condensazione di gas ossidati su particelle già esistenti, aerosol organico secondario (SOA). I precursori gassosi possono includere composti organici ad alta volatilità (VOC) coma ad esempio terpene, isoprene, xilene e toluene, oppure composti organici a intermedia volatilità (IVOC). Tuttavia, le relative emissioni e reazioni in atmosfera di tali precursori sono ancora oggi poco comprese. Inoltre, a tipiche condizioni atmosferiche, una grande quantità del POA tende a evaporare rendendo il risultante materiale gassoso (SVOC) un potenziale precursore per il SOA.

I modelli chimici di trasporto (CTMs), usati in combinazione con misure ambientali e in smog chamber, rappresentano strumenti importanti per l'identificazione e la quantificazione degli aerosol organici e relative sorgenti. Un approccio promettente e dettagliato per descrivere la formazione ed evoluzione del materiale organico in atmosfera è il Volatility Basis set (VBS). Mediante tale approccio uno spazio 2-dimensionale (2D-VBS) è impiegato per predire la composizione ed evoluzione del particolato organico in atmosfera. Una dimensione classifica la pressione di vapore saturo (C^*) in diverse classi di volatilità. Una seconda, consente di predire l'evoluzione del rapporto ossigeno carbonio (O:C) quando il materiale organico funzionalizza o frammenta a seguito dell'interazione con svariati radicali (OH, O_3, NO_3). Le risorse computazionali per l'utilizzo di un modello 2D-VBS sono molto elevate per normali di CTMs. Per tale motivo viene solitamente applicato con alcune modificazioni e semplificazioni in maniera tale da trovare un giusto compromesso tra complessità e applicabilità. I CTMs sono stati applicati in passato su diverse scale spaziali (regionali e globali) con differenti schemi per rappresentare l'evoluzione del particolato organico nella troposfera. Tuttavia, nonostante recenti

miglioramenti, tali modelli tendono ancora a sottostimare la frazione organica con risultati a volte ambigui.

Di conseguenza, il proposito di questo lavoro è:

1) Applicare per la prima volta in Europa un modello VBS utilizzando l'Air Quality Model with Extension (CAMx) e confrontare i dati modellati con misure di particolato organico condotte con l'aerosol mass spectrometer (AMS). Due specifici episodi in estate (Giugno 2006) e inverno (Febbraio-Marzo 2009) sono stati selezionati per effettuare tali confronti.
2) Parametrizzare il modello VBS con nuovi esperimenti di combustione della legna eseguiti in smog chamber a diverse temperature.
3) Implementare la nuova parametrizzazione nel modello CAMx e confrontare i nuovi risultati con la precedenti applicazioni per la frazione organica primaria (POA), secondaria (SOA) e totale.

Campagne di misura del programma EMEP (European Monitoring and Evaluation Programme) sono state utilizzate per analizzare la performance del modello fotochimico CAMx-VBS durante Giugno 2006, Gennaio-Febbraio 2007, Settembre-Ottobre 2008 e Febbraio-Marzo 2009 all'interno del progetto Europeo EURODELTA-III. Analisi di sensitività sono state eseguite per investigare le incertezze legate agli inventari emissivi di particolato organico usati e alla loro volatilità. Le concentrazioni di NO_2 e CO sono risultate sottostimate per tutte e quattro le campagne di misura con una fraction bias (MFB) attesa tra -54% e -28% per NO_2 e -31% e -11% per CO. Tali discrepanze sono state attribuite principalmente alla risoluzione del dominio utilizzato e alla sovrastimata diluizione giornaliera. Le concentrazioni di SO_2 e O_3 d'altra parte sono risultate sovrastimate con una MFB tra 14% e 36% per SO_2 e tra 2% e 48% per O_3 con il periodo invernale di Febbraio e Marzo 2009 meglio rappresentato. La sovrastima nelle concentrazioni di SO_2 è stata attribuita principalmente alle incertezze legate alla distribuzione verticale delle emissioni dal momento che buona parte degli SO_2 viene rilasciata da sorgenti puntuali ad altezze più elevate nell'atmosfera. La sottostima delle concentrazioni di NO_2 potrebbe influenzare direttamente anche le concentrazioni di O_3, riducendo la capacità di distruzione di quest'ultimo durante le ore notturne. Inoltre, una validazione condotta presso la stazione remota di Mace Head, ha indicato una notevole influenza delle concentrazioni di O_3 assegnate ai bordi del dominio sulle aree più interne dello stesso. Le concentrazioni di $PM_{2.5}$ sono state riprodotte in maniera soddisfacente dal modello (fraction error (MFE) $\leq$ +50% and -30% < MFB < +30% per 3 dei 4 periodi investigati). Le concentrazioni di $PM_{2.5}$ sono state ulteriormente validate per Febbraio-Marzo 2009 con misure AMS effettuate presso 11 stazioni presenti nel dominio Europeo. Il modello è stato in grado di riprodurre la massa totale di aerosol misurata con AMS sebbene la frazione inorganica sia risultata sovrastimata e quella organica sottostimata. La sovrastima della frazione organica è stata attribuita principalmente alle

incertezze relative alle emissioni di ammoniaca (NH_3), la quale è ampiamente utilizzata come fertilizzante durante il periodo di Febbraio e Marzo mentre differenti test di sensitività condotti con il modello VBS hanno indicato che la combustione da legna è la sorgente primaria di particolato organico in tale periodo. Test di sensitività per il periodo estivo (Giugno 2006) hanno rivelato che le emissioni di precursori biogenici in fase gassosa, rappresentano la sorgente principale di particolato organico durante i periodi estivi.

Recenti esperimenti di combustione della legna effettuati in smog chamber sono stati utilizzati per parametrizzare ulteriormente il modello VBS. Più di 30000 simulazioni sono state eseguite in maniera da determinare i parametri chimici e fisici affetti da maggiore incertezza: velocità di reazione, yields, ed entalpie di vaporizzazione della frazione organica primaria e secondaria. La nuova parametrizzazione è stata in grado di riprodurre gli esperimenti di combustione in maniera relativamente soddisfacente con circa 25% di errore sulla massa organica totale e 15% sul rapporto O:C.

Nella parte finale di questo lavoro, la nuova parametrizzazione è stata implementata nel modello CAMx e i risultati confrontati con la precedente applicazione durante il periodo invernale Febbraio-Marzo 2009. Le sorgenti dell'aerosol organico come predette dal modello CAMx sono state ulteriormente confrontate con la tecnica positive matrix factorization (PMF) eseguita sui dati AMS. Un considerevole miglioramento nelle performance del modello è stato riscontrato per la frazione organica rispetto alla precedente applicazione (OA maggiorati di circa 60% nel dominio Europeo). Entrambi gli approcci, sembrano suggerire che la frazione organica secondaria rappresenti la sorgente predominante degli OA per la maggior parte dei siti investigati e con concentrazioni assolute sottostimate nel modello CAMx. Le sorgenti primarie costituiscono una frazione minore della frazione organica. Per queste ultime, il modello tende a sottostimare il contributo primario derivante dagli idrocarburi e a sovrastimare il contributo primario derivante della combustione della legna.

1

Introduction

1.1 The Atmosphere of the Earth

The presence of a layer of gases and particles that extends for several kilometers above the surface of the Earth, i.e. the atmosphere, is the result of the gravity force acting on such matter. The Earth's atmosphere could be schematically divided in different sublayers each of them with different chemical and physical properties. The lowest layer of the atmosphere extends approximately up to 10 – 15 km altitude from the surface of the Earth, i.e. the troposphere, and contains most of the atmosphere's mass (see Figure 1.1). Its composition is variable in time and space consisting of c.a. 78% of N_2, 21% of O_2 and 1% of Ar and trace gases together with large amounts of water vapor. Of particular interest is the presence of particles of different size and chemical composition that are commonly referred to as aerosols. Atmospheric aerosols are liquid or solid particles suspended in the air which arise from multiple sources (Baron and Willeke, 2001). They can be directly emitted as particles from both anthropogenic (heating, traffic, cooking) and natural sources (volcanic eruptions, biological materials, deserts, sea-salt, etc.) i.e. primary particles, or later formed in the atmosphere via several physical and chemical mechanisms such as condensation of low-volatility gases, nucleation and chemical reactions, i.e. secondary particles (Hallquist et al., 2009). The size and chemical composition of an aerosol mixture present in the atmosphere is determined by its source and formation pathways. Particles with an aerodynamic diameter $D_p > 2.5$ µm are usually produced by mechanical processes (coarse mode) whereas for nucleation mode particles ($D_p < 10$ nm) homogeneous nucleation is the main source. In between these size ranges, at 10-100nm (Aitken mode) and 0.1-2.5 µm (accumulation mode), particles are generated via coagulation from the nucleation mode which can further grow through condensation (see Figure 1.2).

Atmospheric aerosols have severe adverse health effects on humans and interact with the Earth's radiative balance making it one of the main current environmental concerns. These aspects are discussed in section 1.3 and section 1.4 respectively.

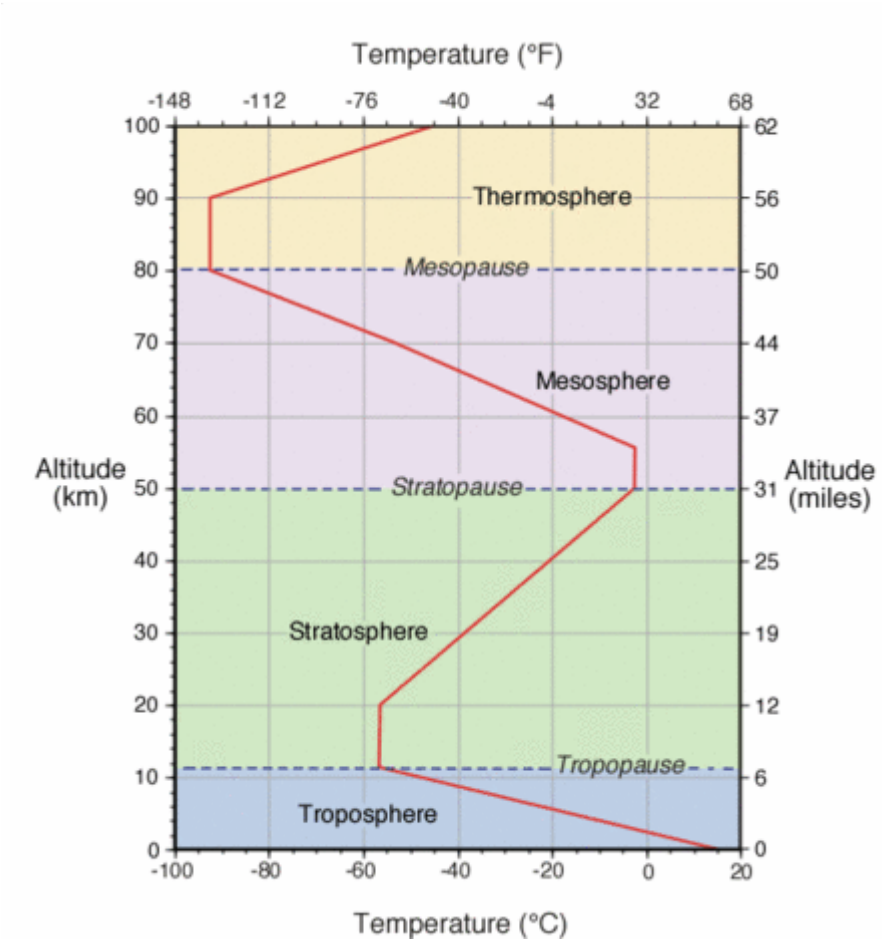

Figure 1.1 *Schematic representation of the different layers of the atmosphere and the vertical change in average global temperature (http://www.physicalgeography.net/).*

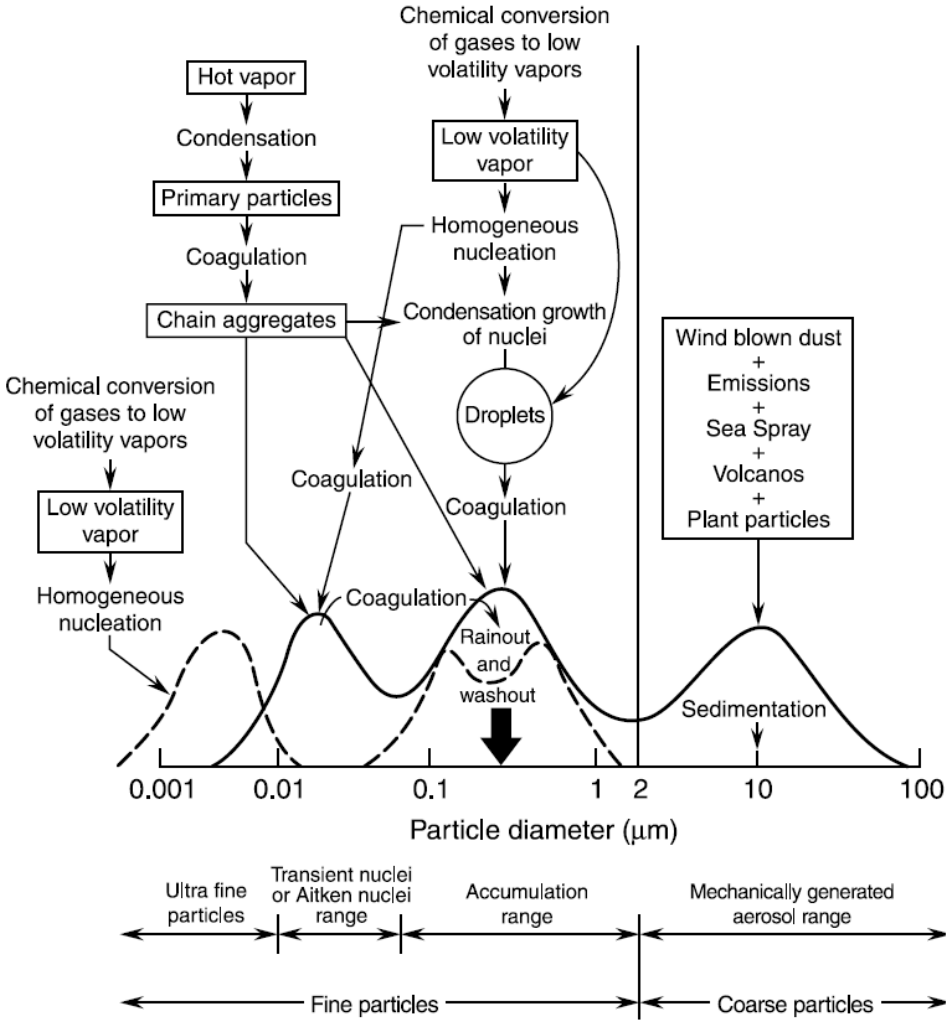

Figure 1.2 *Typical sources, formation, removal pathways and size distributions of atmospheric aerosol (Finlayson-Pitts and Pitts, 2009).*

1.2 Aerosol chemical composition and sources

Atmospheric aerosols can be grouped into two main fractions: organic and inorganic compounds. Inorganic aerosols are usually found in the atmosphere in the form of ammonium nitrate and ammonium sulfate in the fine mode. The main gas-phase species that regulates the availability of different inorganic aerosols is ammonia (NH_3), the most abundant base in the atmosphere mainly emitted from agriculture activities. NH_3 reacts with sulfuric acid (H_2SO_4), an oxidation product of SO_2 which mainly arises from large combustion facilities and ships, to form bisulfate and eventually ammonium sulfate. If NH_3 is in excess i.e. double the sulfate concentrations in moles ("free ammonia"), it can react with nitric acid (HNO_3) to form ammonium nitrate (NH_4NO_3). HNO_3 is mainly produced from the oxidation of NO_x, emitted in large quantities by combustion processes. Organic aerosol (OA), on the other hand, represents a more ubiquitous and complex fraction of the atmospheric fine particulate matter ($PM_{2.5}$) (Hallquist et al., 2009). As shown in Figure 1.3, it comprises a large fraction of $PM_{2.5}$ and it can be either directly emitted as primary organic aerosol (POA) (arising from traffic, coal burning, biomass burning but also from cooking activities) or formed in the atmosphere after the condensation of oxidized gases on pre-existing particles i.e. secondary organic aerosol (referred to as SOA or oxygenated organic aerosol, OOA). Traffic related POA is usually referred to as HOA i.e. hydrocarbon-like organic aerosol whereas biomass burning POA is referred to as BBOA.

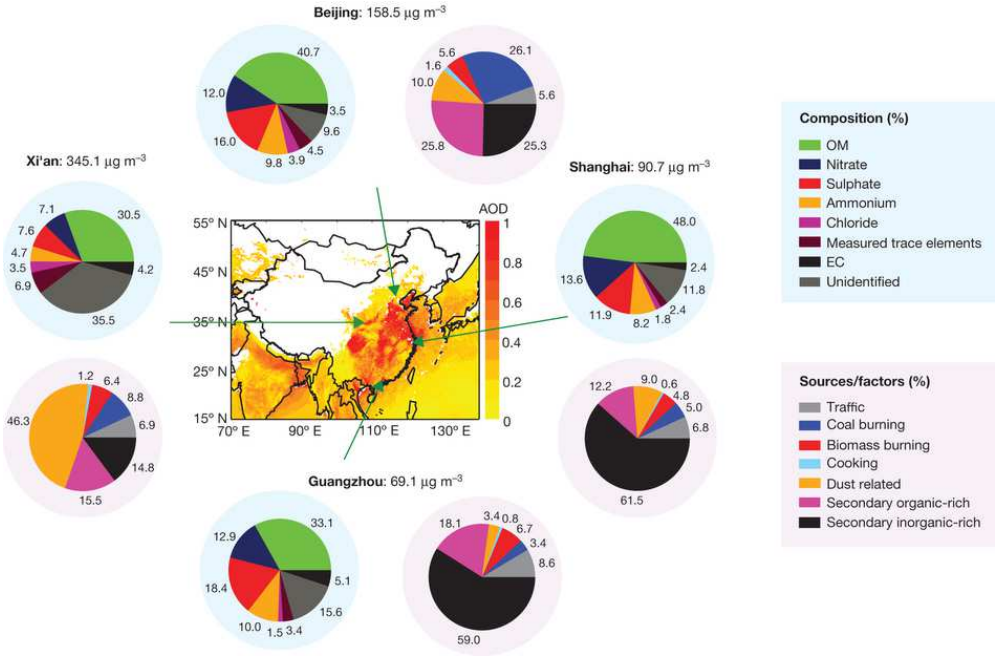

Figure 1.3 *Chemical composition and source apportionment of $PM_{2.5}$ collected during the high pollution events of 5–25 January 2013 at the urban sites of Beijing, Shanghai, Guangzhou and Xi'an. The center map presents aerosol optical depth (AOD) retrieved from satellite (Terra/Modis) (Huang et al., 2014).*

Even though both fractions, POA and SOA, are challenging to quantify in terms of sources and absolute concentrations, multiple state-of-the-art measurements and statistical analysis techniques, e.g. aerosol mass spectrometer (AMS), aerosol chemical speciation monitor (ACSM) in combination with the statistical positive matrix factorization (PMF) analysis (Jayne et al., 2000; Ng et al., 2011; Paatero and Tapper, 1994), are able to elucidate two important aspects of OA: First, a large fraction of OA is of secondary nature (Crippa et al., 2014) and, more surprisingly, SOA is found in large amounts also during winter periods when the overall oxidation potential of the atmosphere is generally reduced (Huang et al., 2014). Second, OA sources are extremely variable in time and space and cannot be entirely explained by considering only a few precursors or chemical processes. As an example, latest source apportionment studies performed in Europe revealed that winter OA is influenced by residential wood burning whereas summer OA is strongly linked to the biological activities of the trees which release larger amounts of volatile organic compounds (VOCs) with increasing temperature and radiation (Canonaco et al., 2015; Crippa et al., 2013; Waked et al., 2014). VOCs are defined as organic compounds with a saturation vapor concentration $C^* \geq 6$ µg/m^3 (Donahue et al., 2012b) and apart from vegetation, they are also emitted by various anthropogenic activities. Another important class of SOA precursors are represented by the intermediate volatility organic compounds (IVOCs), i.e. compounds with a saturation vapor concentration 300 µg/m^3 < (C^*) < 10^6 µg/m^3, also released from anthropogenic and biogenic activities. One more complication is added by the semi-volatile nature of POA (Robinson et al., 2007), which tends to evaporate after dilution from the sources (exhaust pipe, chimneys, etc.) to ambient concentrations. This occurs mainly in the range of 0.3 < (C^*) < 300 µg/m^3 and organic material in this range is referred to as semi-volatile organic compounds (SVOC). Below (C^*) < 0.3 µg/m^3, low-volatility and extremely low-volatility organic compounds (LVOC and ELVOC, respectively) will likely prefer to be in the particle phase. Along this line, also SOA has been identified and classified into semi-volatile SOA (SV-OOA) and low-volatility SOA (LV-OOA) and linked to their oxidation state and O:C ratio (Jimenez et al., 2009).

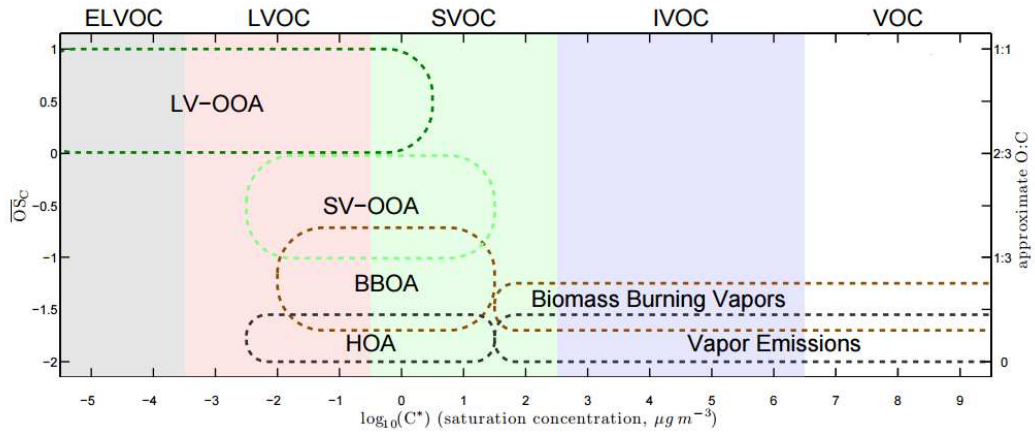

Figure 1.4 *Saturation vapor concentrations (C^* in $\mu g/m^3$), oxidation states and (O:C) ratios for important atmospheric organics. OOA is the analogous of SOA in this representation. Simplified and adapted from (Donahue et al., 2012b).*

Finally, another important component of atmospheric aerosol is represented by elemental carbon (EC) which is an insoluble and chemically inert species primarily emitted during incomplete combustion, e.g. due to traffic, industrial incineration or biomass burning. It consists mainly of pure carbon with a chemical structure similar to graphite. Being a strong light absorber, it influences the climate of the Earth during its lifetime in the atmosphere and reduces the ratio of reflected to incident solar radiation, i.e. albedo, once it is deposited on the snow.

1.3 Health effects of atmospheric aerosols

The World Health Organization (WHO) is the major agency in the world dealing with public health problems. According to new estimates, around 7 million people died in 2012 due to air pollution. This finding doubles previous estimates (WHO, 2014). For outdoor air pollution related deaths 40% were attributed to ischemic heart disease, 40% to stroke, 11% to chronic obstructive pulmonary disease, 6% to lung cancer and 3% to acute lower respiratory infections in children. Especially low- and middle-income countries in South-East Asia and Western Pacific Regions were estimated to have the largest health risk (2.6 million related deaths) (WHO, 2014).

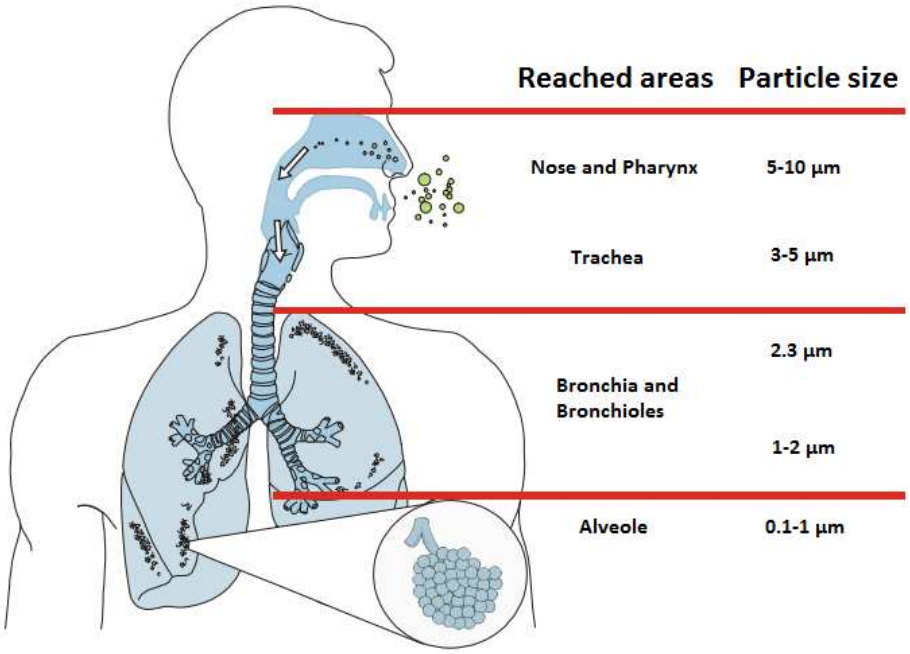

Figure 1.5 *Reached areas of the respiratory system as a function of particle size. Adapted from UGZ (2004).*

Atmospheric aerosols are able to reach different parts of the human respiratory system depending on their size as visible in Figure 1.5, and induce negative health effects e.g. respiratory diseases and cancer (Pope and Dockery, 2006). Particles with a diameter between 5 and 10 µm are usually deposited in the upper part of airways (e.g. nose and throat) whereas particles with smaller size have higher probability to reach deeper areas in the lungs (bronchioles and alveoli). Moreover, ultrafine particles with a diameter D_p < 100 nm, can furthermore accumulate in the alveoli region and reach other vital organ if they diffuse into the circulatory system (Highwood and Kinnersley, 2006).

1.4 Climate effects of atmospheric aerosols

Atmospheric aerosols alter the Earth's radiative balance by interacting with the solar and terrestrial radiation through absorption and scattering. The 5th IPCC report (AR5) (IPCC, 2013) introduced a new terminology to describe the different aerosol effects on climate. The new definitions of aerosol interactions are depicted in Figure 1.6. The effective radiative forcing from aerosol-radiation interactions (ERFari) includes i) the radiative forcing effect due to the aerosol-radiation interaction (RFari previously known as direct effects) which represents the scattering and absorption of solar radiation by aerosol, and ii) the adjustments factor which disentangles the effects of absorbing the radiation in the troposphere which e.g. heats the

surrounding environment and consequently influences cloud formations and properties (previously known as semi-direct effects) (Figure 1.6).

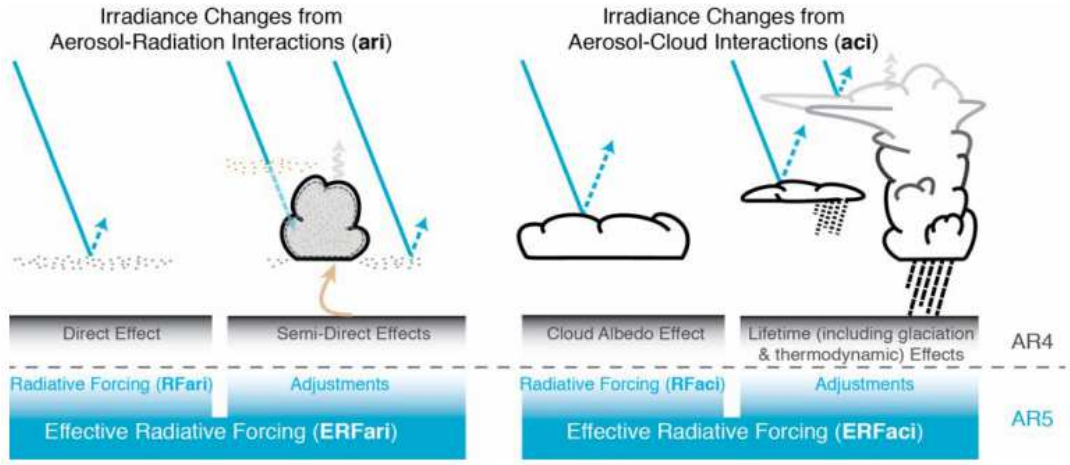

Figure 1.6 *Summary of the aerosol-radiation and aerosol-cloud interactions reported with the new (AR5) and previous (AR4) IPCC terminologies. The blue arrows depict solar radiation, the grey arrows terrestrial radiation, and the brown arrow symbolizes the importance of couplings between the surface and the cloud layer for rapid adjustments (IPCC, 2013).*

The effective radiative forcing from aerosol–cloud interactions (ERFaci), on the other hand, includes the radiative forcing from aerosol-cloud interactions (RFaci), which represents i) the instantaneous effects on cloud albedo due to the changing in concentrations of cloud condensation and ice nuclei ("*Twomey effect*")(Twomey, 1977), and ii) the rapid adjustment, which express the effect on cloud lifetime due to the increased number of CCN ("*Albrecht effect*")(Albrecht, 1989). Figure 1.7 shows the radiative forcing (RF) agents over the 1750-2011 period estimated from both observations and model data (IPCC, 2013). Greenhouse gases (GHG) like carbon dioxide (CO_2), water vapor (H_2O), nitrous oxide (N_2O), ozone (O_3) and methane (CH_4) have positive radiative forcing component in the troposphere i.e. they increase the temperature of the Earth by interfering with the incoming short wave length solar radiation. Figure 1.7 also depicts two important aspects: first, the aerosol-radiation interaction and the aerosol-cloud interaction act as a negative component of the radiative forcing, with about -0.5 W/m^2 each, as already discussed above. Moreover, both kinds of interactions exhibit error bars that are bigger compared to other forcing agent reflecting the high level of uncertainties arising from the current knowledge in the field of atmospheric aerosols and its climate effects.

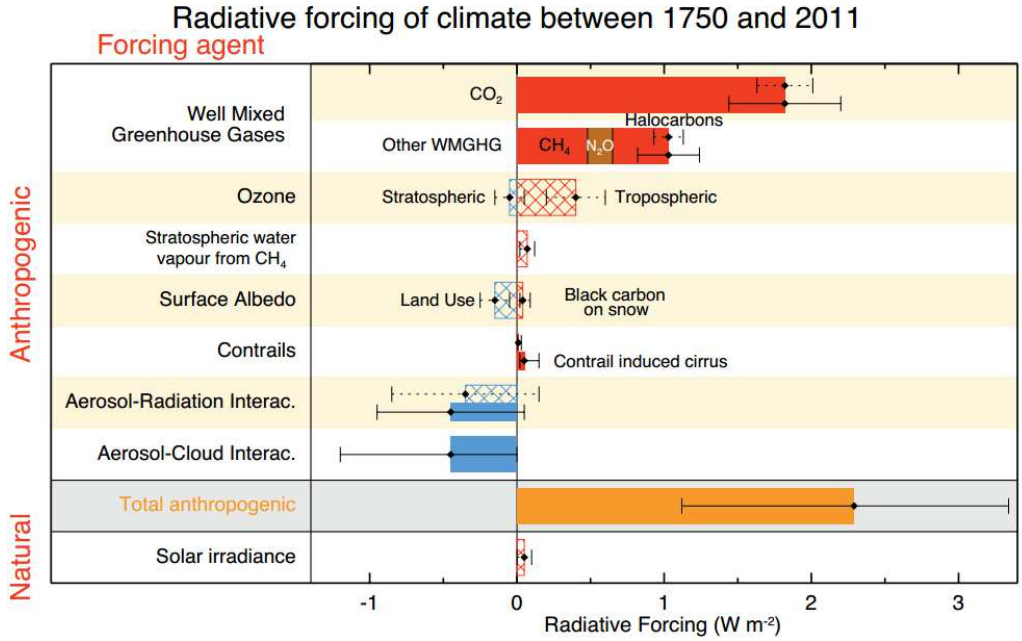

Figure 1.7 *Bar chart for RF (hatched) and ERF (solid) for the period 1750–2011. Uncertainties (5 to 95% confidence range) are given for RF (dotted lines) and ERF (solid lines) (IPCC, 2013).*

2

Air quality modelling and thesis motivation

Human and biogenic activities are both linked to Earth's climate. In this contest, a profound understanding of the main anthropogenic and biogenic sources leading to a specific composition of the Earth's atmosphere is crucial.

Chemical transport models (CTMs) represent valid tools, in combination with measurements and other statistical techniques, to explain and quantify PM sources and their variabilities (Aksoyoglu et al., 2014; Colette et al., 2011). CTMs can be deployed at different scale (e.g. regional, global) with different chemical and physical parameterization with varying degree of complexity (Aksoyoglu et al., 2011; Bergström et al., 2012). Their application requires large data-sets of different kind (meteorological data, land-use types, emissions, etc.). Evaluation of model output with measurement data is needed in order to identify model weaknesses and strengths in reproducing specific pollutant concentrations. In particular several modelling studies performed during targeted measurement campaigns with detailed observation datasets have revealed the difficulties of CTMs in reproducing the observed OA mass, which in most of the applications still remains under-predicted mainly because of the not well reproduced SOA fraction (Bergström et al., 2012; Bessagnet et al., 2014; Hodzic et al., 2009; Woody et al., 2016). Consequently, a great effort has been invested by the modelling community in order to investigate the processes leading to the formation of SOA. As an example, in a very recent global model intercomparison exercise, Aerocom, thirty-one global chemistry transport models (CTMs) and general circulation models (GCMs) were applied to evaluate the status of global modelled OA (Tsigaridis et al., 2014). Results indicated that simulated OA greatly varies between models in terms of POA emissions, SOA formation and complexity of OA parameterizations. The amount of OA remains under-predicted.

In Chapter 4, four European Monitoring and Evaluation Programme (EMEP) intensive measurement campaigns i.e. June 2006, January-February 2007, September-October 2008 and February-March 2009 were modelled within the EURODELTA-III framework (Bessagnet et al., 2014) using the Comprehensive Air Quality Model with Extensions (CAMx) (ENVIRON, 2011). Model validation was performed for common gas-phase species, i.e. NO_2, SO_2, CO, O_3 as well as $PM_{2.5}$. The 2009 winter period was further evaluated against aerosol mass spectrometer measurements (AMS) at 11 different sites in Europe (Crippa et al., 2014). In addition a new organic scheme i.e. the volatility basis sets (VBS) in CAMx model (Koo et al., 2014) was tested for the first time in Europe and several sensitivity tests were performed in order to retrieve the major sources of organic aerosol (OA).

On the other side, smog chamber experiments represent a fundamental aspect of atmospheric science. A series of novel wood combustion experiments were performed at the Paul Scherrer Institute smog-chamber facilities (Bruns et al., 2015). Emission of non-refractory primary organic aerosol (POA) as well as formation of secondary organic aerosol (SOA) and VOCs and IVOCs were characterized with the aerosol mass spectrometer (AMS) and a proton transfer reaction mass spectrometry (PTR-ToF-MS) respectively. In this contest, a hybrid volatility basis set model (VBS) model was developed and constrained with the new chamber data using the brute force approach to retrieve most unknown parameters such as NTVOCs reaction rates and yields as well as enthalpy of evaporation for POA and SOA. Results of the box-modelling study are presented in Chapter 5.

While it is necessary that CTMs correctly reproduce the measured total OA mass, also their capability to predict primary and secondary organic fractions, POA and SOA, should be addressed. SOA have been shown to represent the major fraction of the total ambient OA mass (Crippa et al., 2014; Huang et al., 2014; Jimenez et al., 2009). Even though there have been different attempts in the past to improve the modelled SOA formation at different scales and time periods, model results are still variable (Tsigaridis et al., 2014). In Chapter 6, results of the updated hybrid VBS scheme implemented in CAMx were evaluated using ambient AMS data. The model was applied for the February-March 2009 EMEP intensive measurements campaign and its performance was evaluated for primary and secondary organic aerosol fractions. Comparisons with our first VBS applications were reported as well.

3

Methods

3.1 The EURODELTA framework

The EURODELTA (ED) framework provides the European air quality modelling community with a panel where different teams could provide their experience in terms of air quality modelling related issues. It contributes to the scientific work of the United Nations Economic Commission for Europe (UNECE) Task Force on Measurements and Modelling (TFMM) within the Convention on Long-range Transboundary Air Pollution (CLRTAP). The EURODELTA activities aim to analyze and understand the latest model results and performance, the variabilities between models and sources of uncertainties. The previous EURODELTA exercises, EURODELTA-I and EURODELTA-II, focused on the ability of models to predict recent (2000) and future (2020) air quality in Europe and the effects of emission reduction strategies for targeted pollutants i.e. NO_x, SO_2, VOC and NH_3 in different countries and areas of Europe (European Commission and Joint Research Centre, 2011).

In the latest EURODELTA exercise, i.e. EURODELTA-III (Bessagnet et al., 2014), seven regional air quality models (EMEP, CHIMERE, LOTOS-EUROS, RCG, CMAQ, MINNI and CAMx) were applied in the European domain (see Figure 3.1) for selected periods during the European Monitoring and Evaluation Programme (EMEP) intensive measurement campaigns: 1 – 30 June 2006, 8 January – 4 February 2007, 17 September – 15 October 2008, 25 February – 26 March 2009. Model input data such as anthropogenic emissions, boundary conditions, temporal and vertical distribution profiles of emissions as well as meteorological data were delivered to all the participants for all the selected periods (see section 3.2.2). Different model configurations were deployed by the participant teams in terms of physical and chemical processes as well as vertical resolution of the domain; moreover, some models used different input data such as emissions of biogenic compounds (terpenes, isoprene), derived planetary boundary layer height (PBLH) and aerosol concentrations at the domain boundaries.

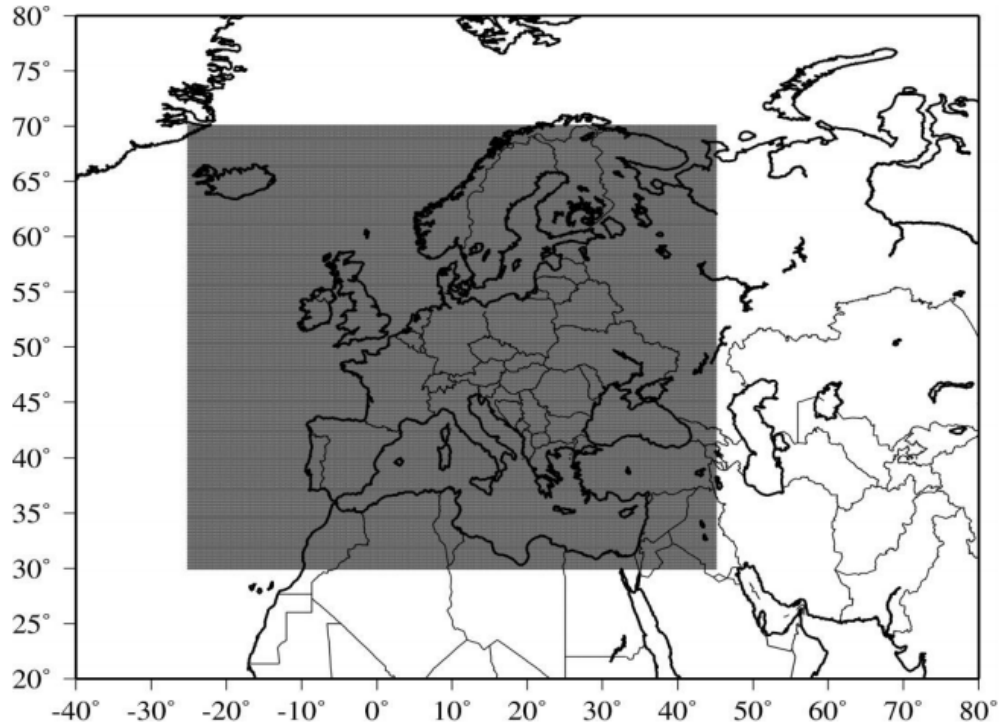

Figure 3.1 *The EURODELTA-III domain, in gray, deployed to perform air quality modelling simulations (Bessagnet et al., 2014).*

3.2 Air quality modelling

3.2.1 The Comprehensive Air Quality Model with Extensions (CAMx)

The Comprehensive Air Quality Model with Extensions (CAMx) (ENVIRON, 2011) was used with different OA schemes, to perform air quality simulations over Europe within the EURODELTA-III exercise. CAMx is a state-of-the-art Eulerian photochemical dispersion model that simulates physical and chemical processes occurring in the atmosphere. Processes like emissions, dispersions, chemical reactions and removal of pollutants are accounted for each cell of the domain by solving the Eulerian continuity equation in a terrain-following height (z) coordinates:

$$\frac{\partial c_l}{\partial t} = -\nabla_H \cdot \mathrm{V}_H c_l + \left[\frac{\partial (c_l \eta)}{\partial z} - c_l \frac{\partial^2 h}{\partial z \partial t}\right] + \nabla \cdot \rho K \nabla \left(\frac{c_l}{\rho}\right) + \frac{\partial c_l}{\partial t}|_E + \frac{\partial c_l}{\partial t}|_C + \frac{\partial c_l}{\partial t}|_R \qquad (3.1)$$

Equation 3.1 predicts the average change in concentration (c) of a specific species (l) in time. Each of the terms on the right side of equation 3.1 accounts for different processes that influence the concentration of a specific species in the model: the first three terms describe the horizontal transport, vertical transport and sub-grid turbulent diffusion where V_H represents the horizontal wind vector, h the model layer interface height, η the net vertical transport rate, ρ the atmospheric density and K the turbulent exchange. In order for the model to resolve these

terms, specific meteorological parameters must be supplied (see section 3.2.2). All the calculations are performed in a so called "*Arawaka C*" configuration grid (Figure 3.2). Parameters like pressure, temperature, cloud cover and water vapor are placed at cell center together with the pollutant concentrations and they represent the average values of the grid cell. Wind components and diffusion coefficients are calculated at the boundaries of each grid cell and they represent the mass transfer inside and outside of each cell boundary.

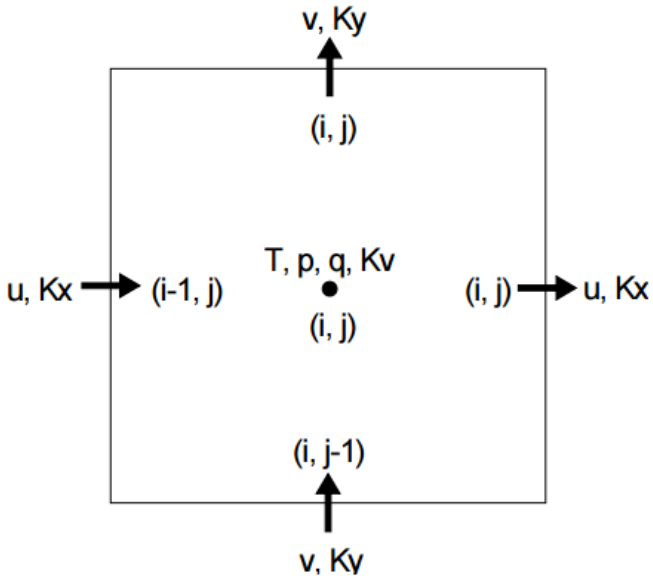

Figure 3.2 *The Arawaka C cell grid configuration used in CAMx. Kx and Ky indicate the diffusion coefficients in the two horizontal directions, u and v the wind speed components and T,p,q,Kv the temperature, pressure, water vapor and vertical diffusivity coefficient, respectively (ENVIRON, 2011).*

The next three terms represent the change in concentration due to emissions (*E*), chemical transformations (*C*) and removal processes (*R*). For the emission term (*E*), anthropogenic and biogenic emissions must be supplied which both usually represent one of the main source of uncertainties. Emissions are usually made available in a gridded format, at different time and spatial resolutions by different agencies in Europe. For this study gridded anthropogenic emissions on a latitude-longitude grid were prepared by *the Institut National de l'Environnement Industriel et des Risques* (INERIS) within the EURODELTA-III exercise and merged together with biogenic emissions calculated by each modeling team using the state-of-the-art biogenic models (see section 3.2.2).

Different chemical mechanisms are available in CAMx in order to simulate the gas-phase chemistry. The chemical carbon bound mechanism 5 (CB05) (Yarwood, 2005) which included 156 chemical reactions and up to 89 species (54 gases species, up to 22 particulates species, and 12 radicals) were used for this work with a new parameterization to treat organic aerosol: the volatility basis set (VBS) scheme (Koo et al., 2014) where a more detailed representation of the evolution of OA in the atmosphere is achieved (see section 3.3). The VBS scheme allows for additional chemical and physical processes to be simulated i.e. evaporation of primary organic

material upon dilution to atmospherically relevant concentrations, oxidation of semi-volatile organic compounds (SVOCs), inclusion of intermediate volatility organic compounds (IVOCs) and multigeneration chemistry of gas-phase material (aging) which must be taken into account especially during winter periods when the anthropogenic activities are enhanced (e.g. wood-burning use for residential heating).

Wet and dry deposition processes are the two main mechanisms affecting the life-time and removal of pollutants from the atmosphere depending on their chemical and physical properties but also on the land-use type and local meteorological conditions. The Zhang resistance model was used to calculate dry deposition of both gas phase and aerosol species (Zhang et al., 2003). The resistance model includes more detailed land-use categories compared to the Wesely (1989) approach (26 land-use categories instead of 11) which no longer represents the current state of the science. The Zhang model accounts for aerodynamic resistance, boundary resistance and the overall canopy resistance. A set of embedded annual surface roughness ranges and monthly leaf area indexes (LAI) are specified for each of the 26 land-use categories, supplied in the CAMx land-use input file. Wet deposition, on the other side, is the principal removal process for aerosol species. In CAMx a scavenging approach is adopted in which the removal of aerosol and gases within and below clouds are scaled with a scavenging coefficient calculated differently for gas and particles (Seinfeld and Pandis, 1998). CAMx accounts for the uptake of gases into the falling precipitation and the growth of cloud droplets in which gases dissolves. For particles, on the same line, both the impaction of particles with the falling precipitation and the growth of the cloud droplets on particles are taken into account. All gases can dissolve into liquid cloud water according to the Henry's Law and aerosols are assumed to be irreversibly scavenged by all precipitation forms and to be hygroscopic and internally mixed.

Finally, photolysis rates must also be supplied for the specific gas-phase chemical mechanism which implies that also their spatial and temporal variation must be provided. For this study the so called "albedo/haze/ozone" tables (also known as AHOMAP files) were prepared using the CAMx preprocessors in order to correct the clear sky photolysis rates. Global distribution of ozone columns, Figure 3.3, were retrieved for each days of the simulation from the TOMS and Ozone Monitoring Instrument (OMI) platforms and post-processed to match resolution of the domain of interest (NASA/GSFC, 2005). Then, the Tropospheric Ultraviolet and Visible (TUV) radiative transfer model (Madronich, 2002) was used to calculate photolysis rates for each specific episode based on the AHOMAP file information. Adjustment for the clouds was then internally performed in CAMx.

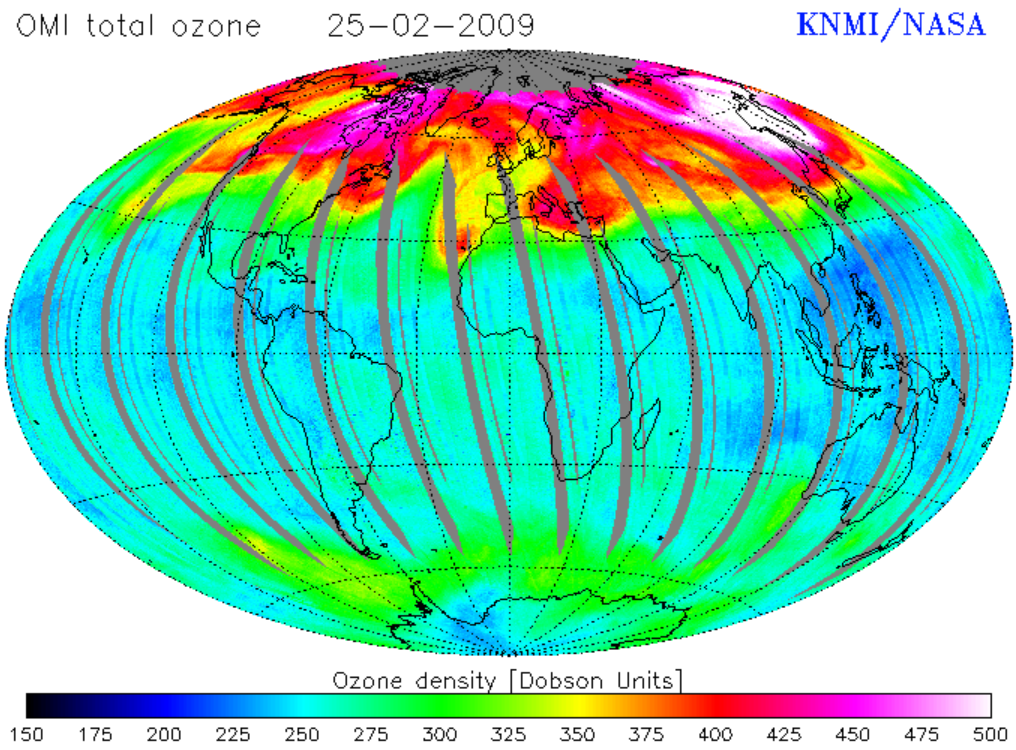

Figure 3.3 *Example of Ozone columns as available from the Ozone Monitoring Instrument (OMI) on the 25 February 2009 (http://www.temis.nl/).*

3.2.2 Emission and meteorological data

A comprehensive simulation of the atmosphere requires large heterogeneous data-sets. For this work the majority of the input data required by CAMx were provided within the EURODELTA-III intercomparison exercise by INERIS. A common domain, covering whole Europe (from 25.125°W to 45.125°E and 29.875°N to 70.125°N) was used for the exercise on a latitude-longitude coordinate system (see section 3.1 and Figure 3.1). The horizontal resolution was set to 0.25° x 0.25° for all the participants whereas no constrain was applied to the vertical resolution. CAMx was set-up with 33 terrain-following σ-levels in order to simulate the vertical structure of the atmosphere ranging up to approximately 350hPa with a lowest layer thickness of about 20 m. The different layer heights in the model matched the original structure of the delivered meteorological data which were calculated from ECMWF IFS (Integrated Forecast System) data at 0.2° resolution. Four-dimensional meteorological parameters i.e. wind speed, wind direction, relative humidity, cloud cover and vertical diffusivity were retrieved and interpolated to CAMx resolution from ECMWF IFS data and post-processed to be used in CAMx. In particular, the vertical diffusivity coefficient (K_z) was estimated from the PBL depth available in IFS following the approach proposed by O'Brien (1970). Initial and boundary conditions were prepared from the MACC (Monitoring Atmospheric Composition and Climate) reanalysis data following the recommendations of the EURODELTA-III exercise (Benedetti et al., 2009; Inness et al., 2013). One half of organic aerosol (OA) was assigned to the primary organic fraction (POA) and the other half considered to be oxidized (SOA). Other aerosol

species that were mapped at the domain boundaries include elemental carbon (EC), dust and sulfate (SO_4^{2-}).

Gridded anthropogenic emissions were calculated and provided by INERIS for all the 4 investigated episodes. Emissions were aggregated from different sources, i.e. TNO-MACC, GAINS and EMEP as well as INERIS expertise on re-gridding residential heating emissions based on population density and French bottom-up data (Kuenen et al., 2011; Vestreng et al., 2007). The final compiled emission inventories consisted of 6 gas phase species i.e. methane, carbon monoxide, ammonia, sulfur oxides, non-methane volatile organic compounds and nitrogen oxides. Particulate matter emissions were also delivered in 6 categories: fine elemental carbon (EC2.5), coarse elemental carbon (EC10), fine primary organic material (fine POA), coarse primary organic material (coarse POA), fine other primary particulate material (non-carbonaceous) and coarse other primary particulate material (non-carbonaceous). Therefore the *two static modes* (CF) representation of the aerosol size distribution was used for this study to represent the diameter of the particles (D*p*) i.e. coarse (2.5µm<D*p*<10µm) and fine (0.039µm <D*p*<2.5µm). Primary emitted material can exist in both size fractions whereas secondary particles are considered to be in the fine mode. Total non-methane volatile organic compounds were prepared to match the chemical mechanism (CB05) using the approach proposed by Passant et al. (2002). Temporal emission profiles were also provided by the EURODELTA-III community as a function of the Selected Nomenclature for Air Pollution (SNAP) codes and countries within the domain in order to represent the cultural habits of different countries.

Biogenic emissions were not provided by the EURODELTA-III community. The Model of Emissions of Gases and Aerosols from Nature, MEGANv2.1 (Guenther et al., 2012), was used to calculate emissions of most common biogenic species i.e. monoterpenes, isoprene, sesquiterpenes, xylene and toluene to be used in CAMx. The same meteorological input described above were used to drive the biogenic emission model with additional information such as plant function type (PFT) from the Community Land Model 4.0, leaf area index data at 8-days resolution from the TERRA/MODIS satellite system and global emission factors of α-pinene, β-pinene, 3-carene, isoprene, limonene, 232-methylbutenol, myrcene, NOx, t-β-ocimene and sabinene available for the MEGANv2.1 model.

3.3 The Volatility Basis Set (VBS) framework

3.3.1 Introduction

Organic aerosols are a complex mixture of hundreds of compounds that are highly variable and reactive in the atmosphere (Hallquist et al., 2009). Jimenez et al. (2009) identified four main classes of organics using aerosol mass spectrometer (AMS) measurements together with positive matrix factorization analysis (PMF): hydrocarbon-like aerosol (HOA), biomass burning aerosol (BBOA), semi-volatile oxygenated organic aerosol (SV-OOA) and low-volatility

oxygenated organic aerosol (LV-OOA). HOA usually arises from traffic emissions and it is considered a primary source of organic aerosol i.e. directly emitted in the atmosphere. It usually correlates with NO_x concentrations which is a typical proxy for traffic related emissions. BBOA, on the other hand is related to wood combustion activities (e.g. residential heating or wild fires) and it is considered as a primary source of organic aerosol. BBOA have been shown to correlate with levoglucosan ambient concentration that is often considered as a chemical tracer for biomass burning (e.g. Favez et al., 2010). The semi-volatile fraction of oxygenated organic is usually a proxy for freshly formed secondary organic aerosol (SV-OOA) that arises for example from the condensation of oxidation products of biogenic precursors in summer and oxidation of semi-volatile biomass burning vapours in winter. The low-volatility part of OOA on the other hand, comprise more oxygenated compounds and it is usually associated with long range transported OOA that has not been removed from the atmosphere, e.g. by wet deposition (Canonaco et al., 2015).

The mechanisms interconnecting the formation and evolution of all these sources are ambiguous and challenging to be represented in CTMs. The volatility basis set (VBS) framework, proposed in a two-dimensional version for the first time in 2011, is an extensive and rigorous attempt to deal with the all the sources and transformation of OA in the atmosphere (Donahue et al., 2012b, 2011).

3.3.2 Organic aerosol in a two-dimensional VBS space

The main challenge in developing an organic chemical model is that OA mixtures are extremely variable and they comprise hundreds or thousands of different compounds. Moreover such mixtures are highly reactive in the atmosphere and they rapidly modify their original chemical structure.

One of the first pioneering attempts to model the formation and evolution of OA in the atmosphere was proposed by Odum et al. (1996) based on the work of Pankow (1994). The Odum schemes deploys four parameters to describe the formation of SOA: two stoichiometric yields and two saturation concentrations to describe the formation of the condensable gases. The main limitation of the Odum approach is that it was parametrized with smog chamber studies performed at high SOA and VOC loads and results extrapolated to ambient conditions were concentrations are in general much lower than the one in chamber studies. Moreover, such approach is not able to account for the semi-volatile nature of primary organic aerosol, which will partition between the gas and particle phase when diluted from the emission sources to background air.

Donahue et al. (2006) developed a new approach to treat the complex behavior of OA: the volatility basis set (VBS) framework. The first version of this approach (one-dimensional VBS) uses different saturation concentration (C^*) bins separated by powers of 10. Usually, the C^* values covers the 0.01 μg m^{-3} to 10^6 μg m^{-3} at 298K. The bins are allowed for shifting, i.e. changing the saturation concentrations, depending on temperature and according to the

Clausius-Clapeyron equation. The partitioning of a compound *i* between the gas and particle phase could be predict in the VBS framework based on work of Pankow (1994):

$$\xi_i = \left(1 + \frac{C_i^*}{C_{OA}}\right)^{-1} \quad (3.2)$$

In Equation 3.2, C_i^* represents the effective saturation concentration of a specific organic compounds (effectively including activity coefficients of the mixture), and C_{OA} the total particle phase mass. The equation implies that at higher C_{OA} values, most of the organic material will be found in the particle phase, whereas lower C_{OA} values will favor the organic material in the gas phase. This implies that partitioning processes take place differently in different part of the globe.

This approach was later extended to a so called two-dimensional VBS model. In a 2D-VBS space four different parameters are used in order to describe the evolution of the organic material: a specific compound with a reference volatility, the carbon-carbon interactions, the oxygen-oxygen interactions and the carbon-oxygen interaction.

The 2D-VBS space relates the saturation concentration of an average OA mixture with the average number of carbons, oxygens and hydrogens (Donahue et al., 2012b, 2011). The change in (C^*) due to addition of oxygens to the OA mixture (functionalization), or reduction of carbons (fragmentation) is inferred by applying a simple group contribution method for predicting vapor pressures and enthalpies of vaporization of multifunctional organic compounds SIMPOL (Pankow and Asher, 2008), to a wide range of pure-compounds saturation concentration available from NIST (National Institute of Standards and Technology) and literature data. Figure 3.4 shows the dependency of the saturation concentration on the carbon and oxygen numbers for oxygenated compounds with functionality found in ambient OA (already corrected for non-linear effects). The compounds were grouped according to their functionalities. Few conclusions can be drawn from Figure 3.4. First, a clear carbon-number trend is visible independent on the molecule class with a net effect on $\log_{10}C°$ of -0.475 decades per carbon. Second, the influence of adding oxygens can also be elucidated. In particular, a carbonyl group (=O) reduces the volatility by 1 decade, an alcohol group (-OH) reduces the volatility by 2.3 decades and one organic acid group (-C(O)OH) by c.a. 3.5 decades. There are evidences that these functional groups are usually the most common ones present in the measured oxygenated organic aerosol fraction (OOA) (Hawkins et al., 2010). An average effect of adding oxygen was therefore retrieved, i.e. it decreases $C°$ by 1.7 decades with respect to a pure hydrocarbon reference point i.e. pentacosane (C_{25}) denoted with dashed black line in Figure 3.4.

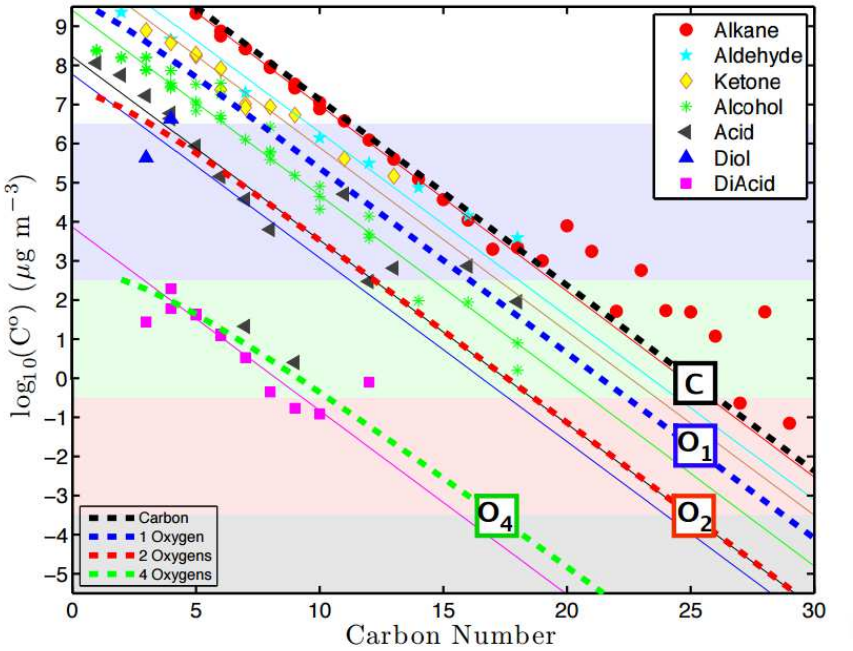

Figure 3.4 *Volatility (C°) predictions with modest nonlinearity in a group-contribution expression. The average effect of oxygenated functionality is shown by thick dashed curves (Donahue et al., 2011).*

Equation 3.2 describes the overall effects of the oxygen-oxygen interactions, carbon-carbon interactions, as well as carbon-oxygen nonideality effects on the saturation concentration for a specific average OA mixture *i*:

$$\log_{10} C_i^0 = \left(n_C^0 - n_C^i\right) b_C - n_O^i b_O - 2\frac{n_C^i n_O^i}{n_C^i + n_O^i} b_{CO} \qquad (3.3)$$

where, $b_{\mathrm{C}} \cong 0.475$, $b_{\mathrm{O}} \cong 2.3$, $b_{\mathrm{CO}} \cong -0.3$ and $n_{\mathrm{C}}^0 \cong 25$ and they represents the carbon-carbon, oxygen-oxygen, carbon-oxygen interaction and carbon numbers of the hydrocarbon reference point respectively The oxygen-oxygen interaction is increased with respect to the previously value, i.e. 1.7 decades increase per oxygen, in order to correct for the low volatility of the diacids.

Equation 3.3 is used to define and extrapolate multiple isopleths at constant numbers of carbon and oxygen as shown in Figure 3.5. The contours in Figure 3.5 describe the average composition of an aerosol mixture in the 2D-VBS space. The dashed oval area, based on extrapolations, represents the oxygenated organic aerosol (OOA) region characterized by organic compounds with carbon numbers between 6 and 10 and oxygen numbers between 4 and 8. Primary organic aerosol emissions (HOA and BBOA) will likely have higher number of carbons and lower numbers of oxygens and thus they will reside in the lower parts of the space between the semi-volatile ranges of saturation concentration.

In Chapter 4 a hybrid version of the 2D-VBS framework available in CAMx was evaluated for the first time in Europe using AMS measurements performed at different sites. In Chapter 5 wood burning smog chamber experiments were used to further parameterize the hybrid 2D-VBS

model. Finally in Chapter 6 the updated VBS scheme was implemented in the CAMx and results of the new simulations were compared to our initial CAMx results (Chapter 4).

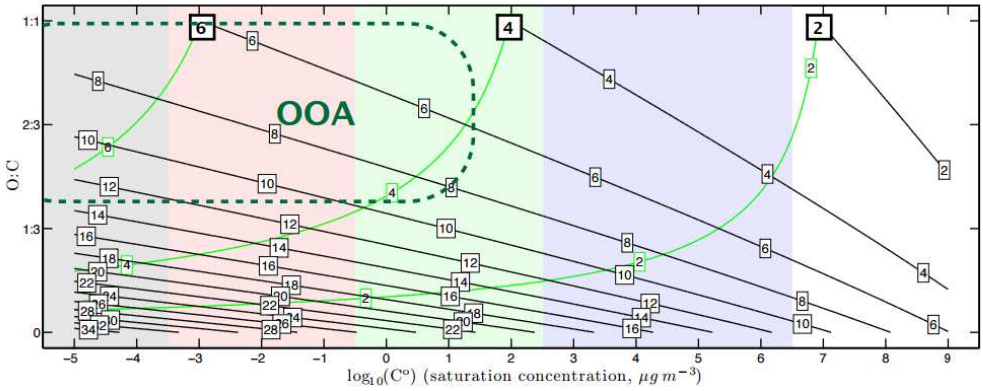

Figure 3.5 *Organic composition in a 2-D space with volatility and oxygenation (O:C) on the x and y axis respectively. Black lines represent the isopleths of carbon numbers and green curves the isopleths of oxygen number. The dashed oval indicated the likely range of oxygenated organic aerosol (OOA) found in the atmosphere (Donahue et al., 2011).*

4

Evaluation of European air quality modelled by CAMx including the volatility basis set scheme

Giancarlo Ciarelli[1], Sebnem Aksoyoglu[1], Monica Crippa[1,*], Jose-Luis Jimenez[2,3], Eriko Nemitz[4], Karine Sellegri[5], Mikko Äijälä[6], Samara Carbone[7,], Claudia Mohr[8], Colin O'Dowd[9], Laurent Poulain[10], Urs Baltensperger[1], and André S. H. Prévôt[1]**

[1]Paul Scherrer Institute, Laboratory of Atmospheric Chemistry, 5232 Villigen PSI, Switzerland
[2]Cooperative Institute for Research in Environmental Sciences, University of Colorado, Boulder, CO 80309, USA
[3]Department of Chemistry and Biochemistry, University of Colorado, Boulder, CO 80309, USA
[4]Center for Ecology and Hydrology, Bush Estate, Penicuik, Midlothian, EH26 0QB, UK
[5]Laboratoire de Météorologie Physique CNRS UMR6016, Observatoire de Physique du Globe de Clermont-Ferrand, Université Blaise Pascal, 63171 Aubière, France
[6]University of Helsinki, Department of Physics, Helsinki, Finland
[7]Atmospheric Composition Research, Finnish Meteorological Institute, P.O. Box 503, 00101 Helsinki, Finland
[8]Karlsruhe Institute of Technology, Institute of Meteorology and Climate Research
[9]School of Physics and Centre for Climate & Air Pollution Studies, Ryan Institute, National University of Ireland Galway, University Road, Galway, Ireland
[10]Leibniz-Institute for Tropospheric Research (TROPOS), Permoserstr. 15, 04318 Leipzig, Germany
[*]now at: European Commission, Joint Research Centre (JRC), Directorate for Energy, Transport and Climate, Air and Climate Unit, Via E. Fermi 2749, I-21027 Ispra (VA), Italy
[**]now at: Institute of Physics, University of São Paulo, Rua do Matão Travessa R, 187, 05508-090 São Paulo, S.P., Brazil

Published in Atmospheric Chemistry and Physics

doi:10.5194/acp-16-10313-2016

Abstract

Four periods of EMEP (European Monitoring and Evaluation Programme) intensive measurement campaigns (June 2006, January 2007, September-October 2008 and February-March 2009) were modelled using the regional air quality model CAMx with VBS (Volatility Basis Set) approach for the first time in Europe within the framework of the EURODELTA-III model intercomparison exercise. More detailed analysis and sensitivity tests were performed for the period of February-March 2009 and June 2006 to investigate the uncertainties in emissions as well as to improve the modelling of organic aerosols (OA). Model performance for selected gas phase species and $PM_{2.5}$ was evaluated using the European air quality database Airbase. Sulfur dioxide (SO_2) and ozone (O_3) were found to be overestimated for all the four periods with O_3 having the largest mean bias during June 2006 and January-February 2007 periods (8.9 pbb and 12.3 ppb mean biases, respectively). In contrast, nitrogen dioxide (NO_2) and carbon monoxide (CO) were found to be underestimated for all the four periods. CAMx reproduced both total concentrations and monthly variations of $PM_{2.5}$ for all the four periods with average biases ranging from -2.1 μg m^{-3} to 1.0 μg m^{-3}. Comparisons with AMS (aerosol mass spectrometer) measurements at different sites in Europe during February-March 2009 showed that in general the model over-predicts the inorganic aerosol fraction and under-predicts the organic one, such that the good agreement for $PM_{2.5}$ is partly due to compensation of errors. The effect of the choice of volatility basis set scheme (VBS) on OA was investigated as well. Two sensitivity tests with volatility distributions based on previous chamber and ambient measurements data were performed. For February-March 2009 the chamber-case reduced the total OA concentrations by about 42% on average. On the other hand, a test based on ambient measurement data increased OA concentrations by about 42% for the same period bringing model and observations into better agreement. Comparison with the AMS data at the rural Swiss site Payerne in June 2006 shows no significant improvement in modelled OA concentration. Further sensitivity tests with increased biogenic and anthropogenic emissions suggest that OA in Payerne were affected by changes in emissions from residential heating during the February-March 2009 whereas it was more sensitive to biogenic precursors in June 2006.

4.1 Introduction

Air pollution is known to cause damage to human health, vegetation and ecosystems. It is one of the main environmental causes of premature death. Only in Europe, more than 400,000 premature deaths were estimated in 2012 with $PM_{2.5}$ (particles less than 2.5 μm in aerodynamic diameter) having the highest relative risk for health damage (WHO, 2014). Air quality models help understanding the processes taking place between emission sources and pollutant concentrations at receptor sites. They are very useful to define control strategies for future legislation. In spite of large improvements in recent years, Chemical Transport Models (CTMs) have still some uncertainties (Solazzo et al., 2012). Various air quality model intercomparison exercises were successfully carried out over the last decades to determine uncertainties in chemical and physical processes governing particulate matter and its precursors (Bessagnet et al., 2014; Solazzo et al., 2012). However, a large variability in particulate matter concentrations was found between different models indicating process parameterization as one of the main reasons for such discrepancies. Moreover, recent studies based on AMS (Aerosol Mass Spectrometer) measurements at different sites in Europe, revealed that the organic fraction dominates the non-refractory PM_1 composition (Crippa et al., 2014). Organic aerosol (OA) can be found in the atmosphere from direct emission by various sources, such as fossil fuel combustion by road vehicle engines or residential wood combustion. Direct emissions of OA are typically referred to as primary organic aerosol (POA) whereas gas-to-particle conversion is referred to as secondary organic aerosol (SOA). Formation mechanisms of SOAs are not very well known yet and their representation in CTMs is still challenging (Bergström et al., 2012; Fountoukis et al., 2014; Hallquist et al., 2009; Langmann et al., 2014; Li et al., 2013; Tsigaridis et al., 2014). In one of our recent aerosol modelling studies we compared model $PM_{2.5}$ prediction with PM_1 AMS measurements for different sites (Payerne and Zürich) and periods (summer and winter) in Switzerland. We found that particulate matter was generally well reproduced by the model with the SOA fraction being under-predicted and POA over-predicted (Aksoyoglu et al., 2011). Traditional CTMs treat POA as non-volatile. Some studies however have revealed the semi-volatile nature of POA, through its dynamic equilibrium of organic aerosol with its gas phase, and the importance of semi-volatile (SVOC) and intermediate volatility (IVOC) organic compounds as SOA precursors (Cappa and Jimenez, 2010; Donahue et al., 2006; Robinson et al., 2007). To describe the absorptive partitioning and ongoing oxidation of the atmospheric material, a volatility basis set (VBS) where organic species are organized into surrogates according to their volatility was developed (Donahue et al., 2012a, 2012b, 2011). Air quality models updated with the VBS scheme started being used (Athanasopoulou et al., 2013; Fountoukis et al., 2014; Jo et al., 2013; Lane et al., 2008; Murphy

et al., 2012; Zhang et al., 2013). Bergström et al. (2012) reported an EMEP model study over Europe for the 2002-2007 period using different assumptions regarding partitioning and aging processes. They could not reproduce the measured OA levels in winter suggesting that residential wood combustion inventories might be underestimated in different parts of Europe. Fountoukis et al. (2014) applied the PMCAMx model to simulate EUCAARI (Kulmala et al., 2011, 2009) and EMEP (Tørseth et al., 2012) campaigns in Europe. They could reproduce most of PM_1 daily average OA observations within a factor of two, with the February-March 2009 period having the largest discrepancies. Zhang et al. (2013) deployed the CHIMERE model with the VBS framework during the MEGAPOLI summer campaign in the Greater Paris region for July 2009. They found a considerable improvement in predicted SOA concentrations which might be even overestimated depending on the emission inventory used. In our study, we applied the regional air quality model CAMx with the VBS scheme for the first time in Europe within the framework of EURODELTA-III model intercomparison exercise. In addition to the base case configuration used in the exercise, more sensitivity tests with the VBS scheme for winter and summer episodes were performed together with a general evaluation of the four EMEP field measurement campaigns.

4.2 Method

4.2.1 The EURODELTA-III exercise

The EURODELTA-III (EDIII) framework is a European model intercomparison exercise between several modelling teams sharing both efforts and technical knowledge in order to reduce model uncertainties and to improve understanding of the performances. It contributes to the scientific work of the United Nations Economic Commission for Europe (UNECE) Task Force on Measurement and Modelling (TFMM) within the Convention on Long-range Transboundary Air Pollution (CLRTAP). In the first phase of the EDIII exercise, 4 periods of the EMEP field measurement campaigns were chosen in order to evaluate the model results:

- 1 June – 30 June 2006
- 8 January – 4 February 2007
- 17 September – 15 October 2008
- 25 February – 26 March 2009

Multiple models were applied on a common domain and driven with the same input data provided by the National Institute for Industrial Environment and Risks (INERIS). However, for some models, different meteorology, boundary conditions and emissions data such as biogenic emissions were used (Bessagnet et al., 2014).

4.2.2 Modelling method

4.2.2.1 CAMx

The Comprehensive Air quality Model with extensions, CAMx-VBS (CAMx5.41_VBS, kindly provided by ENVIRON before its public release) was used in this study. The model domain consisted of one grid with a horizontal resolution of 0.25° x 0.25°. The latitude and longitude grid extended from 25.125°W to 45.125°E and 29.875°N to 70.125°N resulting in 281 x 161 grid cells covering the whole of Europe. Hourly four-dimensional meteorological fields for wind speed and direction, pressure, temperature, specific humidity, cloud cover and rain required by CAMx simulations were calculated from ECMWF IFS (Integrated Forecast System) data at 0.2° resolution. Vertical diffusivity coefficients were estimated following the Kz approach of O'Brien (1970) using PBL depth profiles as available in IFS data. CAMx simulations used 33 terrain-following σ-levels up to about 8000 m above ground level, as in the original IFS data. The lowest layer was about 20 m thick. MACC (Monitoring Atmospheric Composition and Climate) reanalysis data were used to initialize initial and the boundary condition fields (Benedetti et al., 2009; Inness et al., 2013). Elemental carbon, organic aerosol, dust and sulfate were used to model aerosol species at the boundaries of the domain. One half of the OA was assumed to be secondary organic aerosol (SOA) and the other half primary organic aerosol (POA), as recommended in the EDIII exercise. Photolysis rate inputs were calculated using the Ultraviolet and Visible (TUV) radiative transfer and photolysis model (https://www2.acom.ucar.edu/modeling/tropospheric-ultraviolet-and-visible-tuv-radiation-model).

The required ozone column densities to determine the spatial and temporal variation of the photolysis rates were extracted from TOMS data (NASA/GSFC, 2005). Removal processes as dry and wet deposition were simulated using the Zhang resistance model (Zhang et al., 2003) and a scavenging model approach for both gases and aerosols (ENVIRON, 2011), respectively. For the gas phase chemistry the Carbon Bond (CB05) mechanism (Yarwood, 2005) with 156 reactions and up to 89 species was used. Partitioning of inorganic aerosols (sulfate, nitrate, ammonium, sodium and chloride) was performed using the ISORROPIA thermodynamic model (Nenes et al., 1998). Aqueous sulfate and nitrate formation in cloud water was simulated as well using the RADM aqueous chemistry algorithm (Chang et al., 1987).

4.2.2.2 Emissions

Anthropogenic emissions

Annual total gridded anthropogenic emissions were prepared and provided by INERIS for the EDIII exercise, which is based on a merging process of data-bases from different sources, i.e. TNO-MACC (Kuenen et al., 2011), EMEP (Vestreng et al., 2007), GAINS (The Greenhouse Gas and Air Pollution Interactions and Synergies). For specific countries where TNO-MACC emissions were missing (Iceland, Liechtenstein, Malta and Asian countries), the EMEP 0.5° × 0.5° emissions were used and re-gridded using adequate proxies such as "artificial land-use" and EPER (European Pollutant Emission Register) data (http://www.eea.europa.eu/) for industries. Total primary particle emissions were made available by EMEP in two different size ranges: below 2.5µm (fine) and between 2.5µm and 10µm (coarse). Total emissions were later split to estimate the amount of elemental carbon, and organic matter for each of the 10 SNAP codes (Selected Nomenclature for Air Pollution) and country. The final emission inventory thus compiled consisted of 6 gas species namely methane, carbon monoxide, ammonia, sulfur oxides, non-methane volatile organic compounds and nitrogen oxides and 6 categories of particulate matter classes: fine elemental carbon (EC2.5), coarse elemental carbon (EC10), fine primary organic material (fine POA), coarse primary organic material (coarse POA), fine other primary particulate material (non-carbonaceous) and coarse other primary particulate material (non-carbonaceous). $PM_{2.5}$ and PM_{10} emissions were provided by EMEP and they were split to elemental carbon and organic matter using the fractions given by IIASA (International Institute for Applied Systems Analysis) for each source and country. Total non-methane volatile organic compounds were split for the CB05 mechanism using the recommendations of Passant (2002). Hourly, weekly and monthly time profiles were applied to total annual anthropogenic emissions.

Biogenic emissions

Biogenic VOC emissions were calculated using the Model of Emissions of Gases and Aerosols from Nature MEGANv2.1 (Guenther et al., 2012). This model is driven by meteorological variables such as hourly temperature, solar radiation, humidity, wind speed, soil moisture and land cover data including leaf area index (LAI) and plant function type (PFT) as available in the Community Land Model 4.0. 8-Days average satellite data at 0.25° x 0.25° resolution were pre-processed and made available from the TERRA/MODIS satellite system. Sixteen plant function types including needle-leaved evergreen, needle-leaved deciduous, broad-leaved evergreen, broad-leaved deciduous, grass and crop for different climatic zones were prepared for this study at 0.25° x 0.25° resolution together with the global emission factors of α-pinene, β-pinene, 3-carene, isoprene, limonene, 232-methylbutenol, myrcene, NO_x, *t-β-*

ocimene and sabinene. Common BVOC species such as isoprene, terpene, sesquiterpene, xylene and toluene were obtained for each hour and cell in the domain.

4.2.2.3 VBS scheme

A new volatility basis set (VBS) scheme is available in the CAMx model to describe changes in oxidation state and volatility. A total of four basis set simulates the evolution of organic aerosol in the atmosphere (Koo et al., 2014). POA emissions were split in hydrocarbon-like organic aerosol (HOA-like) and biomass burning organic aerosol (BBOA-like) emissions and allocated in two different basis sets. HOA-like emissions include emissions from all SNAP sectors except SNAP2 (non-industrial combustion plants) and SNAP10 (agriculture) which were assigned to BBOA-like emissions. Two other sets were used in the model to allocate secondary organic aerosol from anthropogenic (i.e. xylene and toluene) (ASOA) and biogenic (i.e. isoprene, monoterpene and sesquiterpene) (BSOA) gaseous precursors. These two sets also allocate oxidation products of POA vapours, from each of the two primary sets (HOA-like and BBOA-like). The 2D volatility space retrieved by Donahue et al. (2011; 2012a,b) was used to distribute the organic molecular structures for each of the volatility bins and different sets (Table A.1 1). Five volatility bins represent the range of semi-volatile organic compounds (SVOCs) ranging from 10^{-1} μg m^{-3} to 10^{3} μg m^{-3} in saturation concentrations (C*). Oxidation processes are modelled by shifting C* by a factor of 10 in the next lower volatility bin, increasing the oxidation state and reducing the carbon number to account for fragmentation. OH reaction rates are assumed to be 4 x 10^{-11} cm^{3} $molecule^{-1}$ s^{-1} for the reaction of semi-volatile primary vapors with OH and 2 x 10^{-11} for further aging of ASOA and POA vapours from HOA-like emissions. More details about the VBS parameterization in CAMx can be found in Koo et al. (2014). Further aging of BSOA is not considered in this study based on previous modelling results showing over-prediction of OA when such process is taken into account (Lane et al., 2008; Murphy and Pandis, 2009). This implies that also further aging of POA vapours from BBOA-like emissions was not considered since it is performed in the same basis set. In this work we focus on the effects of a VBS framework on the total OA fraction. Aging processes and alternative VBS implementations will be discussed together with SOA and POA components in a following paper (Ciarelli et al., 2016b). Three sensitivity tests were performed with different assumptions on the volatility distributions (Table 4.1):

- **NOVBS:** Primary organic aerosol was assumed to be non-volatile. Biogenic (isoprene, monoterpenes and sesquiterpenes) and anthropogenic (xylene, toluene and other aromatics) volatile organic compounds (VOCs) were used as precursors for secondary organic aerosol. Partitioning of condensable gases to secondary organic aerosol was calculated using a semi-volatile equilibrium approach (Strader et al., 1999).

- **VBS_ROB:** Primary organic aerosol was assumed to be volatile and undergo chemical oxidation. The volatility distribution estimated by Robinson et al. (2007) was applied to HOA-like and BBOA-like emissions. Emissions of intermediate volatility organic compounds (IVOCs) were assumed to be 1.5 times those of primary organic aerosol (POA) as suggested by Robinson et al. (2007).

- **VBS_BC:** Primary organic aerosol was assumed to be volatile and undergo chemical oxidation using the approach of Shrivastava et al. (2011) and Tsimpidi et al. (2010). The total primary emissions are roughly 3 times higher than in **VBS_ROB.** Different volatility distributions were applied for HOA and BBOA-like emissions. IVOCs were assumed to be 1.5 times the amount of POA. This implies that for this scenario the SVOC + IVOC mass added is equal to 7.5 times the initial amount of POA. This represents the base case scenario used to evaluate gas phase and $PM_{2.5}$ model performance.

Based on the **VBS_BC** base case scenario, two other sensitivity tests were performed with respect to emissions:

- **VBS_BC_2xBVOC:** Increased BVOCs emissions by a factor of 2.

- **VBS_BC_2xBBOA:** Increased BBOA-like emissions by a factor of 2.

Table 4.1 *Volatility distributions used for different scenarios.*

Scenarios	POA emission sources	Emission fraction for volatility bin with C* of				
		0	1	10	100	1000
NOVBS (non-volatile CAMxv5.40)	HOA-like	1.00	-	-	-	-
	BBOA-like	1.00				
VBS_ROB (Robinson et al., 2007)	HOA-like	0.09	0.09	0.14	0.18	0.5
	BBOA-like	0.09	0.09	0.14	0.18	0.5
VBS_BC (Tsimpidi et al., 2010 and Shrivastava et al., 2011)	HOA-like	0.40	0.26	0.40	0.51	1.43
	BBOA-like	0.27	0.27	0.42	0.54	1.50

* Properties of the lowest volatility bins refer to all OA with $C^* \leq 0.1$ μg m^{-3} (non-volatile OA).

4.2.3 Statistical methods

Statistical procedures as available in the Atmospheric Model Evaluation Tool (AMET, (Appel et al., 2010) were used in this study to evaluate model performance. Daily ambient measurements of main gas phase species i.e. O_3, NO_2, CO, SO_2 and fine particulate matter ($PM_{2.5}$) were extracted from the Airbase database in Europe and statistics reported in terms of mean bias (MB), mean error (ME), mean fractional bias (MFB) mean fractional error (MFE) and correlation coefficient (r).

Due to the coarse grid resolution, only rural-background stations, defined as stations far from city sources of air pollution with pollution levels determined by the integrated contribution from all sources upwind of the station (ETC/ACC, 2004), with at least 80% daily average observations available were considered for the statistical analysis. For $PM_{2.5}$ this resulted in 48 stations available for June 2006, 56 for January-February 2007, 90 for September-October 2008 and 110 stations for February-March 2009. $PM_{2.5}$ components were further evaluated for the February-March 2009 period where comprehensive high resolution AMS measurements at 11 European sites were available, i.e., at Barcelona, Cabauw, Chilbolton, Helsinki, Hyytiälä, Mace Head, Melpitz, Montseny, Payerne, Puy de Dôme and Vavihill (Crippa et al., 2014).

4.3 Results and discussions

4.3.1 Model evaluation

Model performance metrics for gas phase species CO, NO_2, O_3 and SO_2 as well as for $PM_{2.5}$ are reported in Table 4.2 and they refer to the base case VBS_BC.

NO_2 and O_3

NO_2 was found to be under-predicted for all the four periods with mean fractional bias between -54% and -28% and NO_2 concentrations being particularly under-predicted during June 2006. Evaluation of the EURODELTA III model inter-comparison exercise showed that all models performed similarly for NO_2 in terms of correlation with *r* values in the range 0.6-0.7 and the spatial correlation was much higher in the range 0.7-0.9 for all models (Bessagnet et al., 2016) with a general underestimation in the afternoon. The NO_2 performance could be influenced by several factors:

- Uncertainties in the emission inventories. Although NO_x emission estimates in Europe are thought to have an uncertainty of about ± 20%, the complete data set used in the inventories has much higher uncertainty (Kuenen et al., 2014). A recent study identified a significant discrepancy between emission estimates and actual flux measurements,

with the highest underestimation being a factor of two in central London mainly due to under-representation of real world road traffic emissions (Vaughan et al., 2016)

- The relatively coarse resolution of the domain which may result in too low NO_x emissions or isolated local events that the model cannot resolve. We report daily average time series of NO_2 for the period of Feb-Mar 2009 for stations in Table 4.2 as well as daily average time series of NO_2 for stations not exceeding 5 ppb (which represents 92% of the stations in Table 4.2) (Figure A.1 1). The model performance for NO_2 significantly improved when the 5 ppb threshold was applied to the dataset. An emission map of NO for 1 March 2009 at 6 AM is reported in Figure A.1 2. High emissions of NO are predicted in the Benelux area, Po Valley, Germany and in some of the eastern European countries. High NO emissions due to ship traffic are also visible especially in the Mediterranean Sea.

- Possible positive artefacts in the chemiluminescence methods for measuring NO_2 may also occur when NO_2 is catalytically converted to NO on the molybdenum surface leading to an over-prediction of measured NO_2 concentrations (Steinbacher et al., 2007; Villena et al., 2012).

- Moreover, an evaluation of planetary boundary layer height (PBLH) within the EDIII shows that although the PBLH was quite well represented in general in the ECMWF IFS meteorological fields, CAMx tends to under-estimate the night-time minima and to over-estimate some daytime peaks, over-predicting the dilution of day time NO_2 concentrations, whereas the wind speed was relatively well reproduced (Bessagnet et al., 2016).

O_3 concentrations were found to be over-predicted for all the four periods with a mean fractional bias ranging from 2% to 48%. Especially in June 2006, when the photochemical activity is higher, the general under-prediction of NO_x in the whole domain reduces the O_3 titration potential during night time.

Model performance for O_3 is also strongly influenced by long-range transport especially during the winter periods when the local chemical production of O_3 is limited. Figure A.1 3 shows the model performance at the Mace Head station located on the west coast of Ireland for all the four periods. Especially in January-February 2007 O_3 concentrations were found to be over-predicted by about 10 to 20 ppb indicating that boundary conditions for O_3 were probably not well represented. In June 2006 and September-October 2008 O_3 was relatively well captured at Mace Head suggesting that the observed positive bias in O_3 concentrations might arise from insufficient NO_x emissions to undergo titration during night time as well as not correctly represented planetary boundary layer dynamics. In February-March 2009 the model tends to

under-predict the O_3 concentration at Mace Head and overall the O_3 model performance shows the lowest bias (2%). Eventually, the under-prediction of O_3 in the boundary condition may counteract the already mentioned deficiencies related to insufficient NO_x emissions.

Table 4.2 *Model gas phase and $PM_{2.5}$ performance for the EDIII field campaigns (base case VBS_BC).*

Species	Number of sites	Observed mean (ppb) ($\mu g\ m^{-3}$ for $PM_{2.5}$)	Modelled mean (ppb) ($\mu g\ m^{-3}$ for $PM_{2.5}$)	MB (ppb) ($\mu g\ m^{-3}$ for $PM_{2.5}$)	ME (ppb) ($\mu g\ m^{-3}$ for $PM_{2.5}$)	MFB [-]	MFE [-]	r
			June 2006					
CO	36	192.0	158.0	-34.2	80.7	-0.12	0.36	0.20
NO_2	320	4.1	2.3	-1.9	2.2	-0.54	0.68	0.55
O_3	460	42.3	51.2	8.9	10.8	0.21	0.24	0.57
$PM_{2.5}$	48	12.0	11.7	-0.3	4.5	-0.07	0.39	0.55
SO_2	263	1.0	1.2	0.2	0.7	0.14	0.67	0.52
			Jan-Feb 2007					
CO	45	248.0	191.0	-57.8	107.0	-0.11	0.37	0.21
NO_2	337	6.5	4.4	-2.2	3.2	-0.28	0.57	0.68
O_3	455	23.5	35.8	12.3	12.6	0.48	0.49	0.61
$PM_{2.5}$	56	11.7	12.8	1.0	6.1	-0.04	0.56	0.69
SO_2	271	1.3	1.7	0.4	1.1	0.36	0.75	0.46
			Sep-Oct 2008					
CO	53	208.0	136.0	-72.0	91.4	-0.31	0.48	0.27
NO_2	370	5.3	3.7	-1.7	2.5	-0.28	0.56	0.62
O_3	465	24.3	32.5	8.2	9.6	0.32	0.37	0.50
$PM_{2.5}$	90	13.0	14.1	1.0	5.7	<0.01	0.46	0.76
SO_2	256	0.9	1.1	0.2	0.8	0.25	0.74	0.37
			Feb-Mar 2009					
CO	57	262.0	170.0	-91.6	119.0	-0.26	0.48	0.37
NO_2	380	6.0	3.9	-2.0	2.8	-0.33	0.56	0.61
O_3	488	32.7	33.0	0.2	7.1	0.02	0.23	0.55
$PM_{2.5}$	110	15.1	13.0	-2.1	6.4	-0.13	0.50	0.71
SO_2	257	1.0	1.3	0.3	0.9	0.23	0.76	0.45

SO_2 and CO

SO_2 concentrations were found to be slightly over-predicted for all the four periods with a mean fractional bias ranging from 14% to 36% for SO_2. The daily variations of modelled and measured SO_2 concentrations for February-March 2009 are reported as well in Figure A.1 1(lower-panel) for the stations in Table 4.2. In general, the daily variations of modelled and measured SO_2 concentrations agree relatively well with each other throughout the period.

Most of the SO_2 emissions arise from high stack point sources which have injection heights of a few hundred meters. It might be that the vertical distribution of SO_2 might affect the model performance in particular near the harbors and coastal areas where ship emissions were allocated in the second layer of the model domain (extending from ~20 to 50 m above ground level) whereas they can reach up to 58 meters in deep draft vessels (SCG, 2004) and also undergo plume rise. Insufficient conversion to sulfate or too low deposition processes might also positively bias the model performance for SO_2.

CO was slightly under-predicted for all periods (mean fractional bias between -11% and -31%), with highest values during the September-October 2008 period (-31%). The late summer-fall period is known to be influenced by agricultural open field burning activities which might be missing from standard emission inventories.

In general, for both SO_2 and CO, the model showed lower correlation coefficients with respect to other gas-phase species (r values from 0.20 and 0.37 for CO and from 0.37 to 0.52 for SO_2).

$PM_{2.5}$

Of all investigated variables, CAMx shows the best statistical performance for $PM_{2.5}$. For all four periods the acceptable model performance criteria recommended by Boylan and Russell (2006) for aerosols were met (MFE ≤ +75 % and −60 % < MFB < +60 %). The fractional bias ranges from less than 1% in September-October 2008 up to -13% in February-March 2009. Also the recommended model performance goals (MFE ≤ +50% and -30% < MFB < +30%) were met for all periods except for January 2007. Modelled average $PM_{2.5}$ concentrations are shown in Figure 4.1. A different spatial distribution is seen for summer and winter. In June 2006 the model predicts higher concentrations in the southern part of the domain especially over the Mediterranean Sea and North Africa (up to 35 μg m^{-3}). On the other hand, the highest concentrations were predicted in the Po valley area (above 40 μg m^{-3}) and in the southern part of Poland during January-February 2007. During the two colder periods (2007 and 2009) elevated concentrations of around 15 μg m^{-3} are also visible close to urban areas such as Paris and Moscow. Figure 4.2 shows $PM_{2.5}$ variations at Airbase rural-background sites in terms of medians, 25th and 75th percentiles. In all the four periods CAMx is able to reproduce the observed monthly variation very well with some over-prediction occurring mainly from the 14th to the 17th of January 2007 and towards the end of the 2008 period.

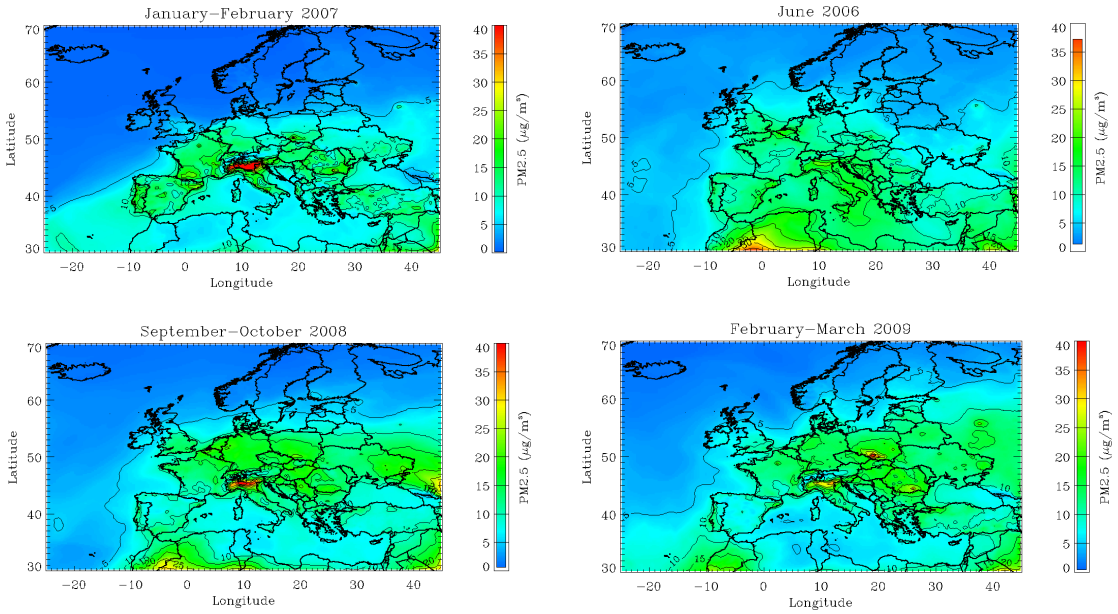

Figure 4.1 *Modelled average $PM_{2.5}$ concentrations for June 2006, January-February 2007, September-October 2008 and February-March 2009 (top to bottom and left to right) based on the base case (VBS_BC). Note that the color scale was limited to a maximum of 40 μg/m^3 to facilitate comparison of the panels.*

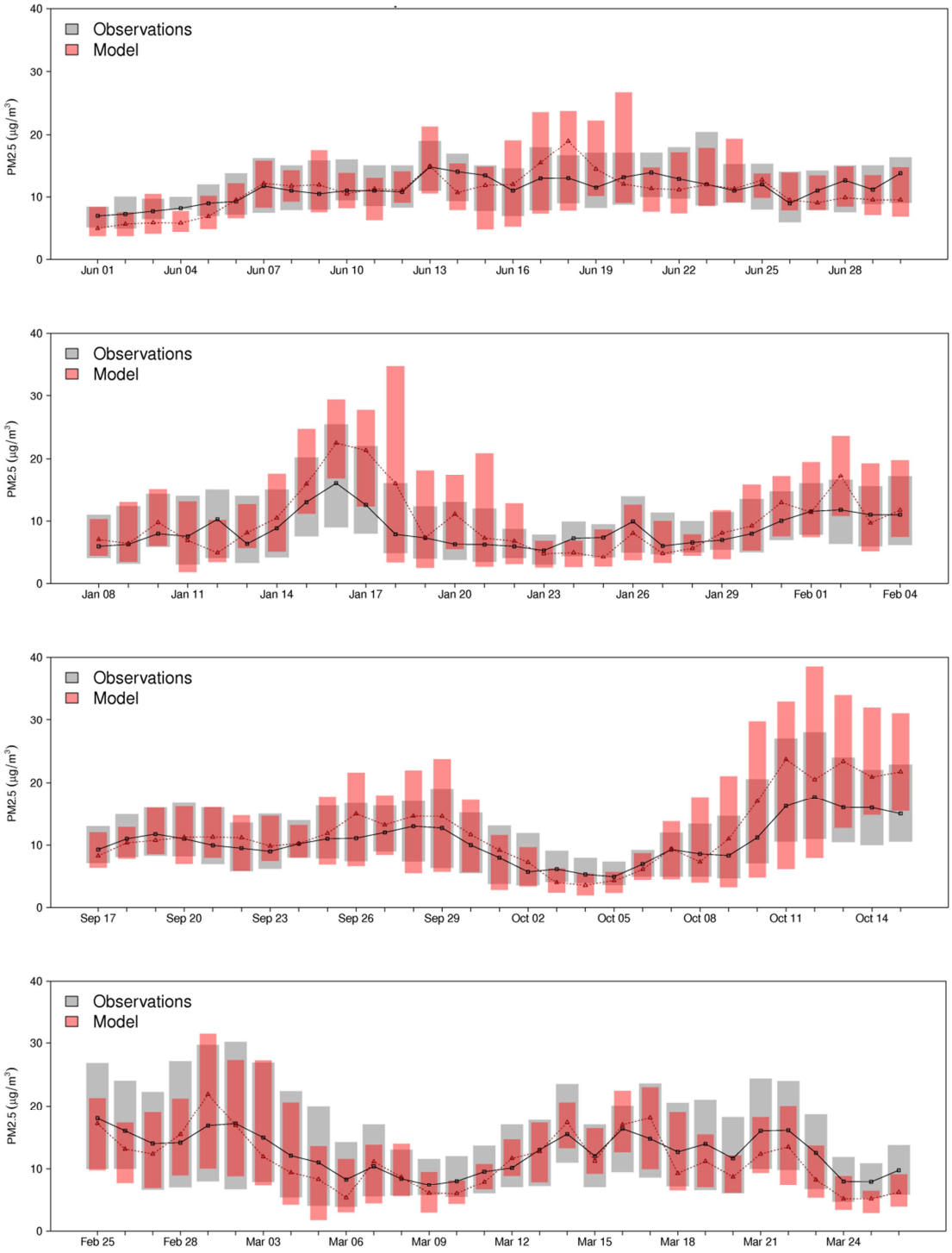

Figure 4.2 *Comparison of modelled (red) and measured (grey) $PM_{2.5}$ concentrations at AirBase rural background sites. The extent of the bars indicates the 25th and 75th percentiles. The black and red lines are observed and modelled medians, respectively. The numbers of sites are 48, 58, 90, and 110 from top to down. Based on the base case (VBS_BC).*

4.3.2 Detailed evaluation of $PM_{2.5}$ components in February-March 2009

The modelled concentrations of non-refractory $PM_{2.5}$ components were compared against aerosol mass spectrometer measurements at eleven European sites for the February-March 2009 period (Crippa et al., 2014). Even though the AMS measures particles with a diameter $D < 1$ µm, the difference between the non-refractory PM_1 and total $PM_{2.5}$ mass is in general rather small as shown in Aksoyoglu et al. (2011), at least for situations without exceedingly high air pollution and situations when sea salt makes a large relative contribution to $PM_{2.5}$. The modelled average total non-refractory $PM_{2.5}$ (sum of nitrate, sulfate, ammonium and OA) concentrations match the measurements quite well with a few exceptions (Figure 4.3 and Table 4.3). The model is able to reproduce both high concentrations observed at the urban site Barcelona and low ones at remote sites like Hyytiälä, Finland. Concentrations of inorganic aerosols are over-predicted and OA are under-predicted at most of the stations (with similar behavior during the other investigated periods, Figure A.1 4 and Figure A.1 5). Very similar results were also presented by other recent studies (Knote et al., 2011). The effect of different schemes to treat OA is discussed in Sect. 4.3.3. At the Cabauw site nitrate was the most dominant species (Mensah et al., 2012). Especially at this site the model strongly over-predicts in particular the nitrate (NO_3^-) fraction (by a factor of 3). A sensitivity test with 50% reduction in ammonia emissions significantly improved the modelled NO3- concentrations at almost all sites (Table A.1 2) suggesting potential uncertainties in NH_3 emissions and their seasonal variability. Other potential reasons for the over-prediction of NO_3^- could be related to uncertainties in the removal process of HNO_3 as well as the dry deposition velocity of NH_3. Substantial over-predictions were found at the higher altitude site of Montseny and Puy de Dôme when compared with first model layer concentrations (~200 and 800 meters a.s.l. respectively at these sites). These sites located at about 720 and 1465 meters a.s.l., are sometimes not within the PBLH during winter periods. At the Montseny site, the relatively coarse resolution of the model could also influence model performance since the site is located in a complex area about 50 km north-east of Barcelona (Pandolfi et al., 2014). Sulfate concentrations (SO_4^{2-}) were over-predicted at almost all sites and especially at Mace Head suggesting that long-range transport of SO_4^{2-} might be positively biased.

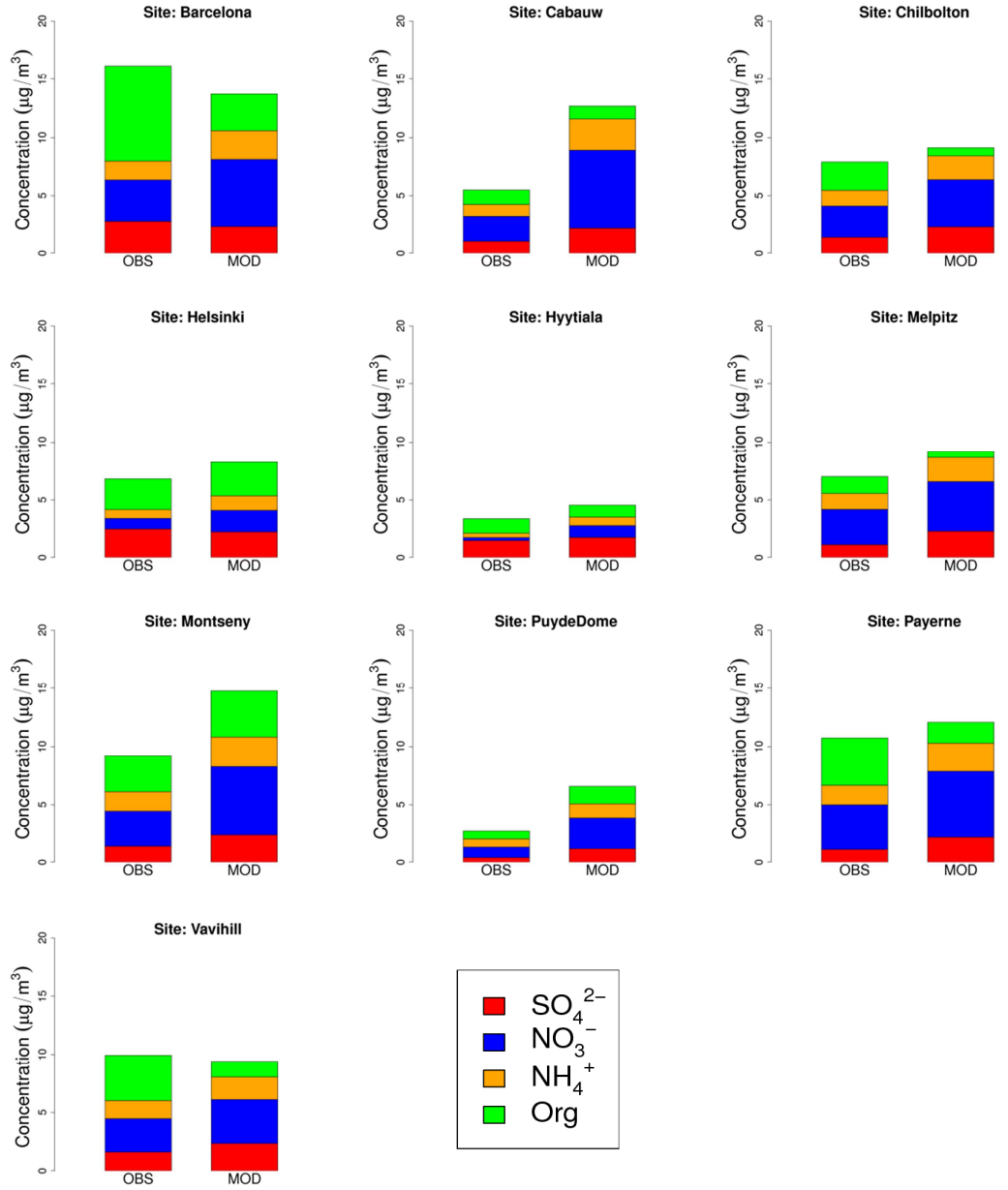

Figure 4.3 *Comparison of observed (OBS) non-refractory PM_1 and modelled (MOD) non-refractory $PM_{2.5}$ at 10 AMS sites in Europe during February-March 2009. Mace Head is reported only in Table 4.3 since the ammonium component is not available.*

Modelled and observed hourly concentrations of NO_3^-, SO_4^{2-}, ammonium (NH_4^+) and OA at Payerne are reported in Figure 4.4 for March 2009 together with meteorological parameters in Figure A.1 6. The model was able to reproduce the meteorological parameters very well for most of the time. The temperature was slightly under-predicted at both night and day-times (with a maximum of -2 °C) whereas both the monthly variation and the absolute values of wind speed and specific humidity were reproduced well with a few under-predictions of high wind-speed (6^{th} and 11^{th} of March and towards the end of the simulation). The model was able to

capture the three NO_3^- and NH_4^+ peaks observed around the 7th, 18th and 23rd of March with a general slight over-prediction throughout the whole period. Indeed, the under-prediction in temperature during day and night time could partially explain the over-prediction of the NO_3^- fraction with more NO_3^- partitioning to the aerosol phase which also apply to the other stations used in this study. An evaluation of modelled temperature at the European scale for the February-March 2009 period confirmed that the model systematically under-predicted the 2 meter surface temperature (Bessagnet et al., 2014).

Table 4.3 *Statistical analysis of nitrate, ammonium, sulfate and organic aerosol for the base case (VBS_BC) for February-March 2009 at different AMS sites.*

Site	Mean observed ($\mu g/m^3$)	Mean modelled ($\mu g/m^3$)	MB $\mu g\ m^{-3}$	ME $\mu g\ m^{-3}$	MFB [-]	MFE [-]
		NO_3^-				
Barcelona	3.6	5.8	2.2	4.0	0.35	0.98
Cabauw	2.2	6.7	4.5	4.6	0.85	1.01
Chilbolton	2.7	4.0	1.3	2.2	0.02	0.76
Helsinki	1.0	1.9	0.9	1.3	0.29	0.92
Hyytiälä	0.2	1.0	0.8	0.8	0.21	1.09
Mace Head	0.6	1.7	1.1	1.1	0.14	0.70
Melpitz	3.1	4.3	1.3	2.4	0.35	0.71
Montseny	3.1	5.9	2.8	4.3	0.38	1.00
Payerne	3.9	5.7	1.8	2.8	0.34	0.61
Puy de Dôme	0.9	2.7	1.8	2.2	1.13	1.30
Vavihill	2.8	3.7	0.9	2.2	0.14	0.78
		NH_4^+				
Barcelona	1.6	2.5	0.9	1.4	0.42	0.71
Cabauw	1.0	2.7	1.7	1.8	0.95	0.97
Chilbolton	1.3	2.0	0.7	1.0	0.39	0.61
Helsinki	0.8	1.3	0.5	0.6	0.51	0.60
Hyytiälä	0.4	0.8	0.4	0.5	0.55	0.70
Melpitz	1.4	2.1	0.7	1.1	0.45	0.69
Montseny	1.7	2.6	0.9	1.6	0.39	0.74
Payerne	1.7	2.5	0.8	1.2	0.36	0.56
Puy de Dôme	0.7	1.2	0.5	0.9	0.83	1.07
Vavihill	1.6	1.9	0.4	0.9	0.17	0.56
		SO_4^{2-}				
Barcelona	2.7	2.3	-0.4	1.3	-0.19	0.48

Cabauw	1.0	2.1	1.1	1.3	0.73	0.85
Chilbolton	1.3	2.2	0.9	1.3	0.45	0.70
Helsinki	2.4	2.2	-0.2	0.9	-0.04	0.43
Hyytiälä	1.4	1.7	0.3	0.7	0.09	0.58
Mace Head	0.4	1.2	0.8	0.9	1.04	1.12
Melpitz	1.1	2.2	1.2	1.4	0.54	0.76
Montseny	1.4	2.3	1.0	1.2	0.55	0.64
Payerne	1.1	2.1	1.1	1.2	0.62	0.70
Puy de Dôme	0.4	1.1	0.8	0.8	1.14	1.19
Vavihill	1.6	2.3	0.7	1.1	0.18	0.54
			OA			
Barcelona	8.2	3.1	-5.1	5.2	-0.80	0.82
Cabauw	1.2	1.1	-0.1	0.5	-0.13	0.50
Chilbolton	2.4	0.7	-1.7	1.7	-1.09	1.10
Helsinki	2.7	2.9	0.3	1.6	0.08	0.62
Hyytiälä	1.3	1.0	-0.3	0.5	-0.48	0.60
Mace Head	0.8	0.4	-0.4	0.4	-0.29	0.70
Melpitz	1.5	0.5	-1.0	1.0	-0.94	0.97
Montseny	3.1	3.9	0.9	1.9	0.31	0.57
Payerne	4.1	1.8	-2.3	2.4	-0.85	0.90
Puy de Dôme	0.6	1.4	0.8	1.0	0.68	0.91
Vavihill	3.9	1.4	-2.5	2.5	-1.04	1.04

All the inorganic components were over-predicted during the first four days of March 2009 with a peak around the 3rd of March, indicating that the PBLH was probably not correctly reproduced by the model during this period. Although the temporal variation was captured, concentrations of OA were under-predicted throughout all the simulation (4.1 μg m^{-3} and 1.8 μg m^{-3} observed and modelled average concentrations). Analysis of the OA fraction is discussed in the next section.

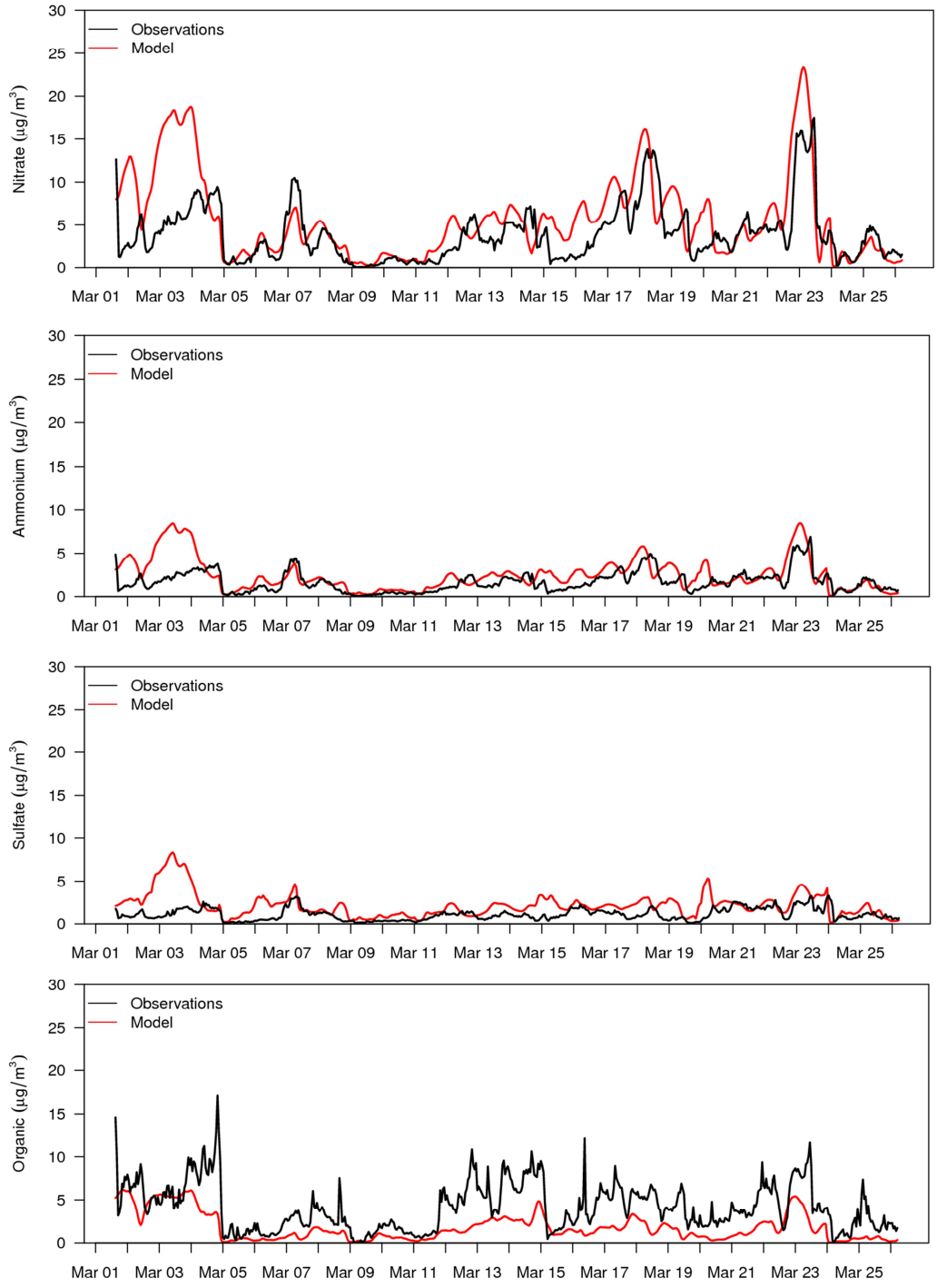

Figure 4.4 *Comparison of observed and modelled nitrate, ammonium, sulfate and organic aerosol at Payerne for March 2009.*

4.3.3 Organic aerosols

4.3.3.1 Sensitivity of OA to the VBS scheme

In this section, effects of different parameterizations of the organic aerosol module on the modelled OA concentrations are discussed. The scatter plots in Figure 4.5 show a comparison of daily average OA concentrations against the same AMS measurements as in Table 4.3 during February-March 2009. Statistics for each scenario are reported in Table 4.4.

Table 4.4 *Statistical analysis of OA for NOVBS, VBS_ROB and VBS_BC scenarios for the 11 AMS sites for February-March 2009.*

Scenario	Mean observed OA (μg m^{-3})	Mean modelled OA (μg m^{3})	MB (μg m^{-3})	ME (μg m^{-3})	MFB [-]	MFE [-]
NOVBS	3.0	1.2	-1.8	2.0	−0.66	0.88
VBS_ROB	3.0	0.7	-2.3	2.4	−1.08	1.19
VBS_BC (base case)	3.0	1.7	-1.2	1.8	−0.47	0.79

When the semi-volatile dynamics of primary organic aerosol is not taken into account (scenario NOVBS), the model under-predicts OA concentrations (MFB: -66%) with observed and modelled average concentrations of 3.0 μg m^{-3} and 1.2 μg m^{-3}, respectively. In the VBS_ROB scenario POA emissions are allowed to evaporate following the volatility distribution proposed by Robinson et al. (2007) and to undergo chemical oxidation. In this case modelled OA concentrations decrease by about 43% with respect to NOVBS, predicting an average OA concentration of 0.7 μg m^{-3}. On the other hand, the VBS_BC scenario improves the OA model performance increasing the OA concentrations by about 47% with respect to NOVBS. Predicted OA concentrations are found to be 1.7 μg m^{-3} on average (MFB: -47%). Similar behavior during winter periods was also shown in recent studies where the same VBS scheme was applied in the U.S. domain (Koo et al., 2014). Figure 4.6 shows the modelled total OA concentration over Europe using NOVBS, VBS_ROB and VBS_BC scenarios. The model predicts high OA values in the Eastern part of the domain as well as over Portugal, France and the Po Valley (VBS_BC). Some hot-spots around large urban areas are also visible, i.e., Paris and Moscow. Higher OA concentrations in the southern part of the domain are observed in the VBS_BC case, likely because of higher temperature and more OH radicals available in that part of the domain leading to an increase in the total organic mass upon reaction with organic vapours. This is in line with the results of Fountoukis et al. (2014) for the February-March 2009

period even though their study predicts lower concentrations over the Po valley. Even though model input data and parameterizations are not the same, the VBS_BC case in particularly, uses a very similar volatility distribution as in Fountoukis et al. (2014).

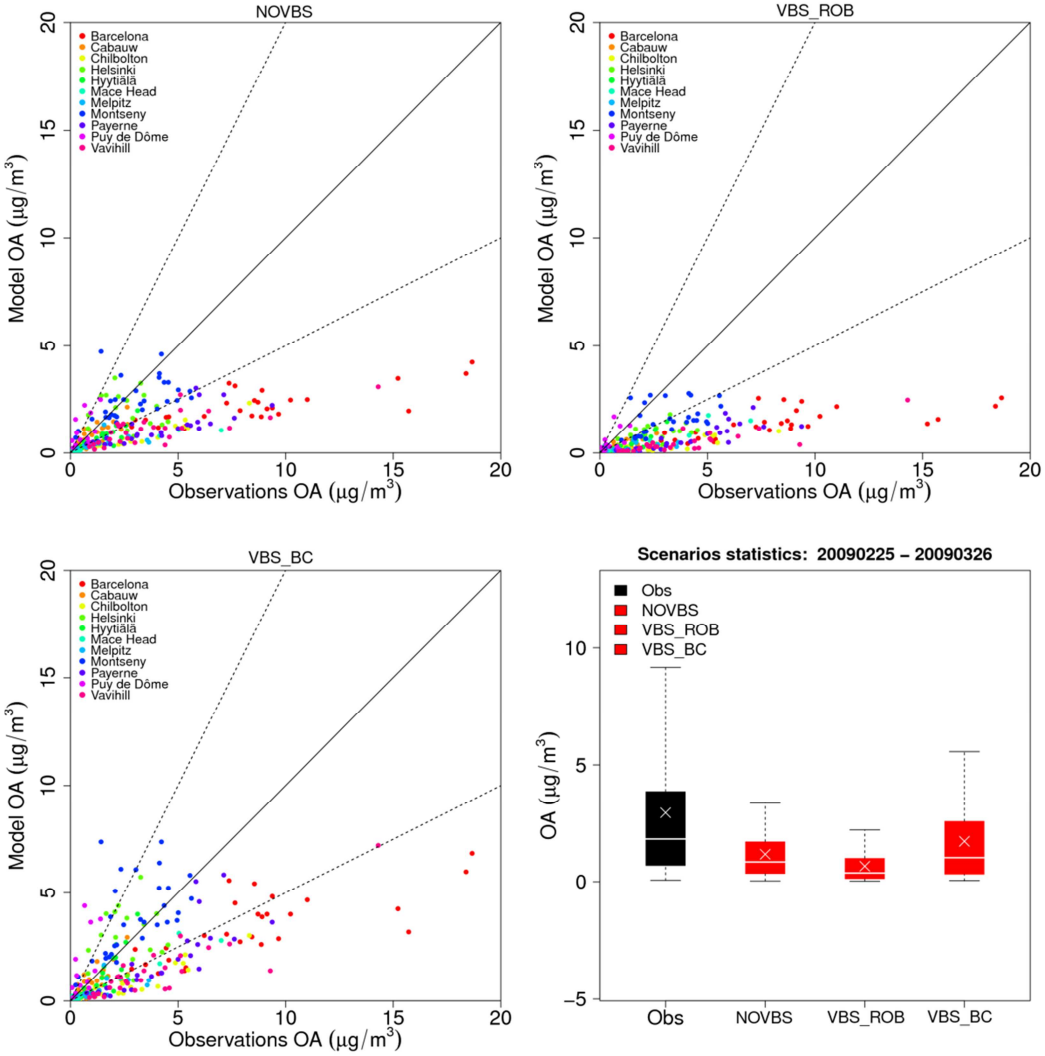

Figure 4.5 *OA daily average scatter plots for NOVBS, VBS_ROB and VBS_BC scenarios for February-March 2009 for stations in Table 3. Solid lines indicate the 1:1 line. Dotted lines are the 1:2 and 2:1 lines. Boxplots indicate medians, 5th, 25th, 75th and 95th quantiles for observations (black) and sensitivity tests (red). The crosses represent the arithmetic means. R^2 is 0.55 for NOVBS, 0.64 for VBS_ROB and 0.59 for VBS_BC (excluding the elevated sited of Puy de Dôme and Montseny).*

Our study predicts relatively lower OA concentrations (MFB: -0.47, MFE: 0.79) compared to those reported by Fountoukis et al. (2014) (MFB: 0.02, MFE: 0.68) for February-March 2009. Unlike Fountoukis et al. (2014) our study does not include fire emissions and marine organic aerosol which may partially explain the differences. Figure 4.7 shows hourly modelled and observed OA concentration at Payerne for March 2009 and June 2006. In March 2009 VBS_ROB results are lower than those in NOVBS whereas OA concentrations in VBS_BC case are higher (see Supplementary Figure A.1 8 and Table A.1 3 for average concentrations

and statistics). In June 2006, the OA mass in VBS_ROB is lower than those in NOVBS while VBS_BC predicts similar concentrations as the NOVBS scenario (2.4 μg m^{-3} and 2.6 μg m^{-3}, respectively, Figure A.1 9 and Table A.1 4). It has to be noted that the NOVBS scenario predicts slightly lower OA concentration for June 2006 in Payerne with respect to our previous application (Aksoyoglu et al., 2011), mainly because of a different biogenic model being used which yields lower monoterpene and sesquiterpene emissions.

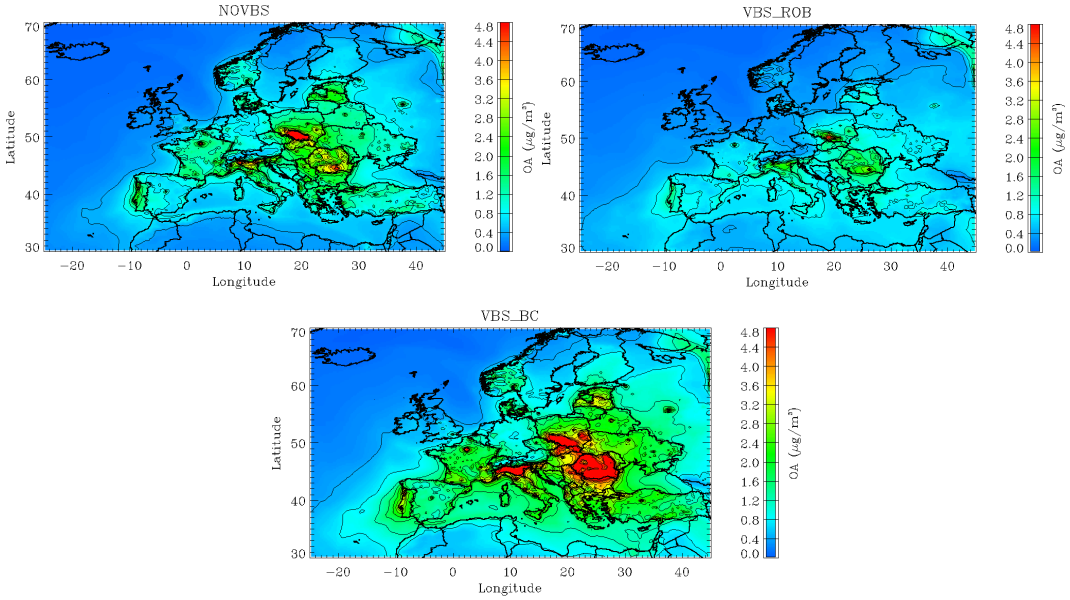

Figure 4.6 *Predicted OA concentrations over Europe for the NOVBS, VBS_ROB and VBS_BC scenario in February-March 2009. Note that the color scale was limited to a maximum of 4.8 μg/m3 to facilitate comparison of the panels.*

Since both BVOCs and BBOA-like emissions are highly uncertain, sensitivity tests with increased biogenic and anthropogenic emissions were performed and results discussed in the next section (4.3.3.2).

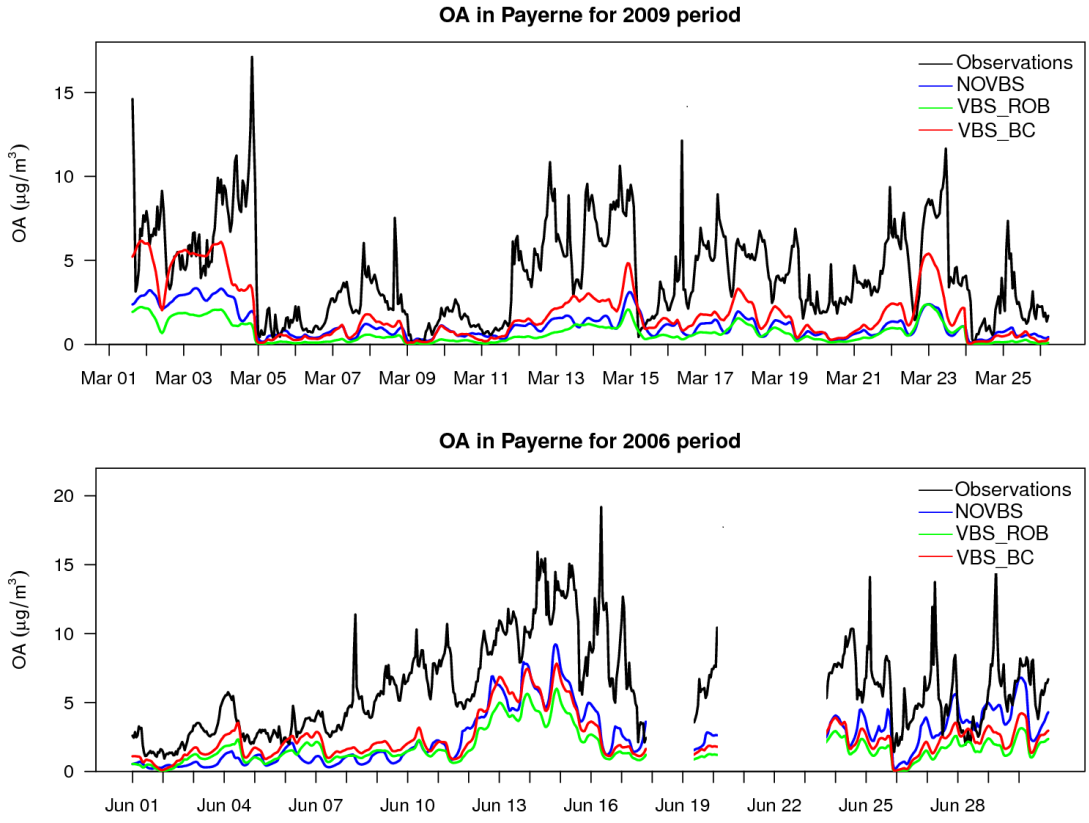

Figure 4.7 *Predicted and observed total OA for scenarios NOVBS, VBS_ROB and VBS_BC in March 2009 (upper panel) and June 2006 (lower panel) at Payerne.*

4.3.3.2 Sensitivity of OA to BBOA-like and BVOC emissions

Emissions of BVOCs compounds (i.e. monoterpenes, isoprene and sesquiterpenes) were doubled in scenario VBS_BC_2xBVOC, whilst primary organic aerosol emissions from SNAP2 and SNAP10 (BBOA-like) were doubled in scenario VBS_BC_2xBBOA, with other emissions and processes represented as in VBS_BC. Figure 4.8 shows modelled and observed OA daily average concentrations for the VBS_BC, VBS_BC_2xBVOC and VBS_BC_2xBBOA scenarios across the sites. Statistics for each scenario are reported in Table 5.

Table 4.5 *Statistical analysis of OA for VBS_BC, VBS_BC_2xBVOC and VBS_BC_2xBBOA scenarios for the 11 AMS sites for February-March 2009.*

Scenario	Mean observed OA (µg m $^{-3}$)	Mean modelled OA (µg m^{3})	MB (µg m^{-3})	ME (µg m^{-3})	MFB [-]	MFE [-]
VBS_BC (base case)	3.0	1.7	-1.2	1.8	−0.47	0.79
VBS_BC_2xBVOC	3.0	1.8	-1.2	1.8	−0.46	0.78
VBS_BC_2xBBOA	3.0	2.8	-0.1	1.9	−0.12	0.69

Increasing biogenic emissions by a factor of two during February-March 2009 resulted in almost no change in the predicted total OA (1.7 μg m^{-3} and 1.8 μg m^{-3} for the VBS_BC and VBS_BC_2xBVOC scenarios, respectively). On the other hand, doubling the BBOA-like emissions (VBS_BC_2xBBOA) during the same period strongly increased the predicted OA mass (up to 2.8 μg m^{-3} on average). As a result the mean fractional bias decreased further, from -47% to -12% averaged across the sites. This could eventually confirm other studies where substantial under-predictions in residential wood burning emissions were underlined (e.g., Bergström et al., 2012). A few points above the 2:1 lines in VBS_BC_2xBBOA mainly belong to the sites of Montseny, Puy de Dôme and Helsinki.

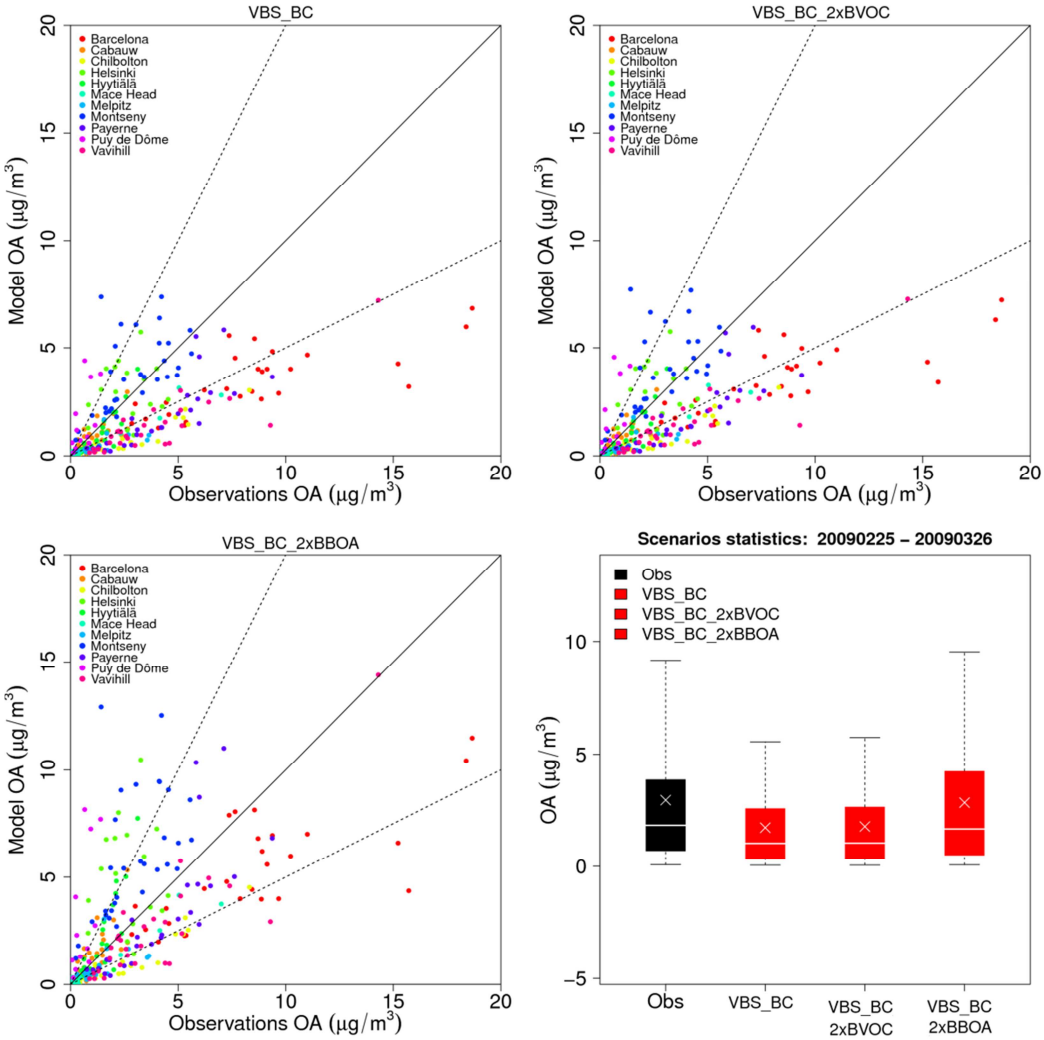

Figure 4.8 *OA daily average scatter plots for VBS_BC, VBS_BC_2xBVOC and VBS_BC_2xBBOA scenarios for February-March 2009 for stations in Table 3. Solid lines indicate the 1:1 line. Dotted lines are the 1:2 and 2:1 lines. Boxplots indicate medians, 5th, 25th, 75th and 95th quantiles for observations (black) and sensitivity tests (red). The crosses represent the arithmetic means.*

During winter periods, it is likely that elevated stations such Montseny and Puy de Dôme are most of the time above the PBLH, as suggested by previous studies for Puy de Dôme (Freney et

al., 2011), whereas model concentrations are extracted from the first layer of the model. In Helsinki, BBOA emissions seem to be overestimated or the dispersion underestimated in the model.

Comparison with a warmer period in June 2006 is reported as well for Payerne where AMS measurements were also available (Figure 4.9). In February-March 2009 increasing BBOA-like emissions (VBS_BC_2xBBOA) reduced the fractional bias from -85% in VBS_BC to -37% (Table A.1 3) with an over-prediction occurring during 1-5 of March (Figure 4.9, upper panel). As already discussed in Section 4.3.2, it is likely that the vertical mixing processes were not correctly represented by the model since also the inorganic components were over-predicted for the same period. Almost no change in the predicted OA mass was found when biogenic emissions were doubled (scenario VBS_BC_2xBVOC) (Figure 4.9, upper panel) due to lower BVOCs emission during winter periods. Increasing BVOCs emissions in June 2006 increased the predicted OA mass at Payerne site especially during the 12-16 June and towards the end of the simulation period, where higher concentrations and temperature (Figure A.1 7) were also observed (Figure 4.9, lower panel).

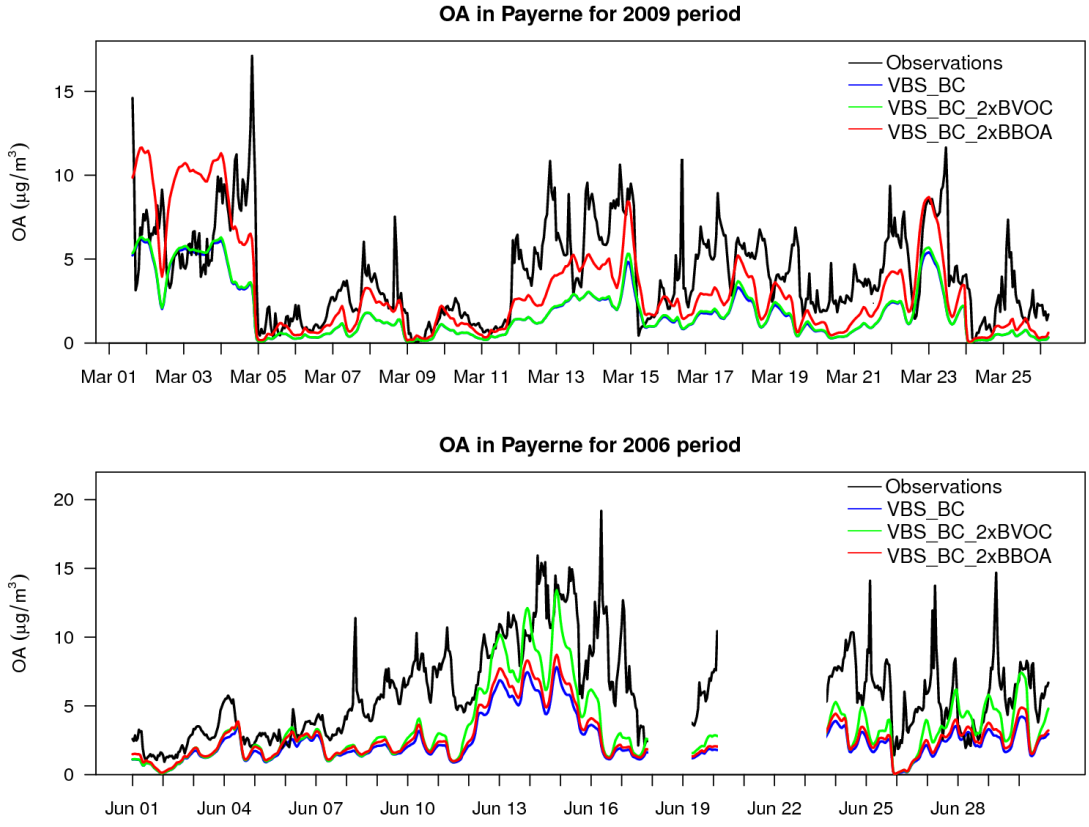

Figure 4.9 *Predicted and observed total OA for scenarios VBS_BC, VBS_BC_2xBVOC and VBS_BC_2xBBOA in March 2009 (upper panel) and June 2006 (lower panel) at Payerne.*

In contrast, similar OA concentrations were predicted in Payerne for VBS_BC and VBS_BC_2xBBOA during June 2006 (with averages of 2.4 μg m^{-3} and 2.8 μg m^{-3}, respectively). This is in line with a recent source apportionment study based on ACSM (aerosol chemical speciation monitor) measurements performed in Zürich for 13 months (February 2011 - February 2012) which revealed substantial differences between the winter (February-March) and summer (June-August) f_{44} / f_{43} space (organic mass fraction measured at mass to charge ratio 44 and 43) indicating that summer OOA (oxygenated organic aerosol) is strongly influenced by biogenic emission and winter OOA by biomass burning emission (Canonaco et al., 2015).

Increased OA concentrations at Payerne in June 2006 with increased biogenic emissions were also found in other modelling studies. Bergström et al. (2012) used the VBS framework with different assumptions regarding aging processes and compared the model results for June 2006 with the AMS results at Payerne. In their study the total OA was found to be under-predicted with lower bias observed when aging processes were taken into account and biogenic emissions were increased by a factor of 3. Even though their model differs from ours in various aspects (number of volatility bins, aging processes parameterization and input data) in two of their scenarios without aging of biogenic SOA, Bergström et al. (2012) predicted an average OA concentration ranging from 2.6 μg m^{-3} to 3.4 μg m^{-3} which is similar to our base case VBS_BC and VBS_BC_2xBVOC scenario (2.4 μg m^{-3} and 3.4 μg m^{-3}, respectively, Table A.1 4).

4.3.3.3 OA components in summer and winter

Comparisons of the primary and secondary organic fraction at the rural site of Payerne during summer (June 2006) and winter (February-March 2009) periods are reported in Figure 4.10. During the winter period the VBS scheme better reproduced the primary and secondary organic aerosol components compared to the NOVBS case. In particular, For the VBS_ROB base case, total OA concentrations were lower compared to the NOVBS case, consistent with the study of Woody et al., (2016) where the same VBS scheme was applied to the US domain. The total OA concentrations in the base case (VBS_BC) and in the scenario with increased biomass burning emissions (VBS_BC_2xBBOA) were higher compared to NOVBS case, even though SOA and POA fractions were not correctly reproduced. Higher contribution from the primary fraction during winter periods was also predicted by the study of Koo et al., (2014) which deployed the same VBS scheme.

Eventually, this might indicate that biomass burning precursors might be missing in this study, or that the oxidation pathways of primary organic material need to be improved in the

model (up to 86% of the reacted primary organic material is still allocated in the primary set as oxidation proceeds, directly increasing the POA fraction).

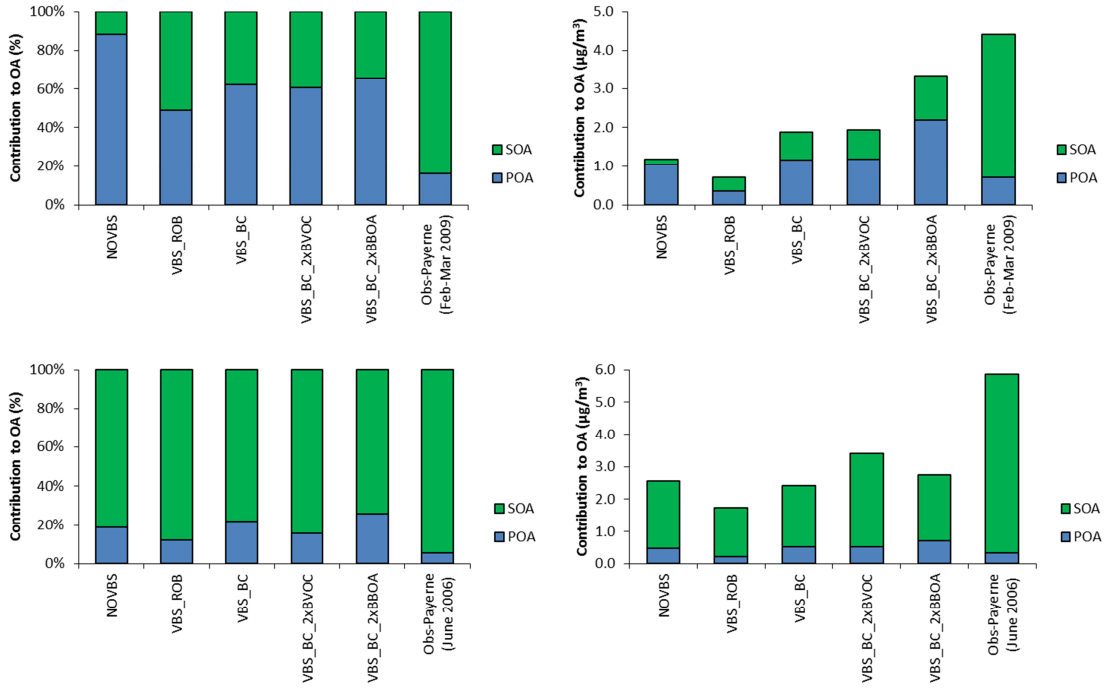

Figure 4.10 *Relative (left) and absolute (right) contributions of predicted and measured POA and SOA fractions to the total OA mass at Payerne for February-March 2009 winter period (upper-panel) and June 2006 (lower-panel) and different model scenarios. NOVBS: (traditional non-volatile POA), VBS_ROB (Robinson et al., 2007), VBS_BC (Tsimpidi et al., 2010, Shrivastava et al., 2011), VBS_BC_2xBVOC (increased biogenic emissions relative to VBS_BC), VBS_BC_2xBBOA (increased biomass burning emissions relative to VBS_BC), Obs-Payerne: AMS-PMF.*

Different behavior was observed for the summer period where the larger contribution of SOA to the total OA retrieved from measurements was also reproduced by the model, even though the total OA concentration was still underestimated. These results for summer are also in line with the study of Koo et al. (2014) for summer periods in the US domain using the same VBS scheme.

4.4 Conclusions

A modelling study using the regional air quality model CAMx with VBS (Volatility Basis Set) scheme was performed for the first time in Europe within the EURODELTA-III model intercomparison exercise. An evaluation for the main gas phase species and $PM_{2.5}$ for four different periods was performed using the European air quality database Airbase as well as

AMS (Aerosol Mass Spectrometer) measurements. The period in February-March 2009 was further analyzed in more detail using different assumptions regarding the volatility of emitted organic aerosol and emissions of precursor. The main findings of this study are summarized below:

- Although total $PM_{2.5}$ mass concentrations and its variations were well reproduced by the model in all four periods, comparisons with AMS measurements for the February–March 2009 period revealed that the good agreement between model and measurements was most of the time due to overestimation of the inorganic fraction, especially NO_3^-, and underestimation of OA. Sensitivity tests with reduced NH_3 emissions generally reduced the positive bias in NO_3^- suggesting potential uncertainties in NH_3 emissions and their seasonal variability.
- In general, for all the four periods, the model under-predicted NO_2 and CO concentrations. On the other hand, O_3 was found to be over-predicted likely because of insufficient NO_x to undergo titration during night-time chemistry or not well captured vertical mixing processes and concentrations at the boundaries. SO_2 was over-predicted presumably mainly because of uncertainties in high stack point sources representation in the model or too low deposition processes.
- Including evaporation and oxidation processes of primary organic particles with the volatility distribution proposed by Robinson et al. (2007) lowered the modelled OA mass both in winter and summer periods. On the other hand, the adjustment of the scheme by Robinson et al. (2007) suggested by Shrivastava et al. (2011) and Tsimpidi et al. (2010) brings model and observations into better agreement by reducing the negative bias for OA by about 29% (MFB) in winter.
- Sensitivity tests with increased BVOCs and BBOA-like emissions suggested that emissions from residential heating represent an important contributor to total OA during winter periods (February-March 2009). The model under-predicted the winter OA concentrations (MFB -47% for base case VBS_BC) more than gas phase pollutants e.g. NO_2 (Table 2). Eventually, increasing BBOA-like emissions by a factor of 2 brought model and observation to a reasonably good agreement even though the model still under-predicts the OA fraction (-12% MFB). This underlines the necessity to better constrain emission inventories with a focus on residential heating. Also the implementation of the VBS scheme for domestic wood burning, which substantially influences both the primary and secondary organic aerosol, should be evaluated.

- A summer period was simulated as well and results were compared at Payerne. In June 2006, the current VBS implementation could not explain the discrepancy between modelled and observed OA. During this period the difference between the model and measurements is likely to be related to BVOCs emissions which are uncertain and difficult to constrain with measurements. In this case the model was sensitive to an increase in biogenic emissions especially during periods with higher temperature and OA concentrations. The latter could confirm the importance of BVOC precursors in summer in Payerne and the way to correctly represent their evolution in the atmosphere.

Acknowledgements

We thank the EURODELTA-III modelling community, especially INERIS for providing various model input data. We are grateful to ENVIRON for providing the CAMx-VBS code before its public release. Calculations of land use data were performed with the Swiss National Supercomputing Centre (CSCS). Ammonia measurements were provided kindly by FUB. We thank D. Oderbolz for developing the CAMxRunner framework to ensure reproducibility and data quality among the simulations and sensitivity tests. We thank M. Tinguely for the visualization software. We also thank G. Pirovano for helping with the pre-processing of Airbase data. This study was financially supported by the Swiss Federal Office of Environment (FOEN). JLJ was supported by NSF AGS-1360834 and EPA STAR 83587701-0. We thank D.A. Day for analysis on the DAURE dataset. Erik Swietlicki for the Vavihill dataset, A. Kiendler-Scharr for Cabauw AMS data, Evelyn Freney for the Puy de Dôme dataset.

5

Constraining a hybrid volatility basis set model for aging of wood burning emissions using smog chamber experiments

Giancarlo Ciarelli[1], Imad El Haddad[1], Emily Bruns[1], Sebnem Aksoyoglu[1], Ottmar Möhler[2], Urs Baltensperger[1] and André S.H. Prévôt[1]

[1]Paul Scherrer Institute, Laboratory of Atmospheric Chemistry, 5232 Villigen PSI, Switzerland
[2]Karlsruhe Institute of Technology, Institute of Meteorology and Climate Research, Germany

Published in Geoscientific Model Development Discussions (GMDD)

doi:10.5194/gmd-2016-163

Abstract

Semi-volatile and intermediate volatility organic compounds (SVOCs, IVOCs) are not included in the current non-methane volatile organic compounds (NMVOCs) emission inventories but may be important for the formation of secondary organic aerosol (SOA). In this study, novel wood combustion aging experiments performed at different temperatures (263 K and 288 K) in a ~7 m^3 smog chamber were modelled using a hybrid volatility basis set (VBS) box model, representing the emission partitioning and their oxidation against OH. We combine aerosol-chemistry box model simulations with unprecedented measurements of non-traditional volatile organic compounds (NTVOCs) from a high-resolution proton transfer reaction mass spectrometer (PTR-MS) and with organic aerosol measurements from an aerosol mass spectrometer (AMS). In so-doing, we are able to observationally-constrain the amounts of different NTVOCs aerosol precursors (in the model) relative to low-volatility and semi-volatile primary organic material (OM_{sv}) which is partitioned based on current published volatility distribution data. By comparing the NTVOCs/OM_{sv} ratios at different temperatures, we determine the enthalpies of vaporization of primary biomass burning organic aerosols. Further, the developed model allows for evaluating the evolution of oxidation products of the semi-volatile and volatile precursors with aging. More than 30,000 box model simulations were performed to retrieve the combination of parameters that fit best the observed organic aerosol mass and O:C ratios. The parameters investigated include the NTVOC reaction rates and yields as well as enthalpies of vaporization and the O:C of secondary organic aerosol surrogates. Our results suggest an average ratio of NTVOCs to the sum of non-volatile and semi-volatile organic compounds of ~4.75. The mass yields of these compounds determined for a wide range of atmospherically relevant temperatures and organic aerosol (OA) concentrations were predicted to vary between 8 and 30 % after 5 hours of continuous aging. Based on the reaction scheme used, reaction rates of the NTVOC mixture range from 3.0×10^{-11} cm^3 $molec^{-1}$ s^{-1} to 4.0×10^{-11} cm^3 $molec^{-1}$ s^{-1}. The average enthalpy of vaporization of SOA surrogates was determined to be between 55,000 J mol^{-1} and 35,000 J mol^{-1} which implies a yield increase of 0.03 - 0.06 % K^{-1} with decreasing temperature. The improved VBS scheme is suitable for implementation into chemical transport models to predict the burden and oxidation state of primary and secondary biomass burning aerosols.

5.1 Introduction

The fact that some semi-volatile compounds can exist in either gaseous or particulate form results in considerable uncertainties in the emission inventories for fine particulate matter ($PM_{2.5}$) and non-methane volatile organic compounds (NMVOCs). Emissions of $PM_{2.5}$ are generally based on emission factors (EF) of primary organic aerosol (POA) which may be over- or under-predicted depending on the measurement method used (Lipsky and Robinson, 2006; Nussbaumer et al., 2008a, 2008b.).

In Europe, residential wood-burning emissions constitute one of the main anthropogenic sources of POA and potentially secondary organic aerosol (SOA), especially during winter periods with contribution from 15% to 50% of the total organic mass (Crippa et al., 2013; Waked et al., 2014). Thus, great effort was devoted in the past to better constrain the uncertainties related to wood burning emissions and their evolution in the atmosphere (Denier van der Gon et al., 2015; May et al., 2013). Recent year-long source apportionment studies based on ACSM (aerosol chemical speciation monitor) measurements in central Europe suggest that winter secondary organic aerosol fingerprints resembles those measured during chamber studies of biomass burning emission aging (Canonaco et al., 2015).

One of the main complications when dealing with organic aerosol (OA) is imposed by the semi-volatile and highly reactive nature of organic material (Robinson et al., 2007). Depending on ambient conditions freshly emitted primary organic particles can undergo evaporation. The fraction of an organic compound *i* in the condensed phase can be inferred based on the absorptive partitioning theory of Pankow (1994) (Eq. 5.1). The critical parameters driving the gas-particle partitioning of this compound are its effective saturation concentration, C_i^*, and the total concentration of organic aerosol, C_{OA}:

$$\xi_i = \left(1 + \frac{C_i^*}{C_{OA}}\right)^{-1}; C_{OA} = \sum_i \xi_i C_i \qquad (5.1)$$

Here, ξ_i is the partitioning coefficient of *i* (condensed-phase mass fraction). C_i^* is a semi-empirical property (inverse of the Pankow-type partitioning coefficient, K_P), reflecting not only the saturation vapor pressure of the pure constituents $\left(p_{L,i}^o\right)$ but also the way they interact with the organic mixture (effectively including liquid phase activities). This formulation essentially determines that at high C_{OA} almost all semi-volatile organic aerosols are in the condensed phase with only species with the highest vapour pressures remaining in the gas phase.

The volatility basis set approach (VBS) was proposed by Donahue et al., (2006) to provide a framework to enable models to represent both the chemical ageing and the associated evolving volatility of particulate organic matter in the atmosphere. The approach is to separate organics

into logarithmically spaced bins of effective saturation concentrations C_i^*, at 298 K and it was later extended (Donahue et al., 2011, 2012a,b) by introducing surrogate compounds with different carbon and oxygen numbers following the group contribution approach based on the SIMPOL method (Pankow and Asher, 2008) (Equation 5.2). The model becomes 2-dimensional, capable of tracking compound volatility and oxidation state (O:C ratios) (Donahue et al., 2012b, 2011):

$$\log_{10} C_i^0 = \left(n_C^0 - n_C^i\right) b_C - n_O^i b_O - 2\frac{n_C^i n_O^i}{n_C^i + n_O^i} b_{CO} \qquad (5.2)$$

where b_c and b_O represent the carbon-carbon and oxygen-oxygen interactions, respectively, b_{CO} describes the non-ideal solution behaviour and n_C^0, equal to 25, represents the reference point for pure hydrocarbons (1 μg m^{-3} of alkene). n_C^i and n_O^i are the carbon and oxygen numbers, respectively, for the ith saturation concentration (C_i^0). For biomass burning in particular, May et al. (2013) revealed that the majority of the emitted primary OA mass is semi-volatile, with 50 to 80 % of the POA mass evaporating when diluted from plume to ambient concentrations or when heated up to 100°C in a thermodenuder. Based on their results, they proposed a volatility distribution function and enthalpies of vaporization for wood burning smoke (May et al., 2013).

Once emitted in the atmosphere, organic compounds are highly reactive towards various oxidants such as the hydroxyl radical (OH), ozone (O_3) and the nitrate radical (NO_3). These oxidants can strongly alter the chemical structure of the reacted precursors by generating secondary products with lower or higher volatilities. Linking partitioning and oxidation processes of thousands of emitted organic compounds is one of the main challenges in atmospheric chemistry. The VBS scheme can delineate the transformation of the surrogates upon their functionalization or fragmentation, by changing the compounds' volatility and O:C ratios, consistently with the dominant representative species in that part of the parameter space. Chemical transport models (CTMs) have been increasingly updated with a VBS scheme with varying complexities (Bergström et al., 2012; Ciarelli et al., 2016a; Murphy et al., 2011; Zhang et al., 2013). A recent landmark paper within the international AeroCom initiative (Tsigaridis et al., 2014), gave a comprehensive audit of the status of organic aerosol schemes in global models, brought together several benchmark observational datasets and intercompared and evaluated the OA simulated by a large number of global aerosol models against them. Results indicate that simulated OA greatly varies between models in terms of POA emissions, SOA formation and complexity of OA parameterizations and the amount of OA remains under-predicted. In the latest EURODELTA-III (EDIII) European model intercomparison, seven different regional models were applied in the European domain during different periods with a

focus on the February-March 2009 EUCAARI winter episode (Bessagnet et al., 2014). All models under-predicted the total measured organic fraction mainly due the uncertainties in SOA representation (Bessagnet et al., 2014). Knote et al. (2011) used the COSMO-ART model to investigate its performance as online-coupled chemistry-climate model. In their study domestic wood burning emissions were not included and POA was assumed to be non-volatile, which resulted in a severe under-prediction of OA over the studied domain (Knote et al., 2011). Bergström et al. (2012) used the EMEP model for the period of 2002-2007 comparing different partitioning and aging schemes, and their results indicate a potential underestimation of wood-burning emissions in Europe. Fountoukis et al. (2014) were among the first to implement the VBS approach into a large-scale aerosol model, following the multiple distribution framework approach proposed by Tsimpidi et al. (2010). They found the approach improved considerably the OA simulated in the model across Europe comparing to a range of observations made during the EUCAARI field campaign (Kulmala et al., 2009, 2011) and from EMEP monitoring network (Tørseth et al., 2012). Recently, an important new initiative to provide improved information on residential wood combustion (RWC) emission inventory for Europe was carried out by Denier van der Gon et al. (2015) and used as an input in two CTMs (PMCAMx and EMEP MSC-W) for the EUCAARI winter periods (February-March 2009). The new RWC emissions, which are higher by a factor of 2-3 compared to previous emission inventories, improved the model performance for total OA (Denier van der Gon et al., 2015). Jo et al. (2013) deployed the GEOS-Chem global model to investigate the effect of using different aging constants on modelled SOA. They concluded that model simulations are improved when chemical aging is taken into account, especially for rural regions (Jo et al., 2013). These novel investigations highlight the critical need for a representation of semi-volatile organic species and their evolution in chemical transport models.

In this study we perform extensive box-model simulations of wood burning combustion aging experiments performed in a ~7 m^3 smog chamber at different temperatures. Most uncertain parameters namely enthalpies of vaporization of SOA, NTVOCs reaction rates and their yields were investigated by means of brute force simulations, and a best fitting solution, within acceptable physical and errors ranges, was retrieved.

5.2 Experimental Method

Beech (*Fagus sylvatica*) logs were combusted in a residential wood burner (model type: Avant, Attika from 2009), following the procedure described in (Heringa et al., 2012) and (Bruns et al., 2015). The resulting emissions were sampled from the chimney through a heated line (473 K), diluted by a factor of ~8-10 using an ejector diluter (473 K, DI-1000, Dekati Ltd.)

and injected into the smog chamber (~7 m^3) through a heated line (423 K). Emissions were only sampled during the stable flaming phase of the burn, for 11-21 min and total dilution factors ranged from ~100 to 200. Four replicate experiments were conducted at 288 K and another four experiments at 263 K. The smog chamber had an average relative humidity of 50% over all eight experiments. Another three experiments were conducted at 90% relative humidity and 263 K. After the characterization of the primary emissions, a single dose of d9-butanol (butanol-D9, 98%, Cambridge Isotope Laboratories) was injected into the chamber, to trace the OH concentration (Barmet et al., 2012). A continuous flow of nitrous acid (2.3-2.6 l min^{-1}, ≥99.999%, Air Liquide) into the chamber served as an OH precursor. The chamber was then irradiated with UV light (40 lights, 90-100 W, Cleo Performance, Philips) for 4.5-6 h (Platt et al., 2013). The evolution of the gas-phase and particulate phase composition and concentration were monitored in real-time throughout aging. Non-refractory primary and secondary particulate emissions were characterized using a high resolution time-of-flight aerosol mass spectrometer (AMS). Equivalent black carbon (eBC) was quantified using a 7-wavelength aethalometer (AE33 Magee Scientific Company, flow rate 2 l min^{-1}) (Drinovec et al., 2015). Particle wall loss rates in the chamber were determined using the decay of eBC assuming all particles were lost equally to the walls and that condensable material partitions only to suspended particles. The average particle half-life in the chamber was 3.4±0.7 h. Non-methane organic gases with a proton affinity greater than that of water were measured using a a high-resolution proton transfer reaction mass spectrometer (PTR-ToF-MS 8000, Ionicon Analytik G.m.b.H.). The PTR-ToF-MS was operated with hydronium ($[H_2O+H]^+$) as reagent, a drift tube pressure of 2.2 mbar, a drift tube voltage of 543 V and a drift tube temperature of 90°C leading to a ratio of the electric field (*E*) and the density of the buffer gas (*N*) in the drift tube (*E*/*N*) of 137 Townsend (Td). The analysis of data PTR-ToF-MS data and the identification of the precursors' chemical nature are described in Bruns et al. (2016). The elemental composition of the detected gases was analyzed using the Tofware post-processing software (version 2.4.5), running in the Igor Pro 6.3 environment (version 6.3, Wavemetrics Inc.). More than 95% of the detected peaks could be assigned to a molecular formula. Approximately 70% of the compounds' chemical structures could be assigned to the observed ions guided by previously reported compounds emitted during residential wood combustion. Here, the lumped sum of the precursors' molar concentrations will be used to constrain the total amount of NTVOCs (Table A.2 1) in the model. Their weighted average O:C ratio, volatility, reaction rate and carbon number will also be presented.

5.3 Box model

The modelling approach involves two steps.

- We first modelled the partitioning of POA for the 11 smog chamber experiments (8 experiments at RH=50% and 3 experiments at RH=90%) before the start of the aging. This step enables constraining the amounts of material in the different volatility bins and the enthalpy of vaporization of the different surrogates used. The simulations proceeded as follows. Using already available volatility distribution data for primary wood burning emissions (Figure 5.1) we inferred the total amount of organic material (gas and particle phase) in the low-volatility and semi-volatile ranges (OM_{sv}), ($0.1 < C_i^* < 1000$ μg m^{-3}), which matched the measured OA concentrations at the beginning of the experiments ($OA_{t=0}$). The amount of OM_{sv} was then compared to the measured NTVOCs, at high and low temperatures and the enthalpies of vaporization of primary compounds were adjusted such that a comparable NTVOCs/OM_{sv} ratio was obtained at both temperatures within our experimental variability. We tested several sets of enthalpies of vaporization characteristic of biomass burning OA derived from May et al. (2013); the different sets were all physically possible and were determined from thermodesorber data by assuming different accommodation coefficients.

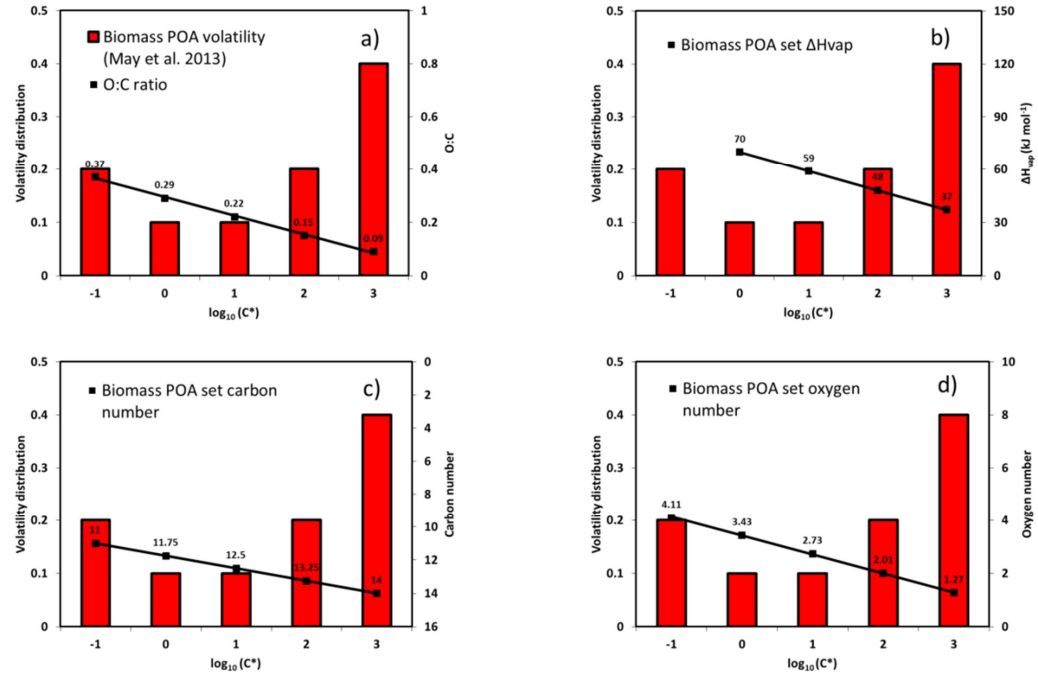

Figure 5.1 *Properties of the wood burning POA set. a) O:C ratio, b) ΔH_{vap} c) C number d) O number. Volatility distribution and enthalpies of vaporization were taken from May et al. (2013). Carbon and oxygen numbers were calculated using the group contribution approach of Donahue et al. (2011). Wood burning POA carbon numbers were placed from 14 to 11 and linearly interpolated between the volatility bins.*

- In step 2, the obtained volatility distributions were used to model the aging of the emissions and SOA formation within a hybrid VBS framework. This framework is adapted from Koo et al. (2014); it describes the formation and further evolution of SOA species from different families of precursors. Unlike previous 2D-VBS schemes, the molecular space was not discretised according to the species saturation concentration and oxidation state (e.g. O:C ratios), but rather every SOA surrogate was given an average molecular composition – $C_xH_yO_z$) – as a function of its volatility and the precursor it derived from. This approach significantly decreases the degree of freedom of the model, while still providing a means to evaluate the bulk aerosol oxidation state based on the knowledge of the surrogate molecular composition. The time-dependent OA mass and O:C ratios were used as model constraints. For step 2, only experiments performed at RH=50% were used, as high RH might favour further uptake of secondary organic material into the bulk phase, effectively increasing aerosol yields (Zuend and Seinfeld, 2012). Such effects are beyond the scope of this study.

In the present study, the bulk micro-physical properties of the condensed phased were not measured. Therefore, for all calculations, we assumed instantaneous reversible absorptive equilibrium of semi-volatile organic species into a well-mixed liquid phase. I.e. the model does invoke diffusion limitations within the condensed phase. These assumptions may influence our results, especially at lower temperatures (e.g. if diffusion limitations were to be considered, higher reaction rates would be required to explain the observations). However, the same assumptions are considered in CTMs and therefore we expect that resulting biases will partially cancel out, providing that the bulk phase properties of chamber and ambient aerosols are not significantly different.

Five volatility bins ranging from 0.1 to 1000 μg m^{-3} in saturation concentration were used to model the partitioning of the POA and SOA fractions. The weighted average carbon and oxygen numbers of the NTVOCs mixture retrieved from PTR-MS measurements were used in combination with the group contribution approach (Eq. 5.2) to estimate the average saturation concentration for SOA precursors yielding about $\sim 10^6$ μg m^{-3}, which falls within the IVOC saturation concentration range limit (Donahue et al., 2012b; Koo et al., 2014; Murphy and Pandis, 2009) (Figure 5.2).

A total number of 3 sets were chosen to describe the evolution of organic material. The first set was used to distribute the primary emissions (set1). Two other sets were used to model the formation and evolution of SOA. Oxidation products of SVOC material arising from primary emissions were allocated to set2, whereas oxidation products from NTVOCs were allocated to set3 (Figure 5.3).

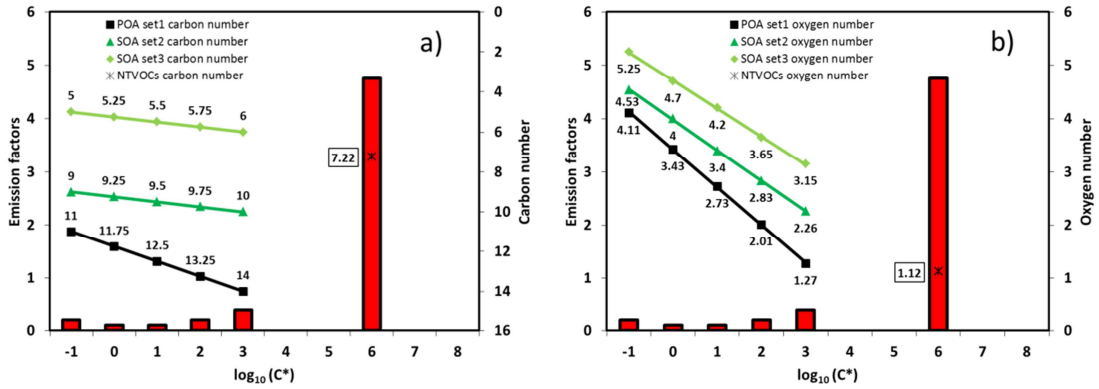

Figure 5.2 *Properties of the wood burning POA and SOA sets. a) C number b) O number. Wood burning SOA carbon numbers were placed from 10 to 5 and linearly interpolated between the volatility bins. Oxygen numbers were calculated using the group approach of Donahue et al. (2011). NTVOCs carbon and oxygen numbers were retrieved from PTR-MS data The red bars indicate the OM emission factors.*

The specific molecular structures for each of the sets and bins were retrieved using the group contribution approach and the Van Krevelen relation (Table 1). Primary wood burning emissions were placed to range from 14 to 11 carbons (set1) in line with previous studies (Donahue et al., 2012b; Koo et al., 2014) and appropriate numbers of oxygen atoms were retrieved (Eq. 5.2). The oxidation of semi-volatile material would tend to increase the compounds' oxygen number and decrease their volatility and carbon number, due to functionalization and fragmentation. We assume that the oxidation of the primary semi-volatile compounds with C_{11}-C_{14} decreases their volatility by one order of magnitude and yields C_9-C_{10} surrogates, placed in set2, based on the work of Donahue et al. (2011, 2012a,b). Based on these assumptions and using the group contribution approach, the oxygen numbers for set 2 is predicted to vary between 2.26 and 4.56 (Figure 5.2). Thus, the model implicitly accounts for the addition of 1.1 to 1.5 oxygen atoms and the loss of 2.75 to 4.25 carbon atoms, with one oxidation step.

Set3, was directly constrained based on the PTR-MS data. The measurements suggested an average NTVOC carbon and oxygen number of about 7 and 1, respectively. Based on reported molecular speciation data (Kleindienst et al., 2007), we expect that the products of C_7 compounds have a C_5-C_6 carbon backbone. These products were placed in set3 following a kernel function based on the distribution of naphthalene oxidation products. At least two oxygens atoms were added to the NTVOC mixture upon their oxidation (Figure 5.2 and Figure 5.3). The overall, O:C ratio in the whole space roughly spans the range from 0.1 to 1.0.

Multigeneration chemistry (aging) is also accounted for by the model. Gas-phase products in the semi-volatile range in set2 and set3, once formed, can further react with a rate constant of 4 x 10^{-11} cm^3 $molecule^{-1}$ s^{-1} as proposed by previous studies (Donahue et al., 2013; Grieshop et al.,

2009; Robinson et al., 2007), further lowering the volatility of the products by one order of magnitude.

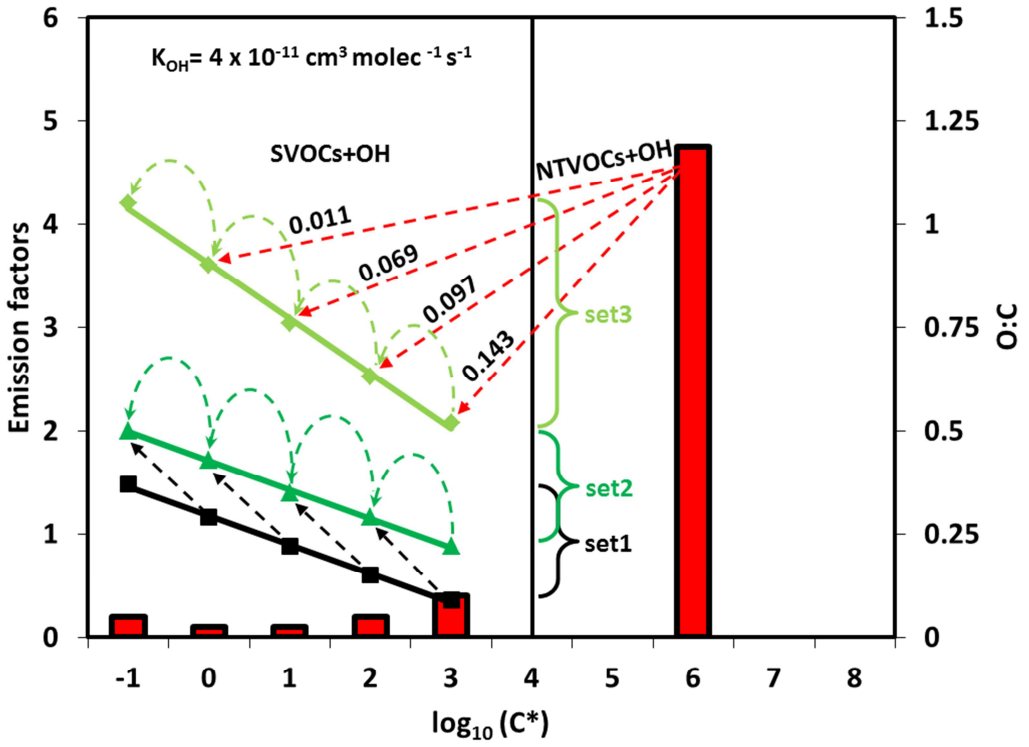

Figure 5.3 *Proposed oxidation scheme: an average mixture of NTVOCs compounds are allowed to react with the hydroxyl radical following a naphthalene kernel mass distribution. Secondary products in the SOA set (set3) are allowed to further react with a reaction rate of* k_{OH} *= 4.0 x* 10^{-11} cm^3 $molec^{-1}$ s^{-1}*. Oxidation products from semi-volatile vapours from the POA set (set1) are allowed for further aging in set2. The numbers on the red arrows indicate the NTVOCs yields for each bin for the best fitting solution (ppm* ppm^{-1}*).*

As the modelled species' average carbon number systematically decreases with aging, this approach effectively takes into consideration the compounds' fragmentation. In parallel, the addition of oxygen reflects the compounds' functionalization with aging and the increase in the measured O:C ratio. Therefore, unlike previous 2D-VBS schemes where functionalization and fragmentation are disentangled, the approach adopted here, by decreasing the number of carbon atoms and increasing the number of oxygens atoms, simultaneously describes both processes.

In addition to the constrains mentioned above, three parameters were determined based on experimentally constrained time-dependent OA mass and O:C ratios, i.e., NTVOCs reaction rates and yields as well as average enthalpies of vaporization values for the set 2 and 3. Detailed explanations are presented in the next two sections.

Table 5.1 *Properties of the VBS space. Oxygen numbers for each volatility bin were calculated using the group-contribution of Donahue et al. (2011). Hydrogen numbers were calculated from the van Krevelen relation (Heald et al., 2010).*

	Log (C*)	Oxygen number	Carbon number	Hydrogen number	O:C ratio	Molecular weight
POA set1	-1	4.11	11.00	17.89	0.37	216
	0	3.43	11.75	20.07	0.29	216
	1	2.73	12.50	22.27	0.22	216
	2	2.01	13.25	24.49	0.15	216
	3	1.27	14.00	26.73	0.09	215
SOA set2	-1	4.53	9.00	13.47	0.50	194
	0	4.00	9.25	14.50	0.43	189
	1	3.40	9.50	15.60	0.36	184
	2	2.83	9.75	16.67	0.29	179
	3	2.26	10.00	17.74	0.23	174
SOA set3	-1	5.25	5.00	4.75	1.05	149
	0	4.70	5.25	5.80	0.90	144
	1	4.20	5.50	6.80	0.76	140
	2	3.65	5.75	7.85	0.63	135
	3	3.15	6.00	8.85	0.52	131

5.3.1 Part1: Inferring OM_{sv} and $NTVOCs/OM_{sv}$ ratios from measurements and partition theory

We seek to determine, based on the PTR-MS and AMS measurements of gas and particle phase organic material at t=0, the ratio $NTVOCs/OM_{sv}$ and the enthalpies of evaporation of compounds of the semi-volatile compounds that represent best the observations at high and low temperatures. We modelled the $OA_{t=0}$ partitioning using two different proposed ΔH_{vapPOA} for wood burning:

$$\Delta H_{vapPOA} = -4\log_{10}(C^*_{298K}) + 85 \quad (5.3)$$

$$\Delta H_{vapPOA} = -11\log_{10}(C^*_{298K}) + 70 \quad (5.4)$$

Eq. 5.3 is the best fitting solution proposed by May et al. 2013, while Eq. 5.4 represents the lower limit for ΔH_{vapPOA} for solution falling within experimental uncertainties (Figure 4 in May et al. 2013). We will refer to these solutions as SOL1 for Eq.5.3, and SOL2 for Eq.5.4. Table

5.2 reports the measured $OA_{t=0}$ for all the 11 experiments, which ranges from 6.0 μg m^{-3} and 22.6 μg m^{-3}. The amount of OM_{sv} that matches the measured $OA_{t=0}$ is reported for both SOL1 and SOL2. The average NTVOCs/OM_{sv} ratios for high temperature and low temperature experiments are reported together with the standard deviation in Table 5.3. For SOL1 we calculated an average ratio of 4.2±1.1 at high temperatures and 7.2±2.6 for low temperatures. SOL2 reduces the differences in the average NTVOCs/OM_{sv} ratios at the two temperatures, and therefore will be used to describe the dependency of the primary organic compounds. For SOL2 the overall NTVOCs/OM_{sv} ratio between high and low temperature experiments is around 4.75. Figure 5.4 shows the resolved equilibrium phase partitioning (Eq. 5.1) between the gas and particle phase at the beginning of each of the 11 smog chamber experiments ($OA_{t=0}$) using SOL2. As expected, most of the material is found in the gas-phase at high temperatures, while at lower temperature only part of the compounds with saturation concentrations (at 20°C) between 100 and 1000 μg m^{-3}, would reside in the gas-phase.

Table 5.2 *Modelled and experimental data for 11 wood burning experiments. OM_{sv} mass at the beginning of each chamber experiments are reported together with measured $OA_{t=0}$ and the initial NTVOCs concentration. The (NTVOCs)/(OM_{sv}) indicates the ratio between the measured NTVOCs and the imposed OM_{sv} mass at the beginning of each experiment for the two different ΔH_{vapPOA} solutions (SOL1 and SOL2).*

	Exp1 T=263K RH=50%	Exp2 T=263K RH=50%	Exp3 T=263K RH=50%	Exp4 T=263K RH=50%	Exp5 T=263K RH=90%	Exp6 T=263K RH=90%	Exp7 T=263K RH=90%	Exp8 T=288K RH=50%	Exp9 T=288K RH=50%	Exp10 T=288K RH=50%	Exp11 T=288K RH=50%
Measured NTVOCs [µg/m^3]	185.1	-	-	79.3	143.5	91.7	68.7	121.5	190.4	174.6	195.7
Measured $OA_{t=0}$ [µg/m^3]	12.3	8.1	16.7	9.3	12.0	17.7	6.0	22.6	17.5	18.7	18.6
SOL1 Modelled OM_{sv} [µg/m^3]	17.3	12.1	22.4	13.6	16.9	23.5	9.5	46.6	37.7	39.8	39.6
SOL2 Modelled OM_{sv} [µg/m^3]	22.7	15.8	29.5	17.8	22.2	31.0	12.3	49.7	40.1	42.4	42.2
SOL1 (NTVOCs)/(OM_{sv})	10.7	-	-	5.1	8.5	3.9	7.2	2.6	5.0	4.4	4.9
SOL2 (NTVOCs)/(OM_{sv})	8.1	-	-	4.4	6.4	3.0	5.6	2.4	4.7	4.1	4.6

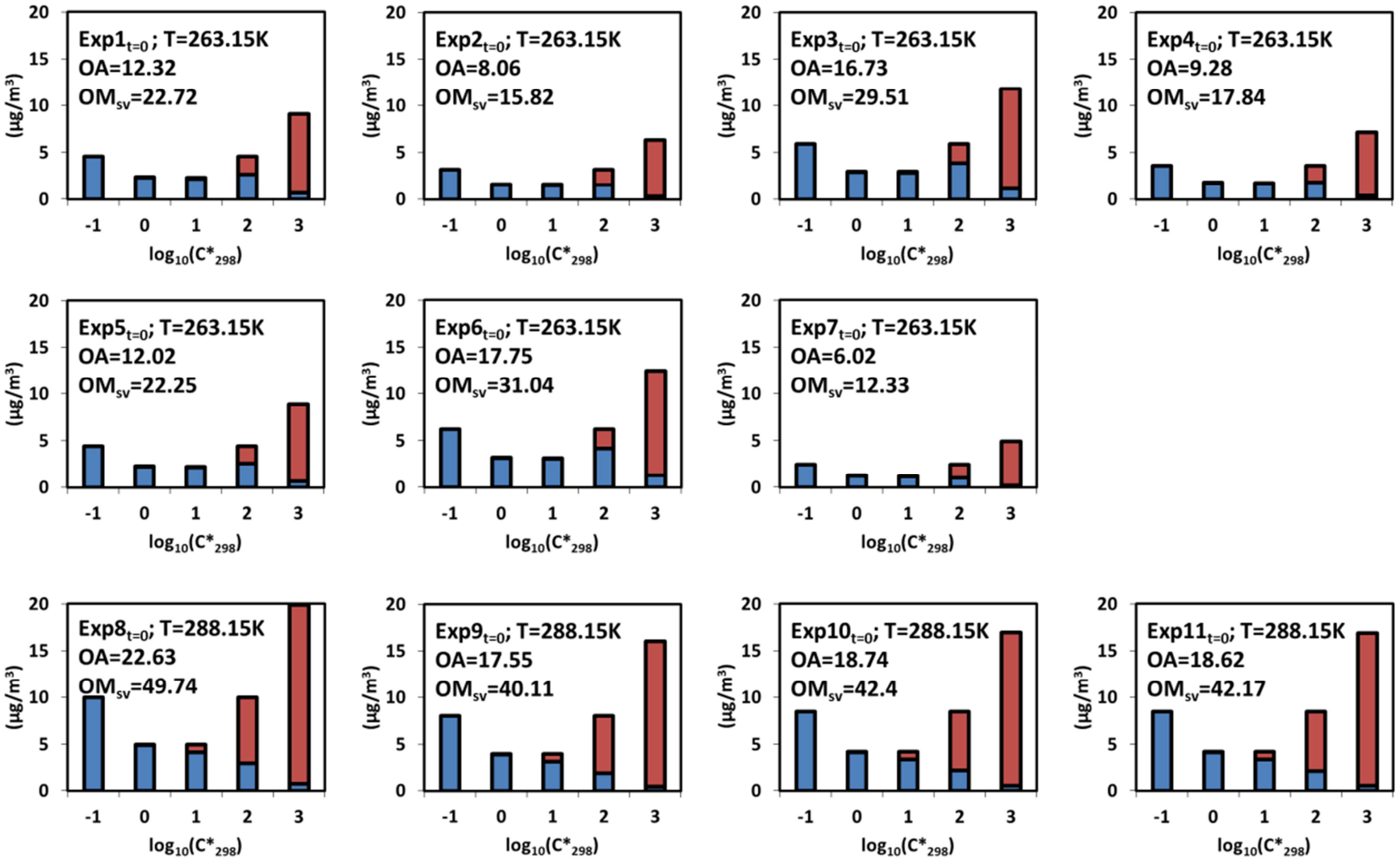

Figure 5.4 *Partitioning of wood burning POA before the start of the aging for 11 smog chamber experiments (SOL2). Gas-phase in red and particle phase in blue.*

Table 5.3 *Solutions used for primary organic aerosol enthalpies of evaporations with averages and standard deviations of the (NTVOCs)/(OM_{sv}) ratio.*

ΔH_{vapPOA} (kJ mol^{-1})	(NTVOCs)/(OM_{sv}) Average High-T (288.15 K)	(NTVOCs)/(OM_{sv}) Average Low-T (263.15 K)
SOL1 $-4\log_{10}(C^{*}_{298K}) + 85$	4.2±1.1	7.2±2.6
SOL2 $-11\log_{10}(C^{*}_{298K}) + 70$	4.0±1.1	5.5±2.0

5.3.2 Part2: Modelling of wood burning aging at low and high temperature

In this section we will focus on the emission aging. Using the NTVOCs/OM_{sv} ratio and the enthalpies of vaporization retrieved in section 3.1.1, we modelled the eight different smog chamber experiments: No. 1, 2, 3, 4 (low temperature) and No. 8, 9, 10, 11 (high temperature) performed at the same relative humidity (RH = 50%). For each of the eight experiments we injected an average mixture of NTVOCs equal to 4.75 times the OM_{sv} mass before the start of the aging. NTVOCs react solely with OH, whose concentration was retrieved from PTR-MS measurements. The temperature dependence of the reaction rates was also taken into account through the Arrhenius equation. The reaction rates ($k_{OH\text{-}NTVOCs}$) and yields (Y) of the NTVOCs as well as enthalpies of vaporization of SOA (ΔH_{vapSOA}) for set2 and set3 were varied within specific physically realistic ranges. We varied $k_{OH\text{-}NTVOCs}$ between 2 and 4 x 10^{-11} cm^3 $molec^{-1}$ s^{-1} in steps of 0.1 x 10^{-11} cm^3 $molec^{-1}$ s^{-1}, and yields between 0.1 and 0.4 ppm ppm^{-1} in steps of 0.01 ppm ppm^{-1}. Values for ΔH_{vapSOA} are still highly uncertain. In this study we explored a wide range of values from 15,000 J mol^{-1} to 115,000 J mol^{-1} in steps of 20,000 J mol^{-1}. The model performance for each combination of *i*,*j* and *k* was evaluated in terms of the root mean square error (RMSE) for the eight experiments and a best fitting solution retrieved as the one that minimized the sum of the errors on both the O:C ratio and OA mass (giving the same weight on both quantities). We performed a total number of $(i \times j \times k \times n_{exp}) = (21 \times 31 \times 6 \times 8) = 31248$ simulations, where n_{exp} are the numbers of aging experiments. Figure 5.5 shows the total errors for the OA mass (left side) and O:C ratio (right side) for different ΔH_{vapSOA}, Y and $k_{OH\text{-}NTVOCs}$.

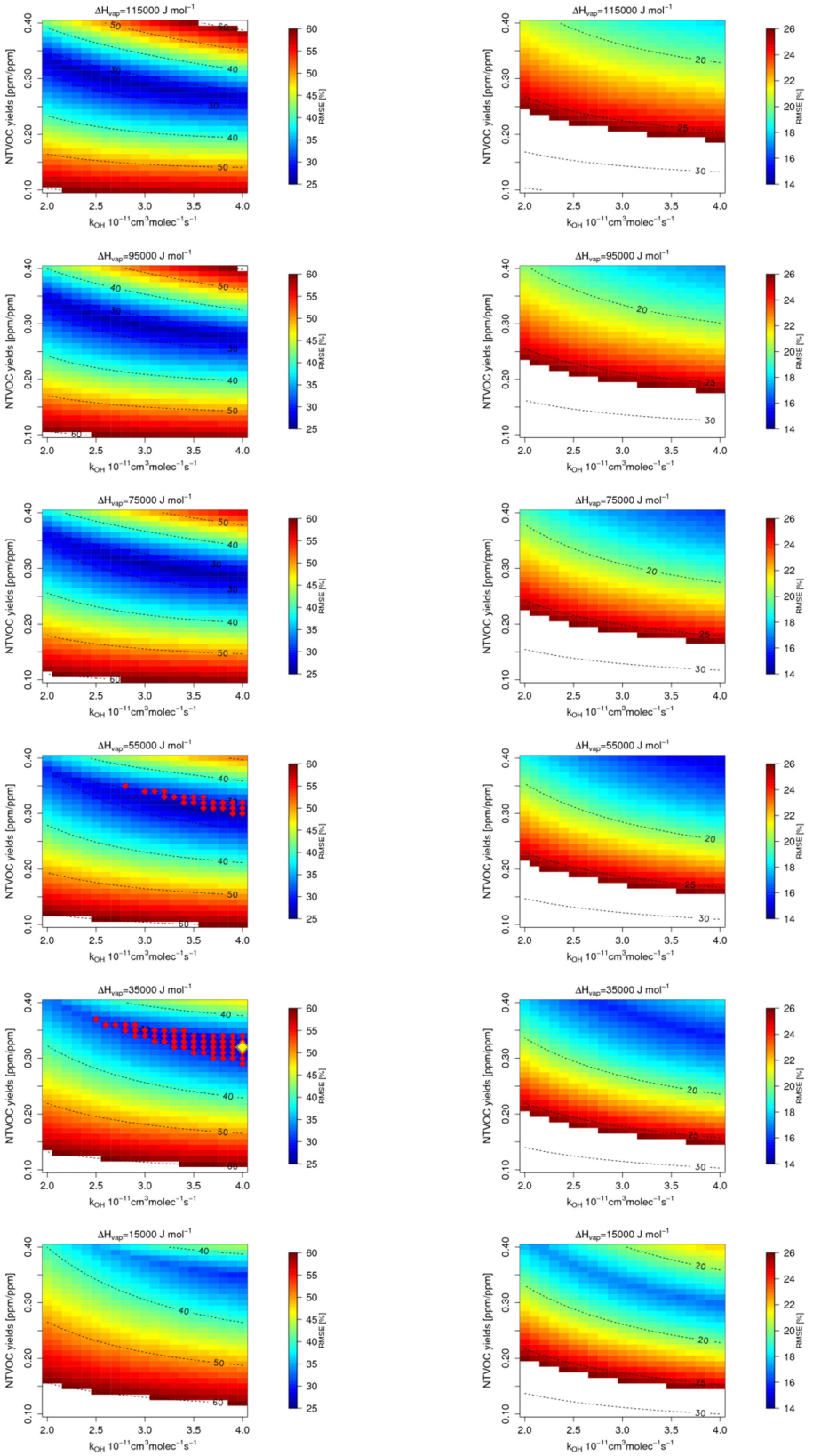

Figure 5.5 *Total error on the OA mass (left side) and on the O:C ratio (right side). White regions have an error larger than 60% for the OA mass and 26% for the O:C ratio. The number of simulations per experiment is 3906. The red diamonds indicate the likelihood ratio test results for solutions within 10% error from the best one (yellow diamond).*

These global errors are root mean squared deviations (i.e. for the eight experiments) adjusted to the number of points per experiment. The error on the OA mass varies from a minimum of ~25% up to more than 60 % whereas the errors on the O:C ratio (Figure 5.5 right side) are lower and they range from approximately 15 % up to more than 30 %. For the OA mass, distinct regions with lower errors are visible in the central part of each panel with different ΔH_{vapSOA}, representing the models that fitted best the measured OA. While a similar observation can be made for the O:C, models with high ΔH_{vapSOA} tend to reproduce the data less faithfully. The diamonds in Figure 5.5 indicate the absolute best fitting solution (in yellow) and the ones retrieved with a likelihood-ratio test allowing for 10% error form the best fit (red diamonds). Regions with lower error are localized for $k_{OH\text{-}NTVOCs} \geq 2.5 \times 10^{-11}$ cm^3 $molec^{-1}$ s^{-1} between ΔH_{vapSOA} values of 35,000 and 55,000 J mol^{-1}.

Figure 5.6 shows the modelled and measured OA mass for all the 8 aging experiments. The primary organic aerosol fraction is reported as well as the SOA fraction from SVOCs and higher volatility NTVOCs. All the low temperature experiments (No. 1, 2, 3, 4 left side of the panel) were reproduced very well along with the concentration gradients at the end of each the experiments even though the model tends in general to slightly over-predict the final OA concentration. The primary fraction slightly increases at the very beginning of the aging phase and it decreases as the experiments proceed as a result of its partitioning to the gas phase and subsequent oxidation. Most of the SOA was predicted to be formed from NTVOCs precursors and only a minor amount from SVOCs. On the other hand, for experiments conducted at higher temperature (No. 8, 9, 10, 11) the OA mass was under-predicted except for experiment No. 8 (see also Figure A.2 1). In this case, SVOCs contribute more significantly to SOA formation compared to low temperature experiments, although the majority of SOA still arises from NTVOCs.

Comparisons between measured and modelled O:C ratios are reported in Figure 5.7. Model and observation results match very well, especially upon aging. Significant differences between measured and modelled O:C ratios at the beginning of the experiments highlight on the one hand the variable nature of primary biomass smoke emissions. This variability cannot be accounted for in the model. On the other hand, for some experiments the model under-predicts the measured O:C ratios suggesting that the model parameters describing the O:C of primary emissions are suboptimal. These parameters include directly the carbon and oxygen number of species in set 1, and indirectly the volatility distributions and enthalpy of vaporization, which are all adopted from previous published data. The average bias in POA O:C ratios is ~30%, well within the experimental uncertainties.

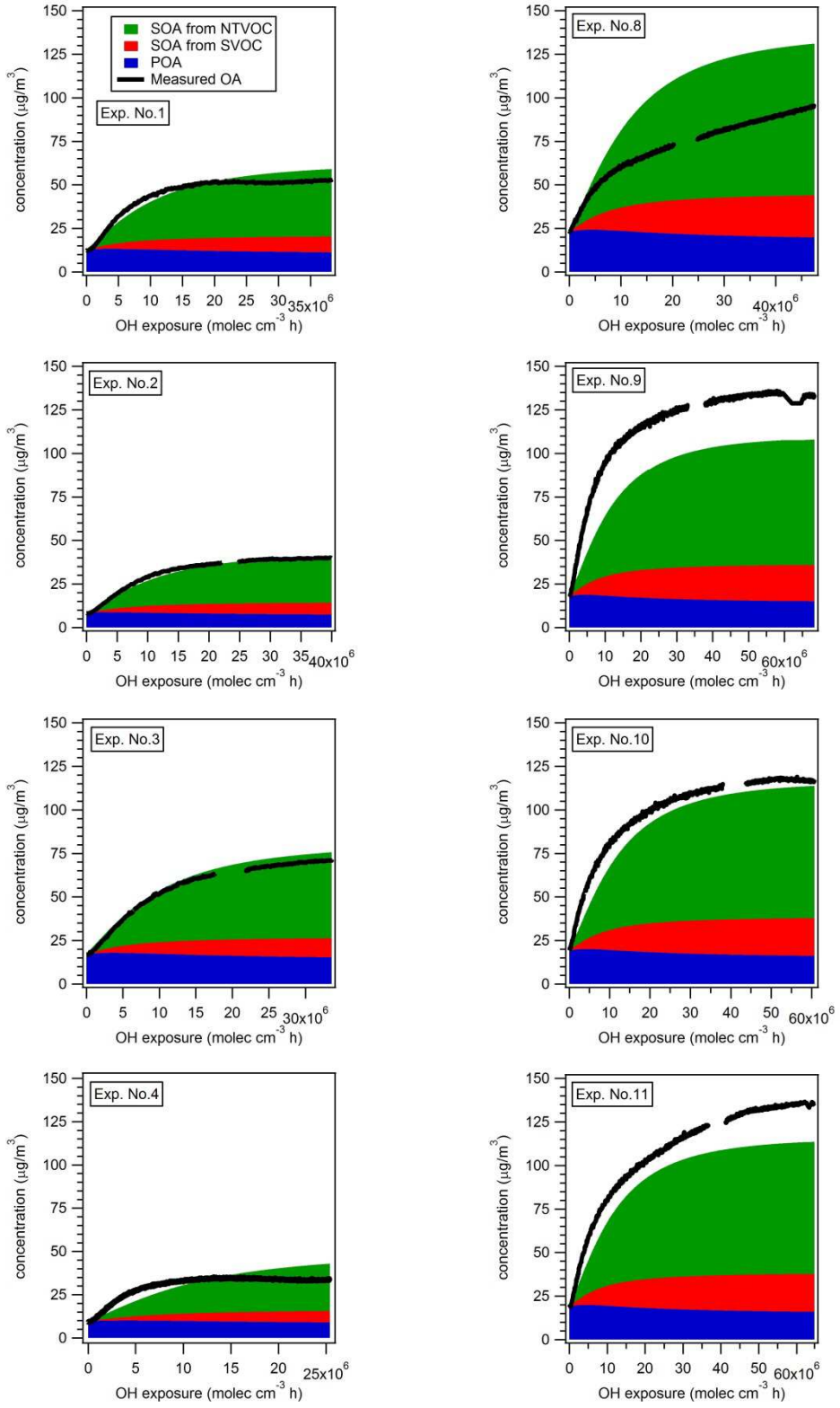

Figure 5.6 *Modelled and observed OA mass for low temperature experiments (left side) and high temperature experiments (right side). The model results for the best fitting solution (yellow diamond in Figure 5.5). SOA from NTVOCs and SVOCs as well as POA are reported in green, red and blue, respectively.*

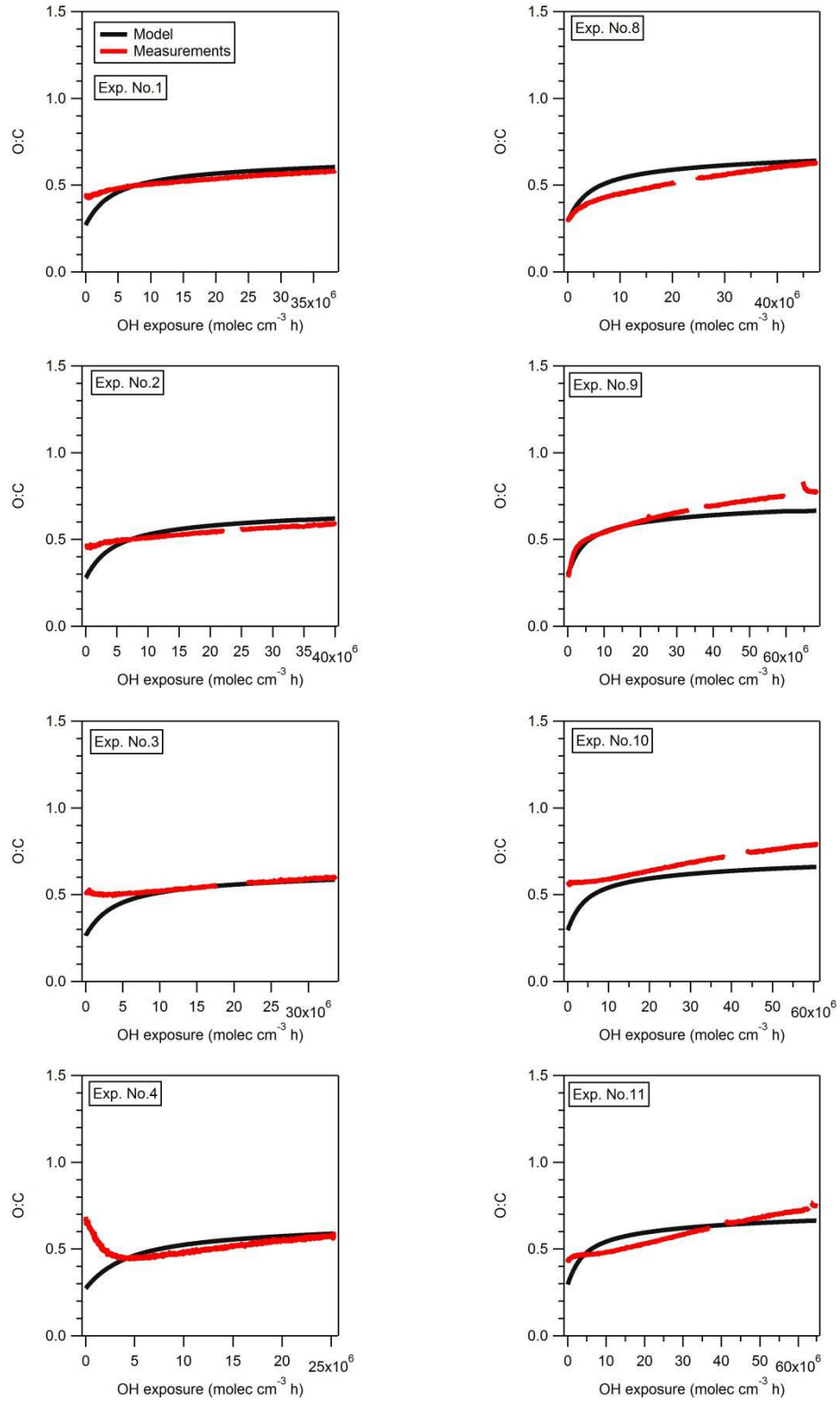

Figure 5.7 *Modelled (black lines) and observed (red lines) O:C ratio for low temperature experiments (left side) and high temperature experiments (right side).*

5.4 Implication for large-scale models

We performed extensive box model simulations of wood burning experiments conducted at two different temperatures (263 and 288 K) in a ~7 m^3 smog chamber facility. By combining new NTVOCs measurements and already available partitioning data for primary wood burning emission, we constrained the amounts of NTVOCs that act as SOA precursors. Our estimates indicate that NTVOCs are approximately 4.75 times the amount of total organic material in the 0.1 and 1000 μg m^{-3} saturation concentration range (OM_{sv}). This ratio can be directly used in CTM models in the absence of explicit NTVOCs emissions for wood burning in combination with the proposed aging scheme. Specific parameters such as NTVOCs reaction rates ($k_{OH\text{-}NTVOCs}$), yields (Y) and enthalpies of vaporization of secondary organic aerosol (ΔH_{vapSOA}) were varied using brute force simulations, and their values were retrieved for best fitting solutions falling within a physically realistic range. The model predicted that the majority of the SOA formed during the aging-phase arose from NTVOCs precursors and only a smaller amount from SVOCs.

Based on our best fitting solutions, we can now predict the OA mass and composition as well as SOA yields at any given temperature, emission load and OH exposure. This is illustrated in Figure 5.8 for 3 different OM emission loads (OM_{sv} + NTVOCs) of 6, 60 and 600 μg m^{-3} and for a wide range of atmospherically relevant temperatures (from 253.15 K to 313.15 K).

Partitioning of POA depends on the temperature and the injection amounts. The primary organic aerosol mass (POA) decreases with temperature by ~0.5% K^{-1} on average with higher effects predicted at higher loads (0.7% K^{-1} at 600 μg m^{-3}, 0.3% at 6 μg m^{-3}). The partitioning coefficient of the primary material increases by about a factor of 1.5 for a 10-fold increase in the emissions. As aging proceeds, POA mass slightly increases as a result of additional partitioning, but after an OH exposure of (1.0-1.5) x 10^7 molec cm^{-3} h, the trend is inversed and POA mass decreases due to the oxidation of semi-volatile primary compounds. This effect is more visible at high loads.

From Figure 5.8, we can also assess the impact of temperature, OH exposure and emission concentrations on SOA yields. The temperature effect on SOA yields is a function of OH exposure, aerosol load, and temperature: i.e. $\partial Y/\partial T = f(T, C_{OA}, OH_{exp})$. SOA yields increase by 0.03, 0.06 and 0.05 % K^{-1} on average for 6, 60 and 600 μg m^{-3} respectively, with higher effects predicted in general at lower temperatures. The temperature effect on the yields is also greater at higher OH exposures (except for very high loads). An analysis typically performed to estimate the volatility distribution of SOA products is based on SOA yields from chamber data performed at different precursor concentrations. We investigated the impact of the OA concentration on the yield at different temperatures and OH exposure. In Figure A.2 2, an

average change in the yield with $\log C_{OA}$ is shown at the different conditions: $(\partial Y/\partial \log C_{OA}) = f(T, OH_{exp})$. Note that an increase in SOA yields with the $\log C_{OA}$ was observed as expected. This increase is not solely due to additional partitioning, but is partially also related to changes in the actual chemical composition and hence volatility distribution of the SOA surrogates, as they age to different extents at different concentrations and different temperatures. We determined a yield increase of 4-9% for a 10-fold increase in emissions, with a higher effect at higher OH exposures and lower temperatures.

From Figure 5.8, one may evaluate the minimum OH exposure values required for SOA to exceed POA. SOA is predicted to exceed POA after~1.5 x 10^7 molec cm^{-3} h, for typical ambient concentrations and temperatures. At low temperatures (263 K) and high loads, SOA might exceed POA at an OH exposure of 9 x 10^6 molec cm^{-3} h, or in 2-10 hours (at OH concentrations of (1-5) x 10^6 molec cm^{-3}), in line with our previously estimated values for biomass burning emissions for the typical conditions of haze events (Huang et al., 2014). Comparatively, at 288.15K an OH exposure of 7 x 10^6 molec cm^{-3} h would be required for SOA to exceed POA, which might be reached within 2 hours or less at typical summer OH concentrations, i.e. (5-10) x 10^6 molec cm^{-3}. These results confirm previous observations that SOA formation is very rapid and the SOA fraction might exceed primary emissions within time-scales of hours, even during haze events.

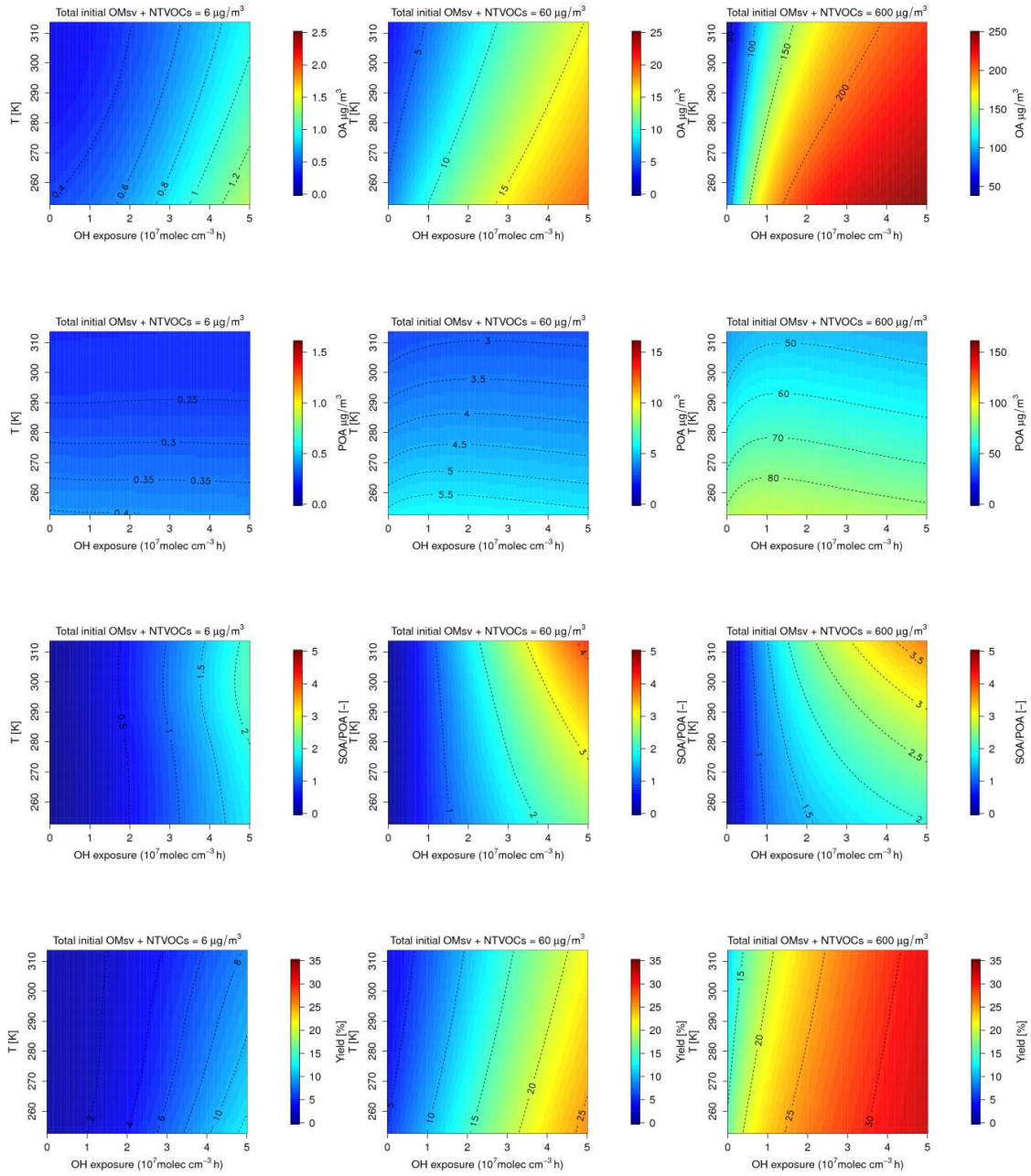

Figure 5.8 *Predicted OA mass (upper panels, note different scales), POA mass, SOA/POA ratio (middle panels) and yields (lower panels) at different OM_{sv} + NTVOCs initial load and atmospheric conditions (T).*

Acknowledgements

This study was financially supported by the Swiss Federal Office of Environment (FOEN).

6

Modelling winter organic aerosol at the European scale with CAMx: evaluation and source apportionment with a VBS parameterization based on novel wood burning smog chamber experiments

Giancarlo Ciarelli[1], Sebnem Aksoyoglu[1], Imad El Haddad[1], Emily A. Bruns[1], Monica Crippa[2], Laurent Poulain[3], Mikko Äijälä[4], Samara Carbone[5], Evelyn Freney[6], Colin O'Down[7], Urs Baltensperger[1] and André S. H. Prévôt[1]

[1]Paul Scherrer Institute, Laboratory of Atmospheric Chemistry, 5232 Villigen PSI, Switzerland
[2]European Commission, Joint Research Centre (JRC), Directorate for Energy, Transport and Climate, Air and Climate Unit, Via E. Fermi 2749, I-21027 Ispra (VA), Italy
[2]Leibniz-Institute for Tropospheric Research (TROPOS), Permoserstr. 15, 04318 Leipzig, Germany
[4]University of Helsinki, Department of Physics, Helsinki, Finland
[5]Institute of Physics, University of São Paulo, Rua do Matão Travessa R, 187, 05508-090 São Paulo, S.P., Brazil
[6]Laboratoire de Météorologie Physique (LaMP), CNRS/Université Blaise Pascal, Clermont-Ferrand, France
[7]School of Physics and Centre for Climate & Air Pollution Studies, Ryan Institute, National University of Ireland Galway, University Road, Galway, Ireland

Submitted to Atmospheric Chemistry and Physics

Abstract

We evaluated a modified VBS (Volatility Basis Set) scheme to treat biomass burning-like organic aerosol (BBOA) implemented in CAMx (Comprehensive Air Quality Model with extensions). The updated scheme was parameterized with novel wood combustion smog chamber experiments using a hybrid VBS framework that accounts for a mixture of wood burning organic aerosol precursors and their further functionalization and fragmentation in the atmosphere. The new scheme was evaluated for one of the winter EMEP intensive campaigns (February-March 2009) against aerosol mass spectrometer (AMS) measurements performed at 11 sites in Europe. We found a considerable improvement for the modelled organic aerosol (OA) mass compared to our previous model application with the mean fractional bias (MFB) reduced from -61% to -29%.

We performed model-based source apportionment studies and compared results against positive matrix factorization (PMF) analysis performed on OA AMS data. Both model and observations suggest that OA was mainly of secondary origin at almost all sites. Modelled secondary organic aerosol (SOA) contributions to total OA varied from 32 to 88% (with an average contribution of 62%) and absolute concentrations were generally under-predicted. Modelled primary hydrocarbon-like organic aerosol (HOA) and primary biomass burning-like aerosol (BBOA) fractions contributed to a lesser extent (HOA from 3 to 30%, and BBOA from 1 to 39%) with average contributions of 13 and 25%, respectively. Modelled BBOA fraction was found to represent 12 to 64% of the total residential heating related OA, with increasing contributions at stations located in the northern part of the domain.

Source apportionment studies were performed to assess the contribution of residential and non-residential combustion precursors to the total SOA. Non-residential combustion and transportation precursors contributed about 30-40% to SOA formation (with increasing contributions at urban and near industrialized sites) whereas residential combustion (mainly related to wood burning) contributed to a larger extent, around 60-70%. Contributions to OA from residential combustion precursors in different volatility ranges were also assessed: our results indicate that residential combustion gas-phase precursors in the semi-volatile range contributed from 6 to 30%, with higher contributions predicted at stations located in the southern part of the domain. On the other hand, higher volatility residential combustion precursors contributed from 15 to 38% with no specific gradient among the stations.

The new retrieved parameterization, although leading to a better agreement between model and observations, still under-predicts the SOA fraction suggesting remaining uncertainties in the new scheme or that other sources and/or formation mechanisms need to be elucidated.

6.1 Introduction

Organic aerosol (OA) comprises the main fraction of fine particulate matter (PM_1) (Jimenez et al., 2009). Even though the sources of its primary fraction (primary organic aerosol, POA) are qualitatively known, uncertainties remain in terms of the total emission fluxes annually released into the troposphere (Kuenen et al., 2014). Moreover, the measured OA load largely exceeds the emitted POA fractions at most measurement sites around the world. A secondary fraction (SOA), formed from the condensation of oxidized gases with low-volatility on pre-existing particles, is found to be the dominant fraction of OA (Crippa et al., 2014; Huang et al., 2014; Jimenez et al., 2009). Such low-volatility products are produced in the atmosphere when higher volatility organic gases are oxidized by ozone (O_3), hydroxyl (OH) radical and/or nitrate (NO_3) radical. The physical and chemical processes leading to the formation of SOA are numerous, very uncertain and currently under debate (Hallquist et al., 2009; Tsigaridis et al., 2014; Fuzzi et al., 2015; Woody et al., 2016).

Available long-term measurements might help in elucidating the composition and origin of OA in different seasons. Canonaco et al. (2015) presented direct evidence for significant changes in the SOA fingerprint between summer and winter from 13 months of OA measurements conducted in Zürich using the aerosol chemical speciation monitor (ACSM). Their results indicate that summer oxygenated OA mainly arises from biogenic precursors whereas winter oxygenated OA is more strongly influenced by wood burning emissions. Moreover, numerous ambient studies of open burning plumes from aircraft do not show a net increase in OA, despite observing oxidation (Cubison et al., 2011; Jolleys et al., 2012). It is therefore necessary that the chemical transport models (CTMs) correctly reproduce OA concentrations by taking into account all the uncertainties and variability of observations.

Most of the CTMs account for common biogenic and anthropogenic high volatility SOA precursors such as terpenes, isoprene, xylene and toluene which have a saturation concentration (C^*) higher than 10^6 μg m^{-3} (Aksoyoglu et al., 2011; Ciarelli et al., 2016a). A few models also include intermediate volatility organic compounds (IVOCs) with a C^* of 10^3 - 10^6 μg m^{-3} and semi-volatile organic compounds (SVOCs) with a C^* of 0.1 - 10^3 μg m^{-3} co-emitted with POA (Bergström et al., 2012; Ciarelli et al., 2016a; Denier van der Gon et al., 2015; Fountoukis et al., 2014; Ots et al., 2016; Tsimpidi et al., 2010; Woody et al., 2016). In these applications, the volatility distributions of POA and IVOCs emissions are based on the study of Robinson et al.

(2007), where the IVOC mass is assumed to be 1.5 times the total organic mass available in the semi-volatile range.

The standard gridded emission inventories do not yet include SVOCs and their emissions are still highly uncertain as their measurement is strongly affected by the method used (Lipsky and Robinson, 2006). A recent study by Denier van der Gon et al. (2015) reported a new residential wood burning emission inventory including SVOCs, where emissions are higher by a factor of 2-3 on average than those in the EUCAARI inventory (Kulmala et al., 2011). The new emission inventory was used in two CTMs (EMEP and PMCAMx) and it improved the model performance for the total OA (Denier van der Gon et al., 2015). Ciarelli et al. (2016a) showed that allowing for evaporation of primary organic particles as available in European emission inventories degraded OA performance (further under-predicted OA but with POA and SOA components in a better agreement) whereas model performance improved when volatility distributions that implicitly account for missing semi-volatile material (increasing POA emissions by a factor of 3) were deployed.

Various modelling studies were performed by increasing POA emissions by a factor of 3 to compensate for the missing gaseous emissions based on partitioning theory predictions (Ciarelli et al., 2016a; Fountoukis et al., 2014; Shrivastava et al., 2011; Tsimpidi et al., 2010). Figure A.3 1 shows the partitioning of ~1 μg m^{-3} of POA at different temperatures using the latest available volatility distribution for biomass burning (May et al., 2013). The ratio between the available gas and particle phase material in the semi-volatile range is predicted to be roughly 3. This implies that, in these applications, the newly emitted organic mass (POA + SVOCs + IVOCs) is 7.5 times higher than in original emissions (i.e., OM = (3*POA) + (1.5*(3*POA))). This indirect accounting of missing organic material could be used in the absence of more detailed gridded emission inventories, keeping in mind that the amount of higher volatility compounds was specifically derived from studies conducted with diesel engines (Robinson et al., 2007).

Along with ambient measurement studies, novel wood burning smog chamber studies provide more insight into wood burning SOA formation and the nature of its precursors. Bruns et al. (2016) performed several wood-burning aging experiments in a ~7 m^3 smog chamber. Using proton-transfer-reaction mass spectrometry (PTR-MS) they characterized SOA precursors at the beginning of each aging experiment and found that up to 80% of the observed SOA could be explained with a collection of a few SOA precursors that are usually not accounted in regional CTMs (e.g. cresol, phenol, naphthalene). Recently, we used those chamber data to parameterize a hybrid volatility basis set (Ciarelli et al., 2016b). The results provided new direct information regarding the amount of wood burning SOA precursors which could be directly used in CTM applications in the absence of more refined wood burning emissions in gridded

inventories. The box-model application reproduced the chamber data with an error of approximately 25% on the OA mass and 15% on the O:C ratio (Ciarelli et al., 2016b).

In the current study, the updated volatility basis set (VBS) parameterization was implemented in the comprehensive air quality model with extensions (CAMx) model, and simulations were performed in Europe for a winter period in February-March 2009. Results are compared with previous simulations using the original VBS framework (Ciarelli et al., 2016a) and with source apportionment data at eleven sites with different exposure characteristics, obtained using PMF applied to AMS measurements (Crippa et al., 2014).

6.2 Method

6.2.1 Regional modelling with CAMx

The CAMx version 5.41 with VBS scheme (ENVIRON, 2011; Koo et al., 2014) was used in this study to simulate an EMEP measurement campaign between 25 February and 26 March 2009 in Europe. The modelling method and input data were the same as those used in the EURODELTA III (ED III) project, described in detail in Ciarelli et al. (2016a). The model domain covers Europe with a horizontal resolution of 0.25° x 0.25°. Meteorological parameters were calculated from ECMWF IFS (Integrated Forecast System) data at 0.2° resolution. There were 33 terrain-following σ-levels from ~20 m above ground level (first layer) up to about 350 hPa, as in the original IFS data. For the gas phase chemistry, the Carbon Bond (CB05) mechanism (Yarwood, 2005). The ISORROPIA thermodynamic model (Nenes et al., 1998) was used for the partitioning of inorganic aerosols (sulfate, nitrate, ammonium, sodium and chloride). Aqueous sulfate and nitrate formation in cloud water was calculated using the RADM algorithm (Chang et al., 1987). Formation and evolution of OA is treated with a hybrid volatility basis set (VBS) that accounts for changes in volatility and O:C ratio (Koo et al., 2014) with dilution and aging. Particle size distributions were treated with a two static mode scheme (fine and coarse). The results presented in this study refer to the fine fraction ($PM_{2.5}$). We parameterized the biomass burning sets based on chamber data as described in Ciarelli et al. (2016b).

The anthropogenic emission inventory was made available for the ED III community team by the National Institute for Industrial Environment and Risks (INERIS) at 0.25° x 0.25° horizontal resolution. More information regarding the anthropogenic emission inventories are available in Bessagnet et al. (2014, 2016) and Ciarelli et al. (2016a). Hourly emissions of biogenic VOCs, such as monoterpenes, isoprene, sesquiterpenes, xylene and toluene, were calculated using the Model of Emissions of Gases and Aerosols from Nature MEGANv2.1 (Guenther et al., 2012) for each grid cell in the model domain.

6.2.2 Biomass burning organic aerosol scheme

The biomass burning organic aerosol scheme was constrained using recently available wood burning smog chamber data (Bruns et al., 2016) as described in Ciarelli et al. (2016b). The model deploys three different basis sets (Donahue et al., 2011) to simulate the emissions of organics from biomass burning and their evolution in the atmosphere. The first set allocates fresh emissions into five volatility bins ranging with saturation concentrations between 10^{-1} and 10^{3} μg m^{-3} following the volatility distribution and enthalpy of vaporization proposed by May et al. (2013). In order to include gas-phase organics in the semi-volatile range in the absence of more detailed inventory data, we used the approach proposed by previous studies (Shrivastava et al., 2011; Tsimpidi et al., 2010). The second set allocates oxidation products from SVOCs after shifting the volatility by one order of magnitude. The third set allocates oxidation products from traditional VOCs (xylene, toluene, isoprene, monoterpenes and sesquiterpenes) and from non-traditional SOA precursors retrieved from chamber data (~4.75 times the amount of organic material in the semi-volatile range, Ciarelli et al., 2016b). Primary and secondary semi-volatile compounds react with OH in the gas-phase with a rate constant of 4×10^{-11} cm^{3} $molec^{-1}$ s^{-1} (Donahue et al., 2013), which decreases their saturation concentration by one order of magnitude. No heterogeneous oxidation of organic particles or oligomerization processes is included in the model. The new model parameterization described in this study is referred to as VBS_BC_NEW throughout the paper to distinguish from the previous base case called VBS_BC as given in Ciarelli et al. (2016a).

6.2.3 Model evaluation

The model results for the period between 25 February and 26 March 2009 were compared with OA concentrations measured by AMS at 11 European sites. Modelled BBOA, HOA and SOA concentrations were compared with multi-linear engine 2 (ME-2) analysis performed on AMS data (Paatero, 1999) using source finder (SoFi) (Canonaco et al., 2013; Crippa et al., 2014). Elevated sites such as Montseny and Puy de Dôme were also included in the analysis and modelled concentrations for these two sites were extracted from higher layers in order to minimize the artefacts due to topography in a terrain-following coordinate system. This was not the case in our previous application, where model OA concentrations were extracted from the surface layer (Ciarelli et al., 2016a). We assumed POA emissions from SNAP2 (emissions from non-industrial combustion plants in the Selected Nomenclature for Air Pollution) and SNAP10 (emissions from agriculture, about 6% of POA in SNAP2) to be representative of biomass burning like emissions. OA emissions from all other SNAP categories, including emissions from ships, were compared with HOA-resolved PMF factors. Whilst this could be a reasonable

assumption for HOA-like aerosol, it is probably not the case for BBOA-like aerosol, as gridded emissions for SNAP2 also include other emission sources (i.e., coal burning which might be important in eastern European countries like Poland). We could not resolve our emission inventory to that level and the contribution of coal could not be separated for these European cites (Crippa et al., 2014) in contrast to China (Elser et al., 2016) using similar statistical methods. Finally, the SOA fraction was compared to the PMF-resolved oxygenated organic aerosol (OOA) fraction.

Statistics were reported in terms of mean bias (MB), mean error (ME), mean fractional bias (MFB), mean fractional error (MFE) and coefficient of determination (R^2) (see Table A.3 1 for the definition of statistical parameters).

6.3 Results and discussions

6.3.1 Analysis of the modelled OA

Figure 6.1 shows the average modelled OA concentrations and surface temperature for the period between 25 February and 26 March 2009. Temperatures were below 0°C in the north, ranged 5-10°C in central Europe and were above 10°C in the southern part of the domain. Model performance for surface temperature was evaluated within the ED III exercise and found to be reproduced reasonably well, with a general under-prediction of around 1°C (Bessagnet et al., 2014).

A clear spatial variability in the modelled OA concentrations is observed (Figure 6.1). Predicted OA concentrations were higher in eastern European countries (especially Romania and southern Poland) as well as over northern Italy (8-10 μg m^{-3} on average) whereas they were lower in the northern part of the domain. A similar spatial distribution of OA concentrations was also reported by Denier van der Gon et al. (2015) using the EMEP model. Relatively high OA concentrations over the Mediterranean Sea are mainly of secondary origin due to enhanced photochemical activity (more details are found in Section 6.3.2). In addition, the reduced deposition capacity over water leads to higher OA levels.

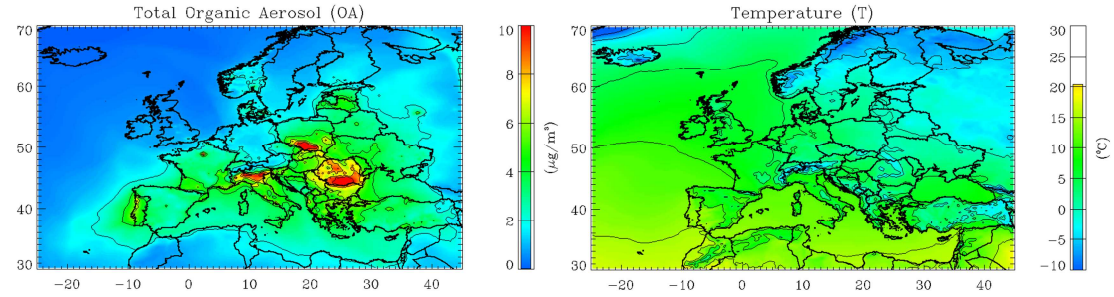

Figure 6.1 *Modelled average total organic aerosol (OA) concentrations (VBC_BC_NEW) and surface temperature (T) for the period between 25 February and 26 March 2009.*

The scatter plots in Figure 6.2 show the modelled (VBS_BC_NEW) versus measured daily average OA concentrations at 11 sites in Europe together with the results from our previous model application (VBS_BC, Ciarelli et al., 2016a) for comparison. The modified VBS scheme (VBS_BC_NEW) predicts higher OA concentrations compared to our previous study using the original scheme (VBS_BC) (~ 60% more OA on average at all sites). Statistical parameters improved significantly (Table 6.1); the mean fractional bias (MFB) decreased from -61% in VBS_BC to -29% in VBS_BC_NEW and the model performance criteria were met (Boylan and Russell, 2006). The coefficient of determination remained almost unchanged for OA in the VBS_BC_NEW case (R^2=0.58) compared to VBS_BC (R^2=0.57) indicating that the original model was able to similarly capture the OA daily variation, but not its magnitude. The majority of the stations show an $R^2 \geq 0.4$. Lower values were found for the elevated sites of Montseny and Puy de Dome (R^2=0.17 and R^2=0.13, respectively) and also at the Helsinki site (R^2=0.06). In spite of the improvements with respect to earlier studies, modelled OA is still lower than measured (mean bias (MB) from -0.1 μg m^{-3} up to -3.1 μg m^{-3}) at most of the sites, with only a slight overestimation at a few locations (MB from 0.3 μg m^{-3} up to 0.9 μg m^{-3}).

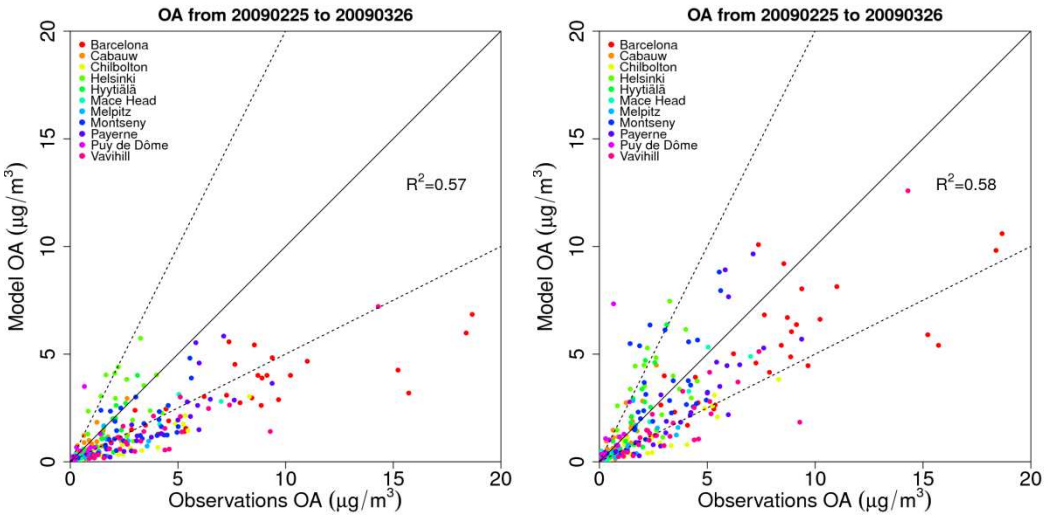

Figure 6.2 *Daily average scatter plots for OA concentrations at 11 AMS sites for the period between 25 February and 26 March 2009 for VBS_BC (left) and VBS_BC_NEW case (right). Solid lines indicate the 1:1 line. Dotted lines are the 1:2 and 2:1 lines.*

The observed OA gradient among the 11 sites was reproduced very well (Figure 6.3). Both measured and modelled OA concentrations were highest in Barcelona. Other sites with concentrations greater than 2 µg m^{-3} were Payerne, Helsinki, Vavihill and Montseny. Barcelona and Helsinki are both classified as urban stations, which justifies the higher OA loads due to the anthropogenic activities (e.g. traffic, cooking and heating). Anthropogenic activities in the area of Barcelona could also affect OA concentrations at Montseny which is about 40 km away. In the case of Payerne and Vavihill, the relatively high OA concentrations might be due to residential heating, where wood is largely used as a combustion fuel during cold periods (Denier van der Gon et al., 2015). For Chilbolton, located not far from London, this might not be the case: the fuel wood usage in the UK is the lowest in Europe (Denier van der Gon et al., 2015). Ots et al. (2016) suggested the possibility of missing diesel-related IVOCs emissions, which might be an important source of SOA in those regions. However, other studies reported substantial contribution from solid fuel combustion to OA (Young et al., 2015). In this case, it might be that difficulties in reproducing the OA concentration are mainly related to the relatively complex area of the site (i.e., close to the English Channel). An evaluation of diurnal variations of HOA and SOA concentrations for this site showed a consistent under-prediction of both components (Figure A.3 2).

Table 6.1 *Statistics of OA for the VBS_BC_NEW case for February-March 2009 at each AMS site as well as an average of all sites for both VBS_BC_NEW and VBS_BC. Bold numbers represent the stations were model performance criteria were met.*

Site*	Mean observed OA ($\mu g\ m^{-3}$)	Mean modelled OA ($\mu g\ m^{-3}$)	MB ($\mu g\ m^{-3}$)	ME ($\mu g\ m^{-3}$)	MFB [-]	MFE [-]	r	R^2
Barcelona (BCN)	8.3	5.1	-3.1	3.7	**-0.4**	**0.5**	0.6	0.4
Cabauw (CBW)	1.2	1.5	0.3	0.7	**0.1**	**0.5**	0.7	0.4
Chilbolton (CHL)	2.4	1.0	-1.4	1.5	-0.9	0.9	0.8	0.6
Helsinki (HEL)	2.7	3.6	0.9	1.8	**0.3**	**0.6**	0.3	0.1
Hyytiälä (SMR)	1.3	1.7	0.3	0.8	**-0.1**	**0.6**	0.8	0.6
Mace Head (MHD)	0.8	0.7	-0.1	0.3	**-0.1**	**0.7**	0.7	0.5
Melpitz (MPZ)	1.5	0.8	-0.6	0.9	-0.6	0.7	0.6	0.3
Montseny (MSY)	3.1	3.5	0.4	2.0	**0.1**	**0.6**	0.4	0.1
Payerne (PAY)	4.1	2.9	-1.2	1.9	**-0.5**	**0.7**	0.7	0.4
Puy de Dôme (PDD)	0.6	1.1	0.4	0.8	0.3	0.8	0.4	0.2
Vavihill (VAV)	3.9	2.1	-1.8	2.0	-0.8	0.8	0.8	0.6
VBS_BC_NEW	3.0	2.3	-0.7	1.6	**-0.3**	**0.7**	0.8	0.6
VBS_BC (Ciarelli et al., 2016a)	3.0	1.4	-1.5	1.8	-0.6	0.8	0.8	0.6

* Model OA concentrations extracted at surface level except for the stations of Puy de Dôme and Montseny.

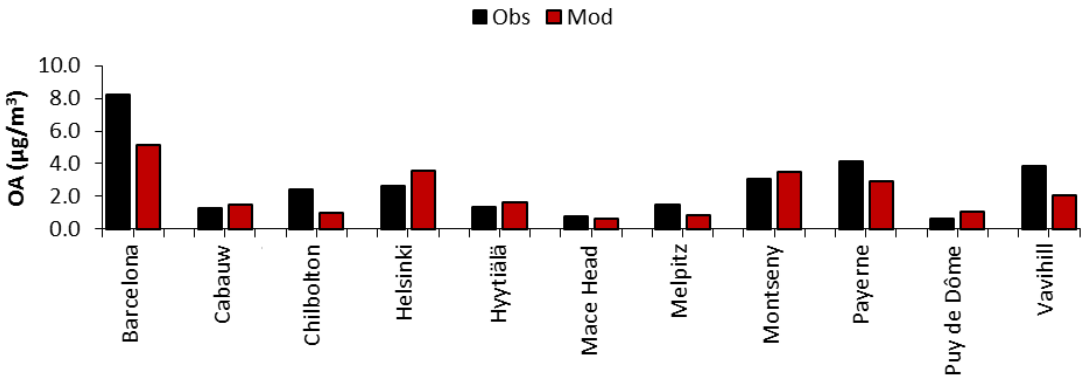

Figure 6.3 *Observed (black) and modelled (VBS_BC_NEW) (red) average OA mass at AMS sites for the period between 25 February and 26 March 2009.*

6.3.2 Analysis of the OA components

The predicted POA spatial distribution (Figure 6.4) resembles the residential heating emission pattern of different countries (Bergström et al., 2012). The highest POA concentrations were predicted in east European countries, France, Portugal and in northern Italy (~3-5 µg m^{-3}) whereas they were less than 1 µg m^{-3} in the rest of the model domain. Very low OA concentrations in Sweden were already shown by previous European studies. Bergström et al. (2012) reported that Swedish organic carbon (OC) emissions from the residential heating sector were lower by a factor of 14 compared to Norway, even though Sweden had much higher wood usage (60% higher) likely due to underestimation of emissions from residential heating in the emission inventory.

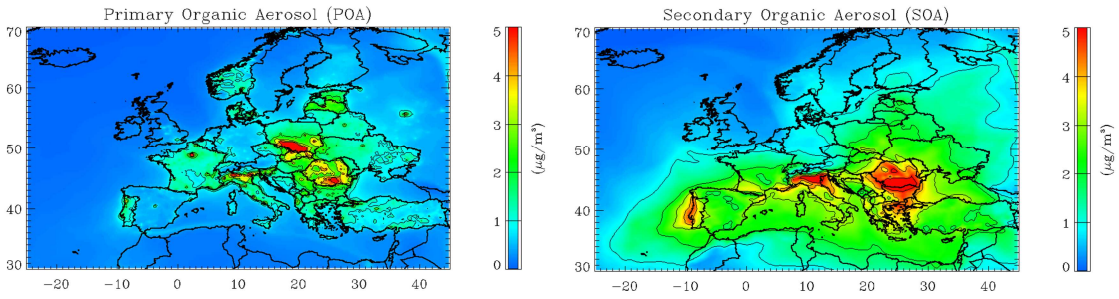

Figure 6.4 *Modelled average POA (left) and SOA (right) concentrations for the period between 25 February and 26 March 2009.*

The spatial distribution of SOA concentrations, on the other hand, is more widespread with a visible north to south gradient (Figure 6.4). Higher SOA concentration were predicted close to primary emission sources (e.g. Poland, Romania, Po Valley and Portugal) but also in most of the countries below 50° latitude and over the Mediterranean Sea where higher OH

concentration, reduced deposition capacity and high contribution from long-range transport are expected (average concentrations around 3-4 μg m^{-3}).

Comparison of results from this study (VBS_BC_NEW) with the earlier one (VBS_BC, Ciarelli et al., 2016a) suggests that the new VBS scheme predicts higher SOA concentrations by about a factor of 3 (Figure 6.5) and improves the model performance when comparing assessed oxygenated organic aerosol (OOA) from measurements with modelled SOA Table 6.3.

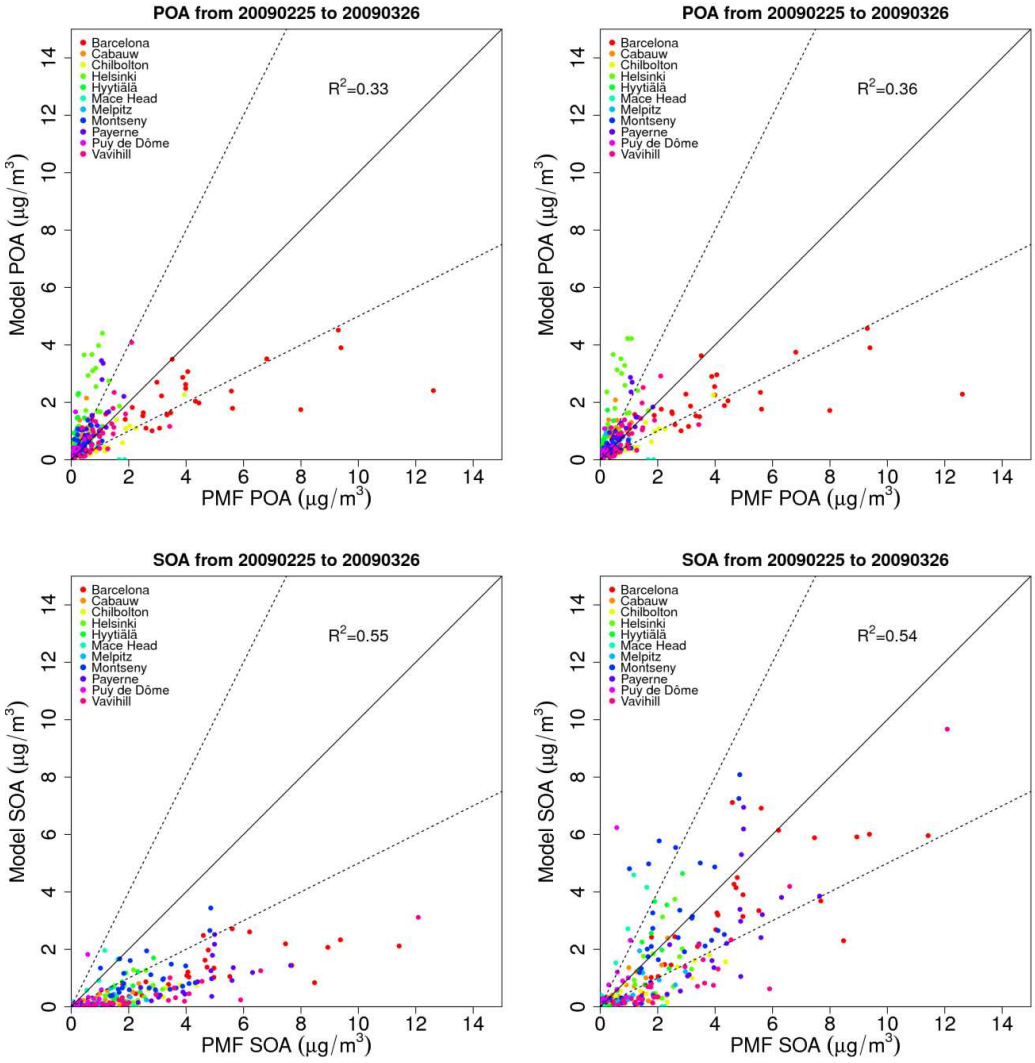

Figure 6.5 *Daily average scatter plots of POA and SOA concentrations at 11 AMS sites for February-March 2009 in VBS_BC (Ciarelli et al., 2016a) (left) and VBS_BC_NEW (right). Solid lines indicate the 1:1 line. Dotted lines are the 1:2 and 2:1 lines.*

POA concentrations, on the other hand, are clustered below 1 μg m^{-3} except in Barcelona, showing an R^2=0.36, (Figure 6.5 and Table 6.2). Although predicted POA concentrations at Barcelona were lower than the measurements, MFB=-47% and MFE=69% were still in the range for acceptable performance criteria (MFE ≤+75% and −60 < MFB < + 60 %, Boylan and Russell, 2006). On the other hand, the model over-predicted the POA concentrations at Hyytiälä (MFB=131% and MFE=131%), Helsinki (MFB=95% and MFE=100%) and Cabauw (MFB=76% and MFE=86%) mainly due to the overestimated BBOA fraction as seen in Figure 6.6.

At most of the sites, OA was dominated by SOA (Figure 6.6 and Figure 6.7) which was underestimated in particular at Chilbolton, Melpitz and Vavihill (Table 6.3). As already mentioned, the under-prediction of SOA concentrations might be attributed to missing SOA precursors or uncertainties in SOA formation mechanisms and removal processes. On the other hand, the remote station of Mace Head showed a positive bias for SOA (MFB = 30%), even though model and measurement concentrations were very similar (0.54 and 0.35 μg m^{-3}, respectively), which could be attributed to an overestimated contribution from the boundaries.

Table 6.2 *Statistics of POA for the VBS_BC_NEW case for February-March 2009 at each AMS site as well as an average of all sites for both VBS_BC_NEW and VBS_BC. Bold numbers represent the stations were model performance criteria were met.*

Site	Mean observed POA (μg m^{-3})	Mean modelled POA (μg m^{-3})	MB (μg m^{-3})	ME (μg m^{-3})	MFB [-]	MFE [-]	r	R^2
Barcelona	4.0	2.0	-2.1	2.4	**-0.5**	**0.7**	0.4	0.2
Cabauw	0.4	0.9	0.5	0.5	0.8	0.9	0.5	0.2
Chilbolton	1.0	0.5	-0.5	0.5	**-0.6**	**0.7**	0.8	0.6
Helsinki	0.8	2.5	1.7	1.7	1.0	1.0	0.2	0.0
Hyytiälä	0.1	0.5	0.4	0.4	1.3	1.3	0.5	0.3
Mace Head	0.2	0.1	-0.1	0.2	0.5	1.0	0.2	0.1
Melpitz	0.3	0.3	0.1	0.2	**0.3**	**0.7**	0.5	0.2
Montseny	0.5	0.4	0.0	0.3	**0.2**	**0.7**	0.3	0.1
Payerne	0.7	1.1	0.3	0.6	**0.5**	**0.7**	0.5	0.3
Puy de Dôme	0.2	0.3	0.1	0.2	0.5	0.9	0.2	0.1
Vavihill	1.1	1.0	-0.1	0.6	**-0.3**	**0.7**	0.5	0.2
VBS_BC_NEW	0.9	0.9	-0.1	0.7	0.3	0.8	0.6	0.3
VBS_BC (Ciarelli et al., 2016a)	0.9	0.9	0.0	0.8	0.3	0.8	0.6	0.4

Table 6.3 *Statistics of SOA for the VBS_BC_NEW case for February-March 2009 at each AMS site as well as an average of all sites for both VBS_BC_NEW and VBS_BC. Bold numbers represent the stations were model performance criteria were met.*

Site	Mean observed SOA ($\mu g\ m^{-3}$)	Mean modelled SOA ($\mu g\ m^{-3}$)	MB ($\mu g\ m^{-3}$)	ME ($\mu g\ m^{-3}$)	MFB [-]	MFE [-]	r	R^2
Barcelona	4.4	3.2	-1.2	1.6	**-0.4**	**0.5**	0.7	0.5
Cabauw	1.0	0.6	-0.4	0.6	-0.7	0.9	0.7	0.4
Chilbolton	1.4	0.5	-0.9	1.0	-1.1	1.2	0.7	0.5
Helsinki	1.8	1.1	-0.7	1.1	-0.7	0.9	0.4	0.2
Hyytiälä	1.2	1.1	-0.1	0.7	-0.7	1.0	0.8	0.6
Mace Head	0.4	0.5	0.2	0.6	0.3	1.0	0.4	0.2
Melpitz	1.2	0.5	-0.7	0.8	-1.0	1.1	0.6	0.4
Montseny	2.6	3.1	0.5	1.8	**0.0**	**0.7**	0.4	0.1
Payerne	3.7	2.0	-1.7	2.1	-0.8	0.9	0.5	0.3
Puy de Dôme	0.6	0.9	0.3	0.8	0.2	0.9	0.2	0.1
Vavihill	2.8	1.1	-1.7	1.7	-1.2	1.2	0.8	0.7
VBS_BC_NEW	2.1	1.4	-0.6	1.2	-0.6	0.9	0.7	0.5
VBS_BC (Ciarelli et al., 2016a)	2.1	0.5	-1.5	1.6	-1.1	1.3	0.7	0.6

The relatively small positive bias at the two elevated sites, Montseny and Puy de Dome (MFB = 4% and 17%, respectively), is most likely the result of difficulties in capturing the inversion layer.

Mostly traffic-related HOA was underestimated at the urban site Barcelona (Table A.3 2, Figure 6.6), with the model not able to reproduce the diurnal variation of HOA at this urban site likely due to poorly reproduced meteorological conditions or too much dilution during day time in the model (Figure A.3 2). The under-prediction of the HOA fraction is consistent with our previous study where model evaluation for NO_2 revealed a systematic under-estimation of the modelled concentration (Ciarelli et al., 2016a). The course resolution of the domain (0.25° x 0.25°) may result in too low emissions especially at urban sites. The majority of the NO_x ($NO+NO_2$) emissions in Europe arises from the transportation sector (SNAP7), which might have much larger uncertainties than previously thought (Vaughan et al., 2016). An evaluation of planetary boundary layer height (PBLH) within the EDIII shows that although the PBLH was quite well represented in general in the ECMWF IFS meteorological fields, CAMx tends to underestimate the night-time minima and to overestimate some daytime peaks. The other urban

site considered in this study is Helsinki. In this case, HOA concentrations were over-predicted, as seen in Figure 6.6 and Figure A.3 2, which might indicate missing dispersion processes in the model or under-estimated dilution.

The modelled BBOA fraction on the other hand was generally higher than the measurements, with an average MFB of 50% (Table A.3 3, Figure 6.6 and Figure 6.7), which might arise from various factors: 1) In the model, POA emissions from SNAP2 and SNAP10 are assumed to be representative of BBOA emissions which might not be the case for all European countries (other non-wood fuels such as coal, which is allocated to SNAP2 category could not be separated in this study), 2) The under-prediction of the modelled surface temperature (Bessagnet et al., 2014) will directly influence the partitioning of organic material in the semi-volatile range, favouring freshly emitted organic material to condense more to the particle phase, 3) Uncertainties in the adopted volatility distributions and/or in the oxidation processes of semi-volatile organic vapours.

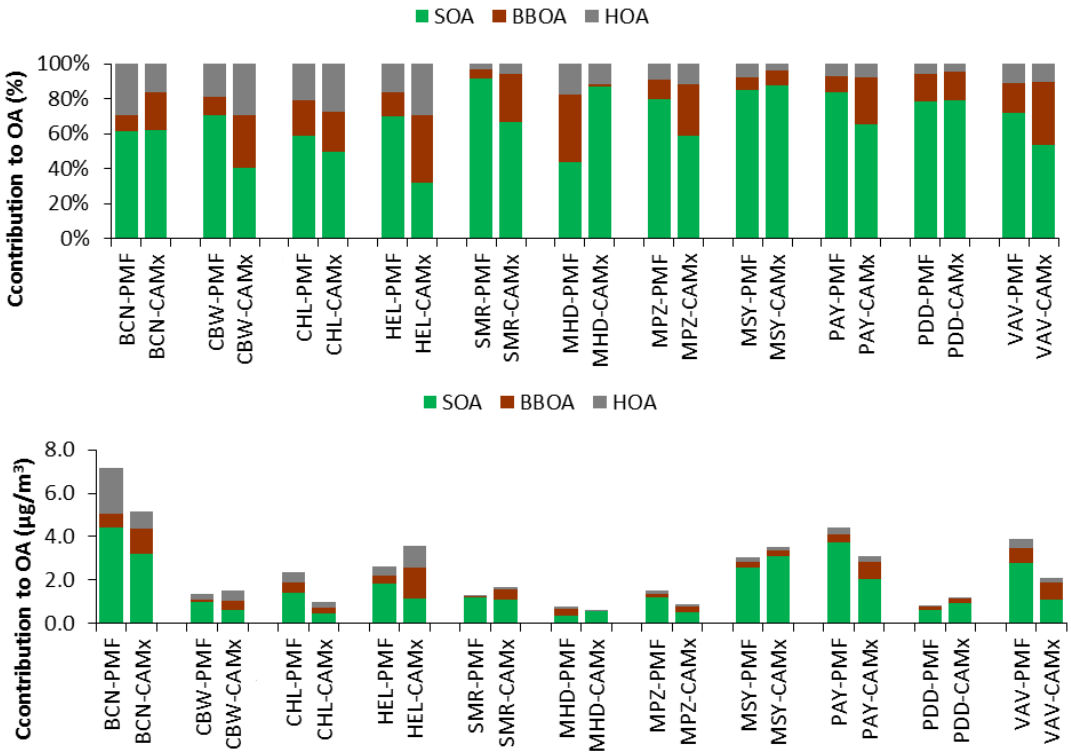

Figure 6.6 *Relative (upper panel) and absolute (lower panel) contribution of HOA, BBOA and SOA to OA concentrations at 11 sites from PMF analysis of AMS measurements (first bar) and CAMx VBS_BC_NEW results (second bar) for the period between 25 February and 26 March 2009.*

The temporal variability of OA concentrations was reproduced quite well: most of the peaks were captured accurately (Figure 6.8); the magnitudes of only a few (Vavihill, Chilbolton and Barcelona) were underestimated. Diurnal variations of HOA, BBOA and SOA components at the rural-background sites suggest that the model was able to reproduce the relatively flat profile

of the measured SOA and the increased BBOA concentrations at night (Figure 6.9). On the other hand, there was a slight underestimation of HOA during the day, especially around noon, likely as a result of too much dilution in the model.

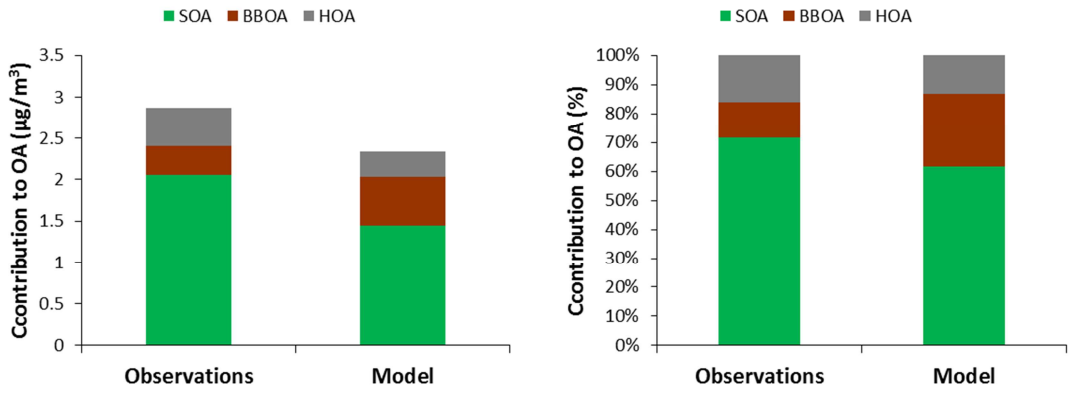

Figure 6.7 *Measured and modelled average absolute (left panel) and relative (right panel) contributions of HOA, BBOA and SOA to OA concentrations for all the 11 sites for the period between 25 February and 26 March 2009.*

In our previous application, we performed a sensitivity study with increased biogenic and residential heating emissions by a factor of two (Ciarelli et al., 2016a). While the model was rather insensitive to the increased biogenic emissions during winter periods, a substantial increase in the OA concentrations was observed when emissions from residential heating were doubled. The model with doubled emissions from residential heating (VBC_BC_2xBBOA), overestimated the POA fraction at most of the sites (Figure 6.10) with smaller effects on SOA, even though a better closure was achieved between modelled and observed OA. The results of the simulations using the new parameterization (VBC_BC_NEW), on the other hand, were closer to the measurement data especially for the SOA fraction (Figure 6.10).

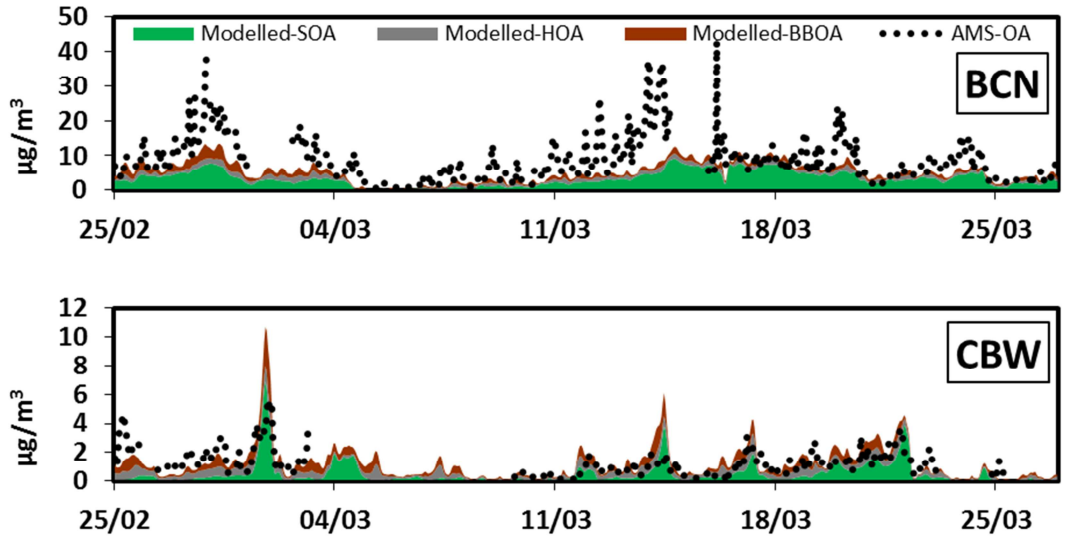

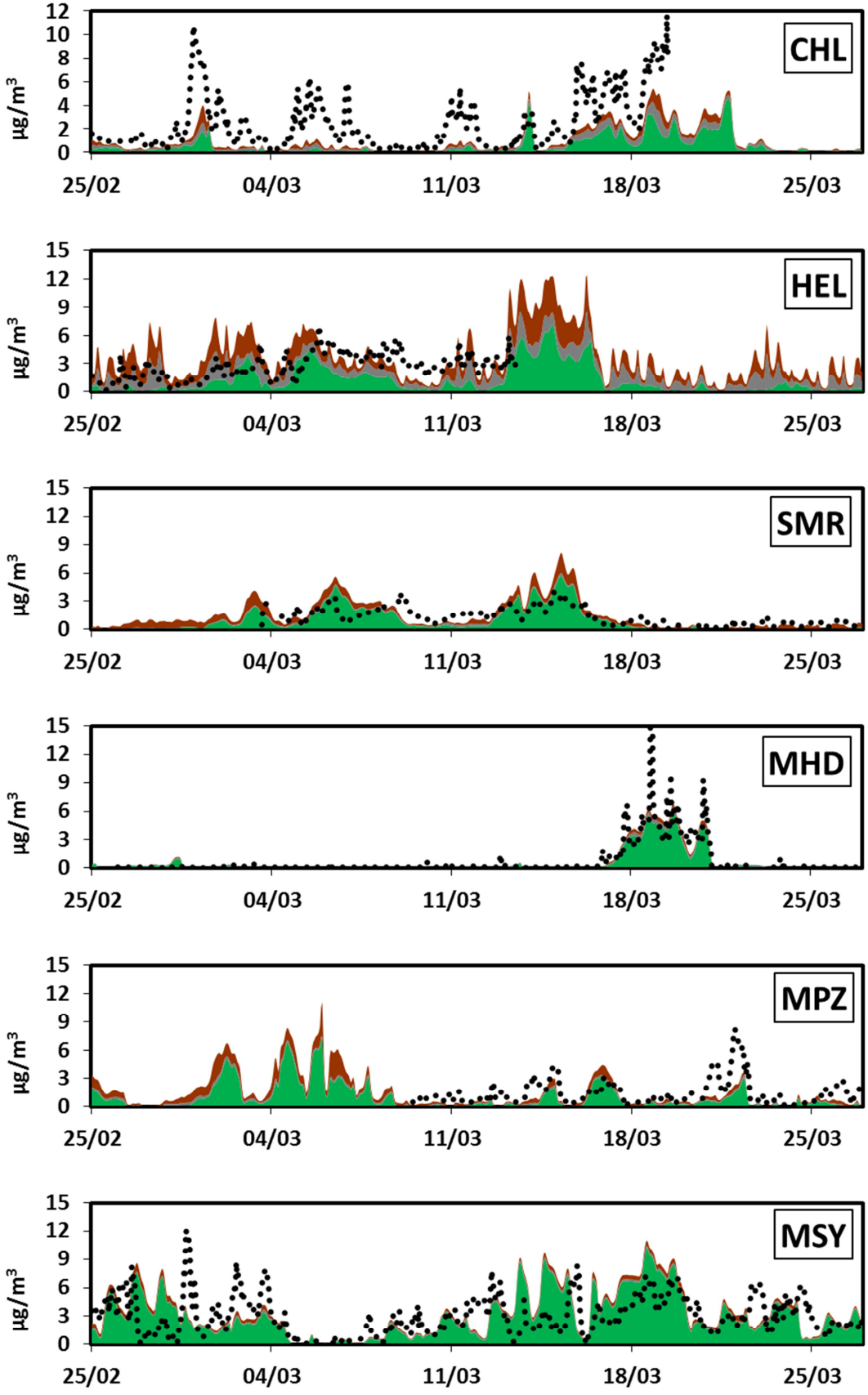
CHL
HEL
SMR
MHD
MPZ
MSY
µg/m³
25/02
04/03
11/03
18/03
25/03

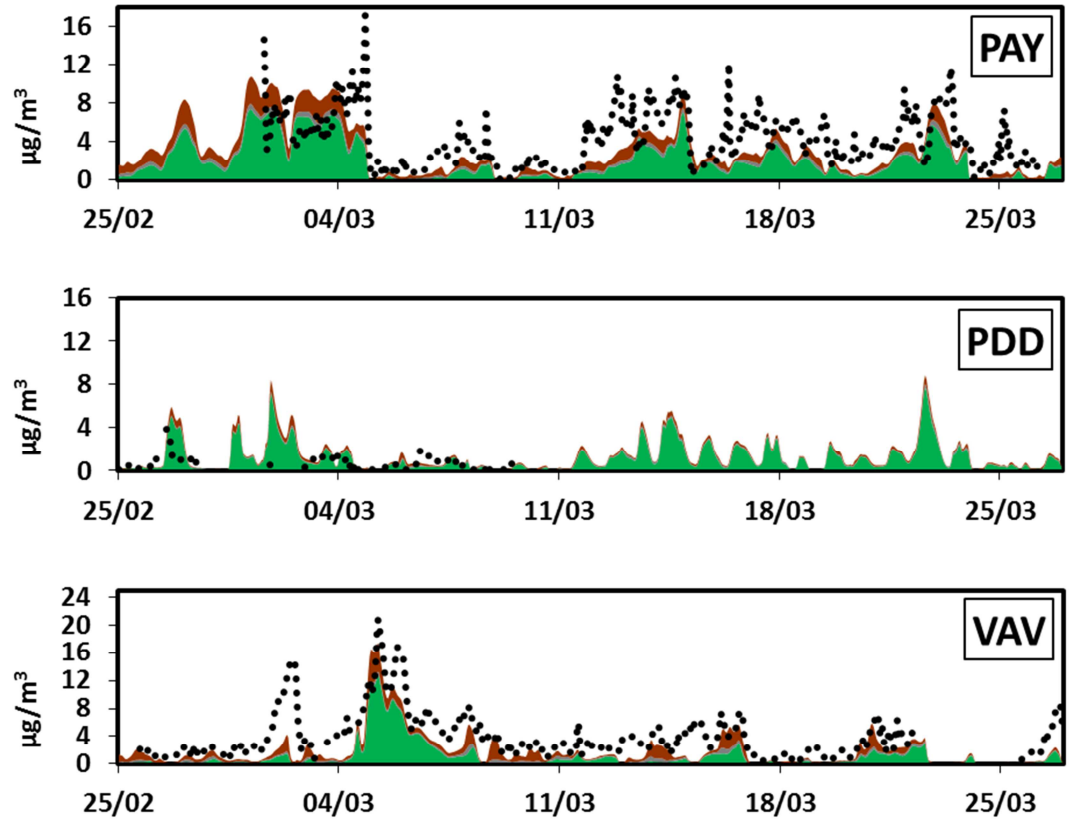

Figure 6.8 *Comparison of measured hourly OA mass concentrations (AMS-OA dotted line), with modelled components HOA, BBOA and SOA.*

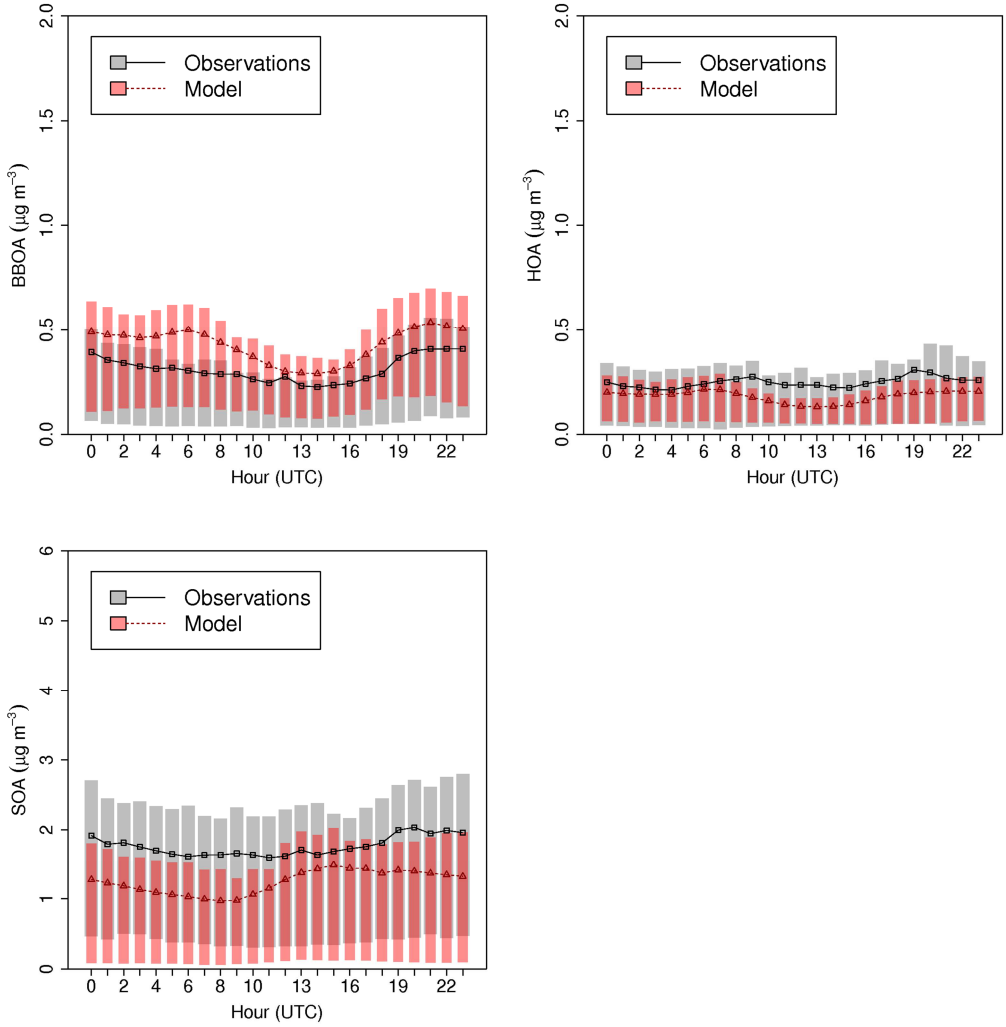

Figure 6.9 *Comparison of modelled (red) and measured (grey) BBOA, HOA and SOA diurnal profiles at the rural-background sites. The extent of the bars indicates the 25th and 75th percentiles.*

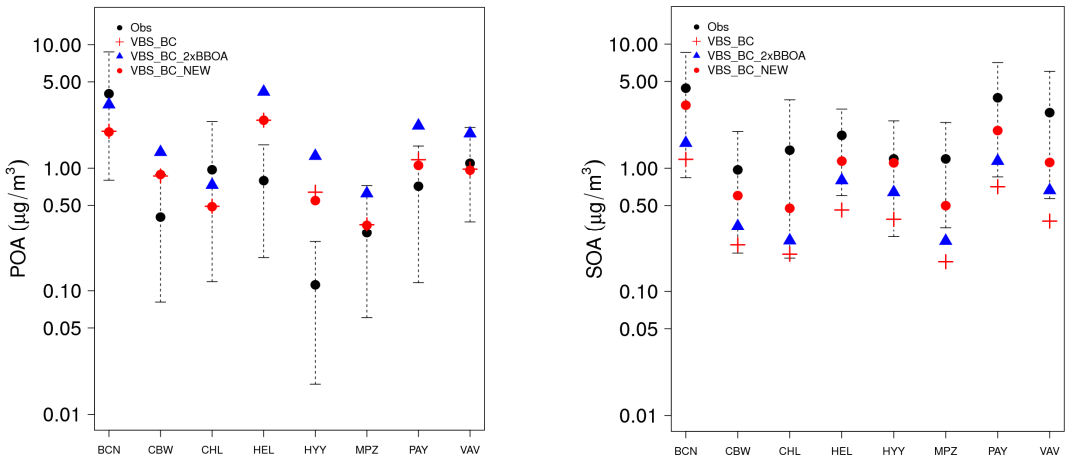

Figure 6.10 *POA (left) and SOA (right) average concentrations at 8 AMS sites for February-March 2009 in the VBS_BC , VBS_BC_2xBBOA and VBS_BC_NEW cases. Dotted lines indicate the 10th and 90th quartile range. Data for the Puy de Dôme and Montseny sites at higher layers are not available for the VBS_BC_2xBBOA scenario.*

6.3.3 Residential versus non-residential combustion precursors

More detailed source apportionment studies were performed in order to assess the importance of residential and non-residential combustion precursors for OA and SOA. The upper panel in Figure 6.11 shows the relative contributions to SOA from residential and non-residential combustion precursors. The model results indicate that non-residential combustion and transportation precursors contribute about 30-40% to SOA formation (with increasing contribution at urban and near-industrialized sites) whereas residential combustion (mainly related to wood burning) contribute to a larger extent, i.e., around 60-70%.

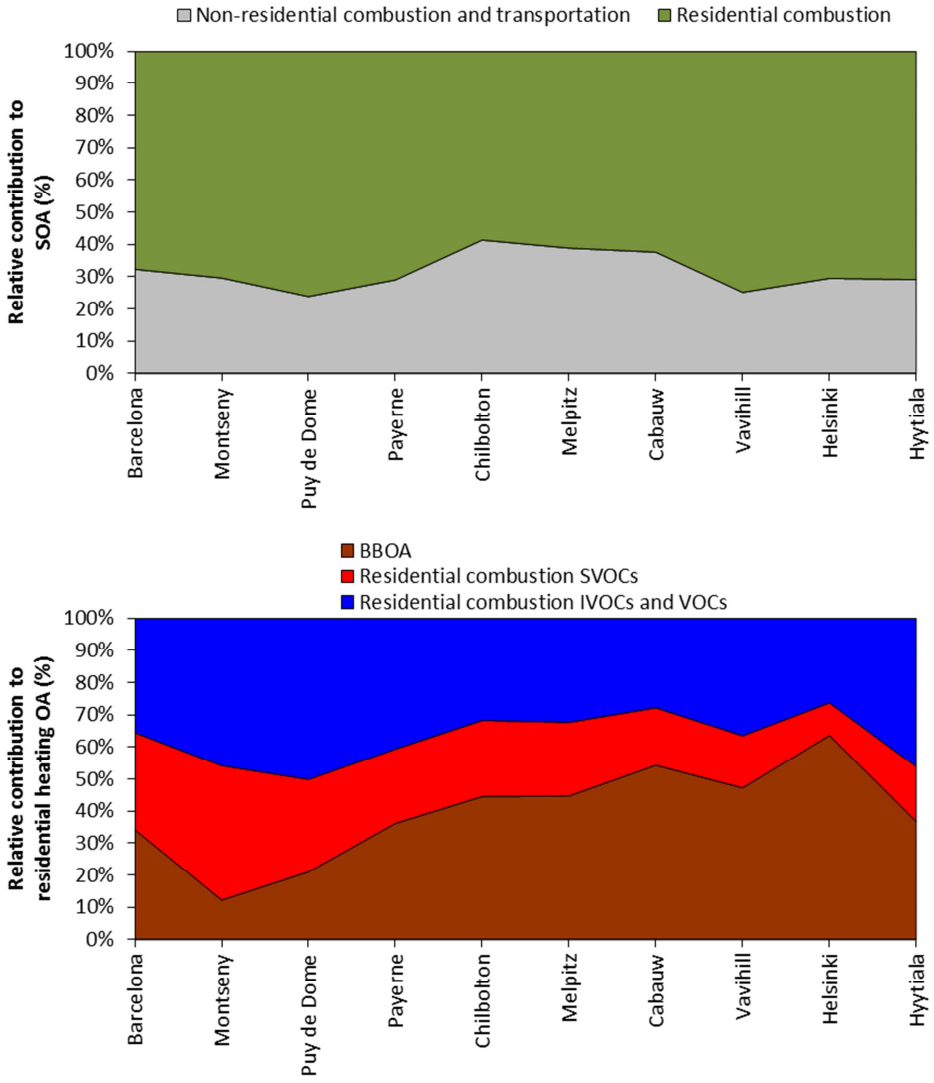

Figure 6.11. *Contribution of residential and non-residential combustion precursors to SOA at different sites (upper panel). Contribution of BBOA, SVOCs and higher volatility organic precursors to residential heating OA (lower panel). Stations are ordered from south to north.*

The residential combustion precursors were further apportioned to semi-volatile and higher volatility precursors (Figure 6.11, lower panel). In particular, SVOC precursors exhibit a south-to-north gradient with increasing contribution to the residential heating related OA for stations located in the southern part of the domain (maximum and minimum contributions of 42 and 17% in Montseny and Hyytiälä, respectively). Such a gradient also reflects the effect of temperature on the partitioning of semi-volatile organic material: the lower temperatures in the northern part of the domain will reduce the saturation concentration of the organic compounds allowing primary organic material to favour the particle phase and reducing the amount of SVOCs available that could act as SOA precursors. In the southern part of the domain, the higher temperature will favour more organic material in the semi-volatile range to reside in the gas-phase, rendering it available for oxidation. On the other hand, no south-to-north gradient was predicted for the higher volatility class of precursors. Source apportionment for different volatilities classes of the non-residential and transportation sectors is currently not implemented for this model application.

A comprehensive summary of the contribution to the total OA from all the sources (i.e. HOA, BBOA, residential combustion semi-volatile precursors, residential combustion higher volatility precursors and non-residential combustion precursors) is shown in Figure 6.12 at each of the measurement sites. Residential combustion precursors in the semi-volatile range contributed from 6 to 30% whereas higher volatility compounds contributed to a larger extent, i.e. from 15 to 38%. SOA from non-residential combustion precursors contributed from 10 to 37% to the total OA. The primary sources HOA and BBOA contributed from 3 to 30% and 1-39%, respectively. These results lead to the conclusion that the overall contribution of residential combustion to OA concentrations in Europe varies between 52% at stations in the UK and 75-76% at stations in Scandinavia.

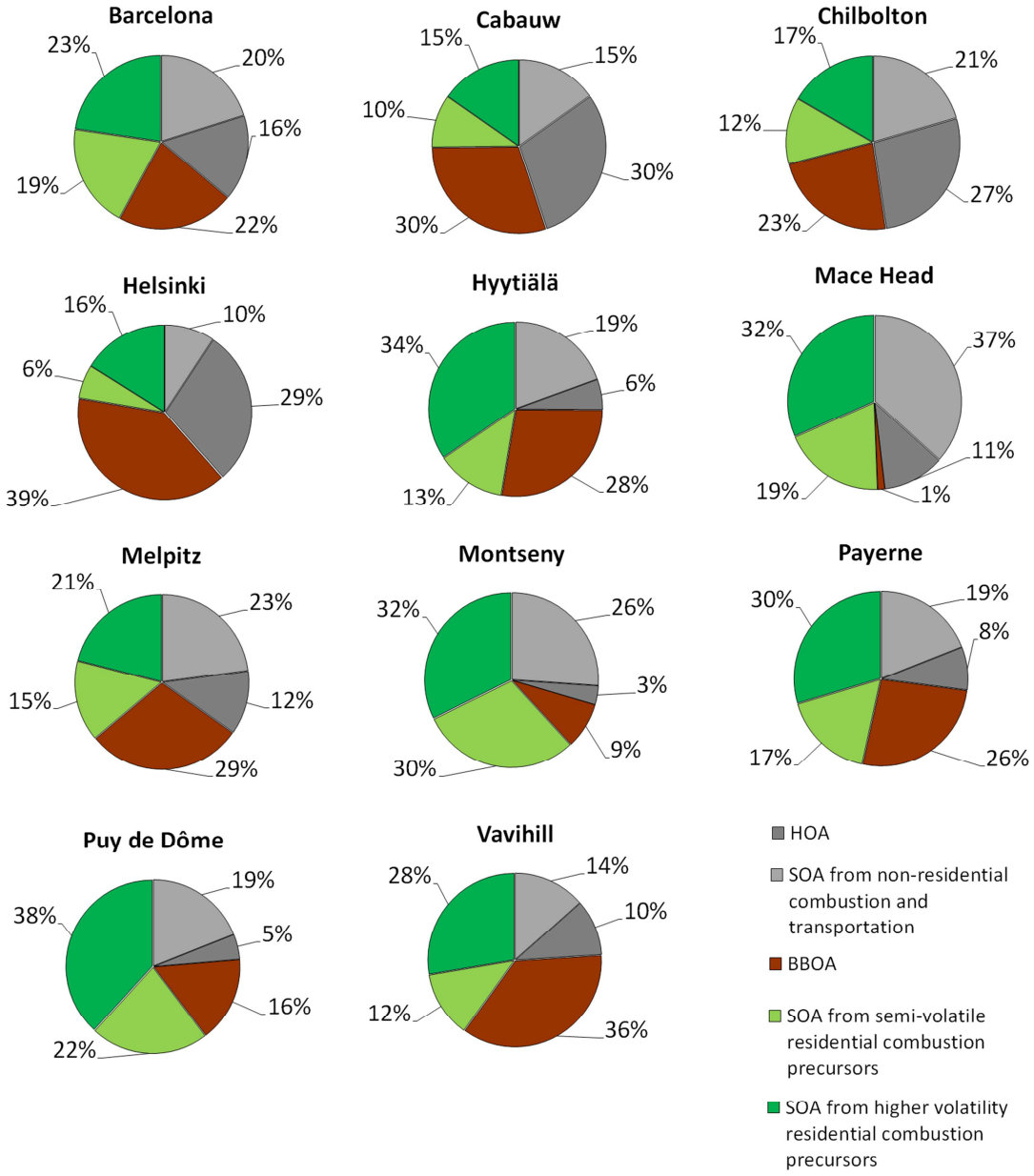

Figure 6.12 *Average modelled composition of OA at the 11 AMS sites for the period between 25 February and 26 March 2009.*

6.4 Conclusion

This study aims to evaluate recent VBS parameterizations in commonly used CTMs and to underline the importance of taking into account updated and more detailed SOA schemes as new ambient and chamber measurements elucidate the high complexity and strong variability of OA. In this context, a new VBS parameterization (based on recent wood burning experiments) implemented in CAMx was evaluated against high-resolution AMS measurements at 11 sites in

Europe during February-March 2009, one of the winter EMEP intensive measurement campaigns. Results obtained from this study were compared with those from our earlier work in which the original VBS scheme in CAMx was applied. A detailed source apportionment for the organic aerosol (OA) fraction was discussed. This study provided the following outcome:

- A considerable improvement was found for the modelled OA concentrations compared to our previous studies mainly due to the improved secondary organic aerosol (SOA) performance. The average bias for the 11 AMS sites decreased by about 60% although the model still underestimates the SOA fraction.
- Both model and PMF source apportionment based on measurements suggested that OA was mainly of secondary origin with smaller primary contribution, with average contribution of 13% and 25% for HOA and BBOA, respectively. The model performance for the HOA fraction was reasonably good at most of the sites except at the urban Barcelona site which could be related to the uncertainties in emissions or too much dilution in the model. On the other hand, the modelled BBOA was higher than the measurements at several stations indicating the need for further studies on residential heating emissions, their volatility distribution and oxidation pathway of the semi-volatile organic gases.
- Emissions from the residential heating sector (SNAP2) largely influenced the OA composition. The model primary BBOA fraction contributed from 46% to 77% of the total primary organic fraction (POA), with an average contribution of 65%. Non-residential combustion and transportation precursors contributed about 30-40% to SOA (with increasing contribution at urban and near-industrialized sites) whereas residential combustion (mainly related to wood burning) contributes to a larger extent, ~ 60-70%. Moreover, the contribution to OA from residential combustion precursors in different range of volatilities was also investigated: residential combustion gas-phase precursors in the semi-volatile range contributed from 6 to 30% with a positive south-to-north gradient. On the other hand, higher volatility residential combustion precursors contributed from 15 to 38% showing no specific gradient among the stations.

Acknowledgements

We thank the EURODELTA III modelling community, especially INERIS, TNO as well as ECMWF for providing various model input data. Calculations of land use data were performed at the Swiss National Supercomputing Centre (CSCS). We thank D. Oderbolz for developing the CAMxRunner framework to ensure reproducibility and data quality among the simulations and sensitivity tests. M. Tinguely for the visualization software and, RAMBOLL ENVIRON for their valuable comments. This study was financially supported by the Swiss Federal Office of Environment (FOEN). The research leading to these results received funding from the European Community's Seventh Framework Programme (FP7/2007-2013) under grant agreement no. 290605 (PSI-FELLOW), from the Competence Center Environment and Sustainability (CCES) (project OPTIWARES) and from the Swiss National Science Foundation (WOOSHI grant 140590). We thank D.A. Day for analysis on the DAURE dataset. Erik Swietlicki for the Vavihill dataset, Claudia Mohr for the Barcelona dataset, A. Kiendler-Scharr for Cabauw AMS data, Eriko Nemitz for the Chilboton data, Karine Sellegri for the Puy de Dôme dataset and Jose-Luis Jimenez for the measurements data in Montseny. The AMS measurements were funded through the European EUCAARI IP. We would like to acknowledge EMEP for the measurement data used here, HEA-PRTLI4, EPA Ireland, and the Science Foundation Ireland for facilitating measurements at Mace Head.

7

Findings and outlook

Organic aerosols constitute the major fraction of the total particulate matter (PM) mass. Despite recent scientific and technological advancement in the field of atmospheric science, their sources, formation mechanisms and transformation in the atmosphere are still not fully understood. In addition, various epidemiological studies underlined their negative effect on human health marking them as one of the main environmental concern of the present day. In this thesis intensive air quality modelling studies were performed at European scale within the EURODELTA-III model intercomparison exercise and model performances evaluated against different measurement networks. The work presented here, specifically focused on winter organic aerosol as novel wood burning smog chamber experiments and ambient aerosol mass spectrometer (AMS) measurements became available during the last years.

Four periods of EMEP (European Monitoring and Evaluation Programme) intensive measurement campaigns (June 2006, January 2007, September-October 2008 and February-March 2009) were evaluated against rural-background stations as in the European air quality database Airbase for selected gas phase species, i.e. NO_2, O_3, CO, SO_2 as well as $PM_{2.5}$. The model systematically under-predicted CO and NO_2 concentrations for all the four campaign likely because of insufficient emission or over-estimated daytime dilution (NO_2 mean fraction bias ranging (MFB) ranging from -54% in June 2006 and -28% for January-February 2007 and September-October 2008). Conversely O_3 and SO_2 concentration were found to be over-predicted, with MFB for O_3 around 48% in January-February 2007 and 2% for February-March 2009. Eventually, in addition to the not well represented dilution, the under-prediction in NO_2 concentrations might have reduced the night-time titration of O_3 which partially justify its over-prediction. A great influence of O_3 concentrations mapped at the boundary of the domain was found on the modelled inland O_3 concentration with the bias in the January-February 2007

period mainly attributed to an over-prediction of the O_3 at the boundary of the domain. The over-prediction of SO_2 on the other hand, was mainly attributed to uncertainties in emission injection height since most of the SO_2 are released by large combustion facilities at higher altitude in the domain. The daily variation of $PM_{2.5}$ observed at all the available Airbase rural-background stations was reproduced very well for all the four investigated periods (number of station varying from 48 in June 2006 and 110 in February-March 2009) with some days of high $PM_{2.5}$ loads for stations close to the southern border of the domain (Viznar station in Spain and Ayia Marina in Cyprus) not captured by the model, probably because of missing representation of Saharan dust events.

Comparisons with AMS measurements for the February-March 2009 period suggested that the model is able to capture the total non-refractory PM_1 mass with the inorganic fraction, especially NO_3^-, being over-predicted and the OA under-predicted. Sensitivity tests with reduced NH_3 emissions generally reduced the positive bias in NO_3^- suggesting potential uncertainties in NH_3 emissions and their seasonal variability. The organic fraction was investigated in more details by testing different assumption regarding evaporation and oxidation of primary organic material. A volatility basis set (VBS) framework was evaluated for the first time in Europe within the CAMx model, and evaluated against 11 aerosol mass spectrometer (AMS) measurements performed in the European domain during February-March 2009.Our first application underlined potential underestimation of primary organic emission from the residential heating sector (SNAP2 in the Selected Nomenclature for sources of Air Pollution). In particular, a better agreement between model and observations (mean fractional bias (MFB) of -47% for OA) was achieved when semi-volatile organic gases (SVOCs) were included in the model by multiplying the available gridded emission of primary organic aerosol (POA) by a factor of 3, as also indicated by partitioning theory data, recent VBS applications and new revisited emission inventories. On the other hand the under-prediction of the OA mass during the June 2006 episode was mainly attributed to BVOCs emissions and their evolution in the atmosphere which are uncertain and difficult to constrain with measurements. In this case the model was sensitive to an increase in biogenic emissions especially during periods with higher temperature and OA concentrations.

We performed extensive box model simulations of wood burning experiments conducted at two different temperatures (263 and 288 K) in a ~7 m^3 smog chamber facility. By combining new non-traditional volatile organic compounds NTVOCs measurements and already available partitioning data for primary wood burning emission we constrain the amounts of NTVOCs that act as SOA precursors. Our estimates indicated that the amount of NTVOCs emitted are approximately 4.75 times the amount of total organic material in the 0.1 and 1000 μg m^{-3} saturation concentration range (OM_{sv}). This ratio could be directly used in CTMs in the absence of explicit NTVOCs emissions for wood burning in combination with the proposed aging scheme. Specific parameters such as NTVOCs reaction rates ($k_{OH\text{-}NTVOCs}$), yields (Y) and enthalpies of evaporation of secondary organic aerosol (ΔH_{vapSOA}) were varied using brute force

simulations and values for best fitting solutions falling with physically realistic range were retrieved. Based on the reaction scheme used, reaction rates of the NTVOCs mixture range from 3.0 x 10^{-11} cm^3 $molec^{-1}$ s^{-1} to 4.0 x 10^{-11} cm^3 $molec^{-1}$ s^{-1}. The average enthalpy of evaporation of SOA surrogates was determined to be between 55000 J mol^{-1} and 35000 J mol^{-1} which implies a yield increase of c.a. 0.03 - 0.06 % K^{-1} with decreasing temperature.

The new retrieved VBS parameterization was implemented in the CAMx model and evaluated against ambient data the February-March 2009 period and results compared with our previous application. A considerable improvement compared to our previous study was found for the modelled OA mass due to an enhancement of the secondary fraction (up to 60% more OA compared to our previous application). The total OA mass measured at the 11 AMS site was very well reproduced by the model, in terms of station-to-station gradient and absolute concentrations with only few exceptions for the Barcelona and Chilbolton sites were the model under-predicts the OA concentrations to a larger extent. Both the model and positive matrix factorization (PMF) source apportionment studies suggested that the main fraction of the OA mass is of secondary origin at almost all the sites (with an average contribution of 62%) with the HOA and BBOA primary fraction contributing only to a minor extent (average contribution of 13 and 25%, respectively).

Non-residential combustion and transportation precursors contribute about 30-40% to SOA formation (with increasing contribution at urban and near-industrialized sites) whereas residential combustion (mainly related to wood burning) contributes to a larger extent, ~ 60-70%. Moreover, the contribution to OA from residential combustion precursors in different range of volatilities was also investigated: residential combustion gas-phase precursors in the semi-volatile range contribute from 6 to 30% with a positive south-to-north gradient. On the other hand, higher volatility residential combustion precursors contribute from 15 to 38% showing no specific gradient among the stations.

This work aimed to provide new links between novel available chamber data for wood-burning combustion emissions, simplified but constrained organic aerosol schemes and their application in chemical transport models (CTMs). Taking into account non-traditional SOA precursors together with detailed OA chemistry schemes is becoming more and more necessary as new ambient and chamber measurements are underlining the high complexity and strong variability of OA. Results are encouraging as both the modelling and experimental communities keeps providing larger datasets. In this context, the novel aerosol chemical speciation monitor instrument (ACSM), could provide the air quality modelling community with long-term aerosol composition data that are vital to validate model performance. Multiple ACMSs can be operated on the scale of months to years and simultaneously deployed in different part of the globe due to its relatively easy handling and reduced cost compare to the AMS. This will provide the modelling community with continuous non-refractory organic aerosol measurements in different part of the globe and at the same time, allowing for a more accurate spatial and temporal validation of the modelled non-refractory organic aerosol.

On the other hand, ambient measurements of IVOCs and VOCs are still very rare, for both anthropogenic and biogenic sources. There is a need to improve the measurement network of such compounds in Europe which might help on one side to better constrain the available emission inventories and on the other side to provide an additional estimation of the contribution of these compound to SOA.

Bibliography

Aksoyoglu, S., Keller, J., Barmpadimos, I., Oderbolz, D., Lanz, V.A., Prévôt, A.S.H., Baltensperger, U., 2011. Aerosol modelling in Europe with a focus on Switzerland during summer and winter episodes. Atmospheric Chem. Phys. 11, 7355–7373. doi:10.5194/acp-11-7355-2011

Aksoyoglu, S., Keller, J., Ciarelli, G., Prévôt, A.S.H., Baltensperger, U., 2014. A model study on changes of European and Swiss particulate matter, ozone and nitrogen deposition between 1990 and 2020 due to the revised Gothenburg protocol. Atmospheric Chem. Phys. 14, 13081–13095. doi:10.5194/acp-14-13081-2014

Albrecht, B.A., 1989. Aerosols, cloud microphysics, and fractional cloudiness. Science 245, 1227–1230. doi:10.1126/science.245.4923.1227

Appel, K.W., Gilliam, R.C., Davis, N., Zubrow, A., Howard, S.C., 2011. Overview of the Atmospheric Model Evaluation Tool (AMET) v1.1 for evaluating meteorological and air quality models. Environ. Modell. Softw. 26, 434–443.

Athanasopoulou, E., Vogel, H., Vogel, B., Tsimpidi, A.P., Pandis, S.N., Knote, C., Fountoukis, C., 2013. Modeling the meteorological and chemical effects of secondary organic aerosols during an EUCAARI campaign. Atmospheric Chem. Phys. 13, 625–645. doi:10.5194/acp-13-625-2013

Barmet, P., Dommen, J., DeCarlo, P.F., Tritscher, T., Praplan, A.P., Platt, S.M., Prévôt, A.S.H., Donahue, N.M., Baltensperger, U., 2012. OH clock determination by proton transfer reaction mass spectrometry at an environmental chamber. Atmos Meas Tech 5, 647–656. doi:10.5194/amt-5-647-2012

Baron, P.A. and Willeke, K. Aerosol measurement: principles, techniques, and applications. Wiley, 2001

Benedetti, A., Morcrette, J.-J., Boucher, O., Dethof, A., Engelen, R.J., Fisher, M., Flentje, H., Huneeus, N., Jones, L., Kaiser, J.W., Kinne, S., Mangold, A., Razinger, M., Simmons, A.J., Suttie, M., 2009. Aerosol analysis and forecast in the European Centre for Medium-Range Weather Forecasts Integrated Forecast System: 2. Data assimilation. J. Geophys. Res. Atmospheres 114, D13205. doi:10.1029/2008JD011115

Bergström, R., Denier van der Gon, H.A.C., Prévôt, A.S.H., Yttri, K.E., Simpson, D., 2012. Modelling of organic aerosols over Europe (2002–2007) using a volatility basis set (VBS) framework: application of different assumptions regarding the formation of secondary organic aerosol. Atmos Chem Phys 12, 8499–8527. doi:10.5194/acp-12-8499-2012

Bessagnet, B., Colette, A., Meleux, F., Rouïl, L., Ung, A., Favez, O., Cuvelier, C., Thunis, P., Tsyro, S., Stern, R., Manders, A., Kranenburg, R., Aulinger, A., Bieser, J., Mircea, M., Briganti, A., Cappelletti, A., Calori, G., Finardi, S., Silibello, C., Ciarelli, G., Aksoyoglu, S., Prévôt, A., Pay, M.T., Baldasano, J.M., García Vivanco, M., Garrido, J.L., Palomino, I., Martín, F., Pirovano, G., Roberts, P., Gonzalez, L., White, L., Menut, L., Dupont, J.C., Carnevale, C., Pederzoli, A., 2014. The EURODELTA III exercise – Model evaluation with observations issued from the 2009 EMEP intensive period and standard measurements in Feb/Mar 2009

Bessagnet, B., Pirovano, G., Mircea, M., Cuvelier, C., Aulinger, A., Calori, G., Ciarelli, G., Manders, A., Stern, R., Tsyro, S., García Vivanco, M., Thunis, P., Pay, M.-T., Colette, A., Couvidat, F., Meleux, F., Rouïl, L., Ung, A., Aksoyoglu, S., Baldasano, J.M., Bieser, J., Briganti, G., Cappelletti, A., D'Isodoro, M., Finardi, S., Kranenburg, R., Silibello, C., Carnevale, C., Aas, W., Dupont, J.-C., Fagerli, H., Gonzalez, L., Menut, L., Prévôt, A.S.H., Roberts, P., White, L., 2016. Presentation of the EURODELTA III inter-comparison exercise - Evaluation of the chemistry transport models performance on criteria pollutants and joint analysis with meteorology. Atmospheric Chem. Phys. Discuss. 1–61. doi:10.5194/acp-2015-736

Boylan, J.W., Russell, A.G., 2006. PM and light extinction model performance metrics, goals, and criteria for three-dimensional air quality models. Atmos. Environ. 40, 4946–4959. doi:10.1016/j.atmosenv.2005.09.087

Bruns, E.A., El Haddad, I., Slowik, J.G., Kilic, D., Klein, F., Baltensperger, U., Prévôt, A.S.H., 2016. Identification of significant precursor gases of secondary organic aerosols from residential wood combustion. Sci. Rep. 6, 27881. doi:10.1038/srep27881

Bruns, E.A., Krapf, M., Orasche, J., Huang, Y., Zimmermann, R., Drinovec, L., Močnik, G., El-Haddad, I., Slowik, J.G., Dommen, J., Baltensperger, U., Prévôt, A.S.H., 2015. Characterization of primary and secondary wood combustion products generated under different burner loads. Atmospheric Chem. Phys. 15, 2825–2841. doi:10.5194/acp-15-2825-2015

Canonaco, F., Crippa, M., Slowik, J.G., Baltensperger, U., Prévôt, A.S.H., 2013. SoFi, an IGOR-based interface for the efficient use of the generalized multilinear engine (ME-2) for the source apportionment: ME-2 application to aerosol mass

spectrometer data. Atmospheric Meas. Tech. 6, 3649–3661. doi:10.5194/amt-6-3649-2013

Canonaco, F., Slowik, J.G., Baltensperger, U., Prévôt, A.S.H., 2015. Seasonal differences in oxygenated organic aerosol composition: implications for emissions sources and factor analysis. Atmos Chem Phys 15, 6993–7002. doi:10.5194/acp-15-6993-2015

Cappa, C.D. and Jimenez, J.L., 2010. Quantitative estimates of the volatility of ambient organic aerosol. Atmospheric Chem. Phys. 10, 5409–5424. doi:10.5194/acp-10-5409-2010

Chang, J.S., Brost, R.A., Isaksen, I.S.A., Madronich, S., Middleton, P., Stockwell, W.R., Walcek, C.J., 1987. A three-dimensional Eulerian acid deposition model: Physical concepts and formulation. J. Geophys. Res. Atmospheres 92, 14681–14700. doi:10.1029/JD092iD12p14681

Ciarelli, G., Aksoyoglu, S., Crippa, M., Jimenez, J.-L., Nemitz, E., Sellegri, K., Äijälä, M., Carbone, S., Mohr, C., O'Dowd, C., Poulain, L., Baltensperger, U., Prévôt, A.S.H., 2016a. Evaluation of European air quality modelled by CAMx including the volatility basis set scheme. Atmospheric Chem. Phys. 16, 10313–10332. doi:10.5194/acp-16-10313-2016a

Ciarelli, G., El Haddad, I., Bruns, E., Aksoyoglu, S., Möhler, O., Baltensperger, U., Prévôt, A.S.H., 2016b. Constraining a hybrid volatility basis set model for aging of wood burning emissions using smog chamber experiments. Geosci. Model Dev. Discuss. 1–31. doi:10.5194/gmd-2016-163

Colette, A., Granier, C., Hodnebrog, ø., Jakobs, H., Maurizi, A., Nyiri, A., Bessagnet, B., D'Angiola, A., D'Isidoro, M., Gauss, M., Meleux, F., Memmesheimer, M., Mieville, A., Rouïl, L., Russo, F., Solberg, S., Stordal, F., Tampieri, F., 2011. Air quality trends in Europe over the past decade: a first multi-model assessment. Atmospheric Chem. Phys. 11, 11657–11678. doi:10.5194/acp-11-11657-2011

Crippa, M., Canonaco, F., Lanz, V.A., Äijälä, M., Allan, J.D., Carbone, S., Capes, G., Ceburnis, D., Dall'Osto, M., Day, D.A., DeCarlo, P.F., Ehn, M., Eriksson, A., Freney, E., Hildebrandt Ruiz, L., Hillamo, R., Jimenez, J.L., Junninen, H., Kiendler-Scharr, A., Kortelainen, A.-M., Kulmala, M., Laaksonen, A., Mensah, A.A., Mohr, C., Nemitz, E., O'Dowd, C., Ovadnevaite, J., Pandis, S.N., Petäjä, T., Poulain, L., Saarikoski, S., Sellegri, K., Swietlicki, E., Tiitta, P., Worsnop, D.R., Baltensperger, U., Prévôt, A.S.H., 2014. Organic aerosol components derived from 25 AMS data sets across Europe using a consistent ME-2 based source apportionment approach. Atmospheric Chem. Phys. 14, 6159–6176. doi:10.5194/acp-14-6159-2014

Crippa, M., DeCarlo, P.F., Slowik, J.G., Mohr, C., Heringa, M.F., Chirico, R., Poulain, L., Freutel, F., Sciare, J., Cozic, J., Di Marco, C.F., Elsasser, M., Nicolas, J.B., Marchand, N., Abidi, E., Wiedensohler, A., Drewnick, F., Schneider, J., Borrmann, S., Nemitz, E., Zimmermann, R., Jaffrezo, J.-L., Prévôt, A.S.H., Baltensperger, U., 2013. Wintertime aerosol chemical composition and source apportionment of the organic fraction in the metropolitan area of Paris. Atmos Chem Phys 13, 961–981. doi:10.5194/acp-13-961-2013

Cubison, M.J., Ortega, A.M., Hayes, P.L., Farmer, D.K., Day, D., Lechner, M.J., Brune, W.H., Apel, E., Diskin, G.S., Fisher, J.A., Fuelberg, H.E., Hecobian, A., Knapp, D.J., Mikoviny, T., Riemer, D., Sachse, G.W., Sessions, W., Weber, R.J., Weinheimer, A.J., Wisthaler, A., Jimenez, J.L., 2011. Effects of aging on organic aerosol from open biomass burning smoke in aircraft and laboratory studies. Atmos Chem Phys 11, 12049–12064. doi:10.5194/acp-11-12049-2011

Denier van der Gon, H.A.C., Bergström, R., Fountoukis, C., Johansson, C., Pandis, S.N., Simpson, D., Visschedijk, A.J.H., 2015. Particulate emissions from residential wood combustion in Europe – revised estimates and an evaluation. Atmos Chem Phys 15, 6503–6519. doi:10.5194/acp-15-6503-2015

Donahue, N.M., Robinson, A.L., Stanier, C.O., Pandis, S.N., 2006. Coupled Partitioning, Dilution, and Chemical Aging of Semivolatile Organics. Environ. Sci. Technol. 40, 2635–2643. doi:10.1021/es052297c

Donahue, N.M., Epstein, S.A., Pandis, S.N., Robinson, A.L., 2011. A two-dimensional volatility basis set: 1. organic-aerosol mixing thermodynamics. Atmos Chem Phys 11, 3303–3318. doi:10.5194/acp-11-3303-2011

Donahue, N.M., Henry, K.M., Mentel, T.F., Kiendler-Scharr, A., Spindler, C., Bohn, B., Brauers, T., Dorn, H.P., Fuchs, H., Tillmann, R., Wahner, A., Saathoff, H., Naumann, K.-H., Mohler, O., Leisner, T., Muller, L., Reinnig, M.-C., Hoffmann, T., Salo, K., Hallquist, M., Frosch, M., Bilde, M., Tritscher, T., Barmet, P., Praplan, A.P., DeCarlo, P.F., Dommen, J., Prevot, A.S.H., Baltensperger, U., 2012a. Aging of biogenic secondary organic aerosol via gas-phase OH radical reactions. Proc. Natl. Acad. Sci. 109, 13503–13508. doi:10.1073/pnas.1115186109

Donahue, N.M., Kroll, J.H., Pandis, S.N., Robinson, A.L., 2012b. A two-dimensional volatility basis set – Part 2: Diagnostics of organic-aerosol evolution. Atmos Chem Phys 12, 615–634. doi:10.5194/acp-12-615-2012

Donahue, N.M., Chuang, W., Epstein, S.A., Kroll, J.H., Worsnop, D.R., Robinson, A.L., Adams, P.J., Pandis, S.N., 2013. Why do organic aerosols exist? Understanding aerosol lifetimes using the two-dimensional volatility basis set. Environ. Chem. 10, 151. doi:10.1071/EN13022

Drinovec, L., Močnik, G., Zotter, P., Prévôt, A.S.H., Ruckstuhl, C., Coz, E., Rupakheti, M., Sciare, J., Müller, T., Wiedensohler, A., Hansen, A.D.A., 2015. The "dual-spot" Aethalometer: an improved measurement of aerosol black carbon with real-time loading compensation. Atmos Meas Tech 8, 1965–1979. doi:10.5194/amt-8-1965-2015

Elser, M., Huang, R.-J., Wolf, R., Slowik, J.G., Wang, Q., Canonaco, F., Li, G., Bozzetti, C., Daellenbach, K.R., Huang, Y., Zhang, R., Li, Z., Cao, J., Baltensperger, U., El-Haddad, I., Prévôt, A.S.H., 2016. New insights into PM2.5 chemical composition and sources in two major cities in China during extreme haze events using aerosol mass spectrometry. Atmos Chem Phys 16, 3207–3225. doi:10.5194/acp-16-3207-2016

ENVIRON, 2011. User's Guide, Comprehensive Air Quality Model with Extensions (CAMx), Version 5.40, Environ International Corporation, California.

ETC/ACC, 2004. Improvement of classifications European monitoring stations for AirBase – a quality control. Technical Paper.

European Commission, Joint Research Centre, 2011. EURODELTA - II Evaluation of a Sectoral Approach to Integrated Assessment Modelling Including the Mediterranean Sea. Dictus Publishing, Saarbrücken.

Favez, O., El Haddad, I., Piot, C., Boréave, A., Abidi, E., Marchand, N., Jaffrezo, J.-L., Besombes, J.-L., Personnaz, M.-B., Sciare, J., Wortham, H., George, C., D'Anna, B., 2010. Inter-comparison of source apportionment models for the estimation of wood burning aerosols during wintertime in an Alpine city (Grenoble, France). Atmos Chem Phys 10, 5295–5314. doi:10.5194/acp-10-5295-2010

Finlayson-Pitts and B.J., Pitts, J.N., 2009. Chemistry of the upper and lower atmosphere: theory, experiments, and applications, Academic Press, San Diego, Calif.

Fountoukis, C., Megaritis, A.G., Skyllakou, K., Charalampidis, P.E., Pilinis, C., Denier van der Gon, H.A.C., Crippa, M., Canonaco, F., Mohr, C., Prévôt, A.S.H., Allan, J.D., Poulain, L., Petäjä, T., Tiitta, P., Carbone, S., Kiendler-Scharr, A., Nemitz, E., O'Dowd, C., Swietlicki, E., Pandis, S.N., 2014. Organic aerosol concentration and composition over Europe: insights from comparison of regional model predictions with aerosol mass spectrometer factor analysis. Atmos Chem Phys 14, 9061–9076. doi:10.5194/acp-14-9061-2014

Freney, E.J., Sellegri, K., Canonaco, F., Boulon, J., Hervo, M., Weigel, R., Pichon, J.M., Colomb, A., Prévôt, A.S.H., Laj, P., 2011. Seasonal variations in aerosol

particle composition at the puy-de-Dôme research station in France. Atmospheric Chem. Phys. 11, 13047–13059. doi:10.5194/acp-11-13047-2011

Fuzzi, S., Baltensperger, U., Carslaw, K., Decesari, S., Denier van der Gon, H., Facchini, M.C., Fowler, D., Koren, I., Langford, B., Lohmann, U., Nemitz, E., Pandis, S., Riipinen, I., Rudich, Y., Schaap, M., Slowik, J.G., Spracklen, D.V., Vignati, E., Wild, M., Williams, M., Gilardoni, S., 2015. Particulate matter, air quality and climate: lessons learned and future needs. Atmos Chem Phys 15, 8217–8299. doi:10.5194/acp-15-8217-2015

Grieshop, A.P., Logue, J.M., Donahue, N.M., Robinson, A.L., 2009. Laboratory investigation of photochemical oxidation of organic aerosol from wood fires 1: measurement and simulation of organic aerosol evolution. Atmospheric Chem. Phys. 9, 1263–1277. doi:10.5194/acp-9-1263-2009

Guenther, A.B., Jiang, X., Heald, C.L., Sakulyanontvittaya, T., Duhl, T., Emmons, L.K., Wang, X., 2012. The Model of Emissions of Gases and Aerosols from Nature version 2.1 (MEGAN2.1): an extended and updated framework for modeling biogenic emissions. Geosci. Model Dev. 5, 1471–1492. doi:10.5194/gmd-5-1471-2012

Hallquist, M., Wenger, J.C., Baltensperger, U., Rudich, Y., Simpson, D., Claeys, M., Dommen, J., Donahue, N.M., George, C., Goldstein, A.H., Hamilton, J.F., Herrmann, H., Hoffmann, T., Iinuma, Y., Jang, M., Jenkin, M.E., Jimenez, J.L., Kiendler-Scharr, A., Maenhaut, W., McFiggans, G., Mentel, T.F., Monod, A., Prévôt, A.S.H., Seinfeld, J.H., Surratt, J.D., Szmigielski, R., Wildt, J., 2009. The formation, properties and impact of secondary organic aerosol: current and emerging issues. Atmospheric Chem. Phys. 9, 5155–5236. doi:10.5194/acp-9-5155-2009

Hawkins, L.N., Russell, L.M., Covert, D.S., Quinn, P.K., Bates, T.S., 2010. Carboxylic acids, sulfates, and organosulfates in processed continental organic aerosol over the southeast Pacific Ocean during VOCALS-REx 2008. J. Geophys. Res. 115. doi:10.1029/2009JD013276

Heald, C.L., Kroll, J.H., Jimenez, J.L., Docherty, K.S., DeCarlo, P.F., Aiken, A.C., Chen, Q., Martin, S.T., Farmer, D.K., Artaxo, P., 2010. A simplified description of the evolution of organic aerosol composition in the atmosphere. Geophys. Res. Lett. 37, n/a-n/a. doi:10.1029/2010GL042737

Heringa, M.F., DeCarlo, P.F., Chirico, R., Tritscher, T., Clairotte, M., Mohr, C., Crippa, M., Slowik, J.G., Pfaffenberger, L., Dommen, J., Weingartner, E., Prévôt, A.S.H., Baltensperger, U., 2012. A new method to discriminate secondary organic aerosols from different sources using high-resolution aerosol mass spectra. Atmospheric Chem. Phys. 12, 2189–2203. doi:10.5194/acp-12-2189-2012

Highwood, E.J. and Kinnersley, R.P., 2006. When smoke gets in our eyes: the multiple impacts of atmospheric black carbon on climate, air quality and health. Environ. Int. 32, 560–566. doi:10.1016/j.envint.2005.12.003

Hodzic, A., Jimenez, J.L., Madronich, S., Aiken, A.C., Bessagnet, B., Curci, G., Fast, J., Lamarque, J.-F., Onasch, T.B., Roux, G., Schauer, J.J., Stone, E.A., Ulbrich, I.M., 2009. Modeling organic aerosols during MILAGRO: importance of biogenic secondary organic aerosols. Atmospheric Chem. Phys. 9, 6949–6981. doi:10.5194/acp-9-6949-2009

Huang, R.-J., Zhang, Y., Bozzetti, C., Ho, K.-F., Cao, J.-J., Han, Y., Daellenbach, K.R., Slowik, J.G., Platt, S.M., Canonaco, F., Zotter, P., Wolf, R., Pieber, S.M., Bruns, E.A., Crippa, M., Ciarelli, G., Piazzalunga, A., Schwikowski, M., Abbaszade, G., Schnelle-Kreis, J., Zimmermann, R., An, Z., Szidat, S., Baltensperger, U., Haddad, I.E., Prévôt, A.S.H., 2014. High secondary aerosol contribution to particulate pollution during haze events in China. Nature 514, 218–222. doi:10.1038/nature13774

Inness, A., Baier, F., Benedetti, A., Bouarar, I., Chabrillat, S., Clark, H., Clerbaux, C., Coheur, P., Engelen, R.J., Errera, Q., Flemming, J., George, M., Granier, C., Hadji-Lazaro, J., Huijnen, V., Hurtmans, D., Jones, L., Kaiser, J.W., Kapsomenakis, J., Lefever, K., Leitão, J., Razinger, M., Richter, A., Schultz, M.G., Simmons, A.J., Suttie, M., Stein, O., Thépaut, J.-N., Thouret, V., Vrekoussis, M., Zerefos, C., the MACC team, 2013. The MACC reanalysis: an 8 yr data set of atmospheric composition. Atmospheric Chem. Phys. 13, 4073–4109. doi:10.5194/acp-13-4073-2013

IPCC (Ed.), 2013. Clouds and Aerosols, in: Climate Change 2013 - The Physical Science Basis. Cambridge University Press, Cambridge, pp. 571–658.

Jayne, J.T., Leard, D.C., Zhang, X., Davidovits, P., Smith, K.A., Kolb, C.E., Worsnop, D.R., 2000. Development of an Aerosol Mass Spectrometer for Size and Composition Analysis of Submicron Particles. Aerosol Sci. Technol. 33, 49–70. doi:10.1080/027868200410840

Jimenez, J.L., Canagaratna, M.R., Donahue, N.M., Prevot, A.S.H., Zhang, Q., Kroll, J.H., DeCarlo, P.F., Allan, J.D., Coe, H., Ng, N.L., Aiken, A.C., Docherty, K.S., Ulbrich, I.M., Grieshop, A.P., Robinson, A.L., Duplissy, J., Smith, J.D., Wilson, K.R., Lanz, V.A., Hueglin, C., Sun, Y.L., Tian, J., Laaksonen, A., Raatikainen, T., Rautiainen, J., Vaattovaara, P., Ehn, M., Kulmala, M., Tomlinson, J.M., Collins, D.R., Cubison, M.J., Dunlea, E.J., Huffman, J.A., Onasch, T.B., Alfarra, M.R., Williams, P.I., Bower, K., Kondo, Y., Schneider, J., Drewnick, F., Borrmann, S., Weimer, S., Demerjian, K., Salcedo, D., Cottrell, L., Griffin, R., Takami, A., Miyoshi, T., Hatakeyama, S., Shimono, A., Sun, J.Y., Zhang, Y.M., Dzepina, K., Kimmel, J.R., Sueper, D., Jayne, J.T., Herndon, S.C., Trimborn, A.M., Williams, L.R., Wood, E.C., Middlebrook, A.M., Kolb, C.E.,

Baltensperger, U., Worsnop, D.R., 2009. Evolution of organic aerosols in the atmosphere. Science 326, 1525–1529. doi:10.1126/science.1180353

Jo, D.S., Park, R.J., Kim, M.J., Spracklen, D.V., 2013. Effects of chemical aging on global secondary organic aerosol using the volatility basis set approach. Atmos. Environ. 81, 230–244. doi:10.1016/j.atmosenv.2013.08.055

Jolleys, M.D., Coe, H., McFiggans, G., Capes, G., Allan, J.D., Crosier, J., Williams, P.I., Allen, G., Bower, K.N., Jimenez, J.L., Russell, L.M., Grutter, M., Baumgardner, D., 2012. Characterizing the Aging of Biomass Burning Organic Aerosol by Use of Mixing Ratios: A Meta-analysis of Four Regions. Environ. Sci. Technol. 46, 13093–13102. doi:10.1021/es302386v

Kleindienst, T.E., Lewandowski, M., Offenberg, J.H., Jaoui, M., Edney, E.O., 2007. Ozone-isoprene reaction: Re-examination of the formation of secondary organic aerosol. Geophys. Res. Lett. 34, L01805. doi:10.1029/2006GL027485

Knote, C., Brunner, D., Vogel, H., Allan, J., Asmi, A., Äijälä, M., Carbone, S., van der Gon, H.D., Jimenez, J.L., Kiendler-Scharr, A., Mohr, C., Poulain, L., Prévôt, A.S.H., Swietlicki, E., Vogel, B., 2011. Towards an online-coupled chemistry-climate model: evaluation of trace gases and aerosols in COSMO-ART. Geosci Model Dev 4, 1077–1102. doi:10.5194/gmd-4-1077-2011

Koo, B., Knipping, E., Yarwood, G., 2014. 1.5-Dimensional volatility basis set approach for modeling organic aerosol in CAMx and CMAQ. Atmos. Environ. 95, 158–164. doi:10.1016/j.atmosenv.2014.06.031

Kuenen, J.J.P., Denier van der Gon, H.A.C., Visschedijk, A., Van der Brugh, H., Van Gijlswijk, R., 2011. MACC European emission inventory for the years 2003–2007, TNO report 716 TNO- 060-UT-2011-00588, TNO, Utrecht,.

Kuenen, J.J.P., Visschedijk, A.J.H., Jozwicka, M., Denier van der Gon, H.A.C., 2014. TNO-MACC_II emission inventory; a multi-year (2003–2009) consistent high-resolution European emission inventory for air quality modelling. Atmos Chem Phys 14, 10963–10976. doi:10.5194/acp-14-10963-2014

Kulmala, M., Asmi, A., Lappalainen, H.K., Baltensperger, U., Brenguier, J.-L., Facchini, M.C., Hansson, H.-C., Hov, Ø., O'Dowd, C.D., Pöschl, U., Wiedensohler, A., Boers, R., Boucher, O., de Leeuw, G., Denier van der Gon, H.A.C., Feichter, J., Krejci, R., Laj, P., Lihavainen, H., Lohmann, U., McFiggans, G., Mentel, T., Pilinis, C., Riipinen, I., Schulz, M., Stohl, A., Swietlicki, E., Vignati, E., Alves, C., Amann, M., Ammann, M., Arabas, S., Artaxo, P., Baars, H., Beddows, D.C.S., Bergström, R., Beukes, J.P., Bilde, M., Burkhart, J.F., Canonaco, F., Clegg, S.L., Coe, H., Crumeyrolle, S., D'Anna, B., Decesari, S., Gilardoni, S., Fischer, M., Fjaeraa, A.M., Fountoukis, C., George,

C., Gomes, L., Halloran, P., Hamburger, T., Harrison, R.M., Herrmann, H., Hoffmann, T., Hoose, C., Hu, M., Hyvärinen, A., Hõrrak, U., Iinuma, Y., Iversen, T., Josipovic, M., Kanakidou, M., Kiendler-Scharr, A., Kirkevåg, A., Kiss, G., Klimont, Z., Kolmonen, P., Komppula, M., Kristjánsson, J.-E., Laakso, L., Laaksonen, A., Labonnote, L., Lanz, V.A., Lehtinen, K.E.J., Rizzo, L.V., Makkonen, R., Manninen, H.E., McMeeking, G., Merikanto, J., Minikin, A., Mirme, S., Morgan, W.T., Nemitz, E., O'Donnell, D., Panwar, T.S., Pawlowska, H., Petzold, A., Pienaar, J.J., Pio, C., Plass-Duelmer, C., Prévôt, A.S.H., Pryor, S., Reddington, C.L., Roberts, G., Rosenfeld, D., Schwarz, J., Seland, Ø., Sellegri, K., others, 2011. General overview: European Integrated project on Aerosol Cloud Climate and Air Quality interactions (EUCAARI) – integrating aerosol research from nano to global scales. Atmospheric Chem. Phys. 11, 13061–13143. doi:10.5194/acp-11-13061-2011

Kulmala, M., Asmi, A., Lappalainen, H.K., Carslaw, K.S., Pöschl, U., Baltensperger, U., Hov, Ø., Brenquier, J.-L., Pandis, S.N., Facchini, M.C., Hansson, H.-C., Wiedensohler, A., O'Dowd, C.D., 2009. Introduction: European Integrated Project on Aerosol Cloud Climate and Air Quality interactions (EUCAARI) – integrating aerosol research from nano to global scales. Atmos Chem Phys 9, 2825–2841. doi:10.5194/acp-9-2825-2009

Lane, T.E., Donahue, N.M., Pandis, S.N., 2008. Simulating secondary organic aerosol formation using the volatility basis-set approach in a chemical transport model. Atmos. Environ. 42, 7439–7451. doi:10.1016/j.atmosenv.2008.06.026

Langmann, B., Sellegri, K., Freney, E., 2014. Secondary organic aerosol formation during June 2010 in Central Europe: measurements and modelling studies with a mixed thermodynamic-kinetic approach. Atmospheric Chem. Phys. 14, 3831–3842. doi:10.5194/acp-14-3831-2014

Li, Y.P., Elbern, H., Lu, K.D., Friese, E., Kiendler-Scharr, A., Mentel, T.F., Wang, X.S., Wahner, A., Zhang, Y.H., 2013. Updated aerosol module and its application to simulate secondary organic aerosols during IMPACT campaign May 2008. Atmospheric Chem. Phys. 13, 6289–6304. doi:10.5194/acp-13-6289-2013

Lipsky and E.M., Robinson, A.L., 2006. Effects of Dilution on Fine Particle Mass and Partitioning of Semivolatile Organics in Diesel Exhaust and Wood Smoke. Environ. Sci. Technol. 40, 155–162. doi:10.1021/es050319p

Madronich, S., 2002. The Tropospheric Visible Ultra-violet (TUV) model web page, National Center for Atmospheric Research, Boulder, CO., http://www.acd.ucar.edu/TUV/.

May, A.A., Levin, E.J.T., Hennigan, C.J., Riipinen, I., Lee, T., Collett, J.L., Jimenez, J.L., Kreidenweis, S.M., Robinson, A.L., 2013. Gas-particle partitioning of

primary organic aerosol emissions: 3. Biomass burning. J. Geophys. Res. Atmospheres 118, 2013JD020286. doi:10.1002/jgrd.50828

Mensah, A.A., Holzinger, R., Otjes, R., Trimborn, A., Mentel, T.F., ten Brink, H., Henzing, B., Kiendler-Scharr, A., 2012. Aerosol chemical composition at Cabauw, The Netherlands as observed in two intensive periods in May 2008 and March 2009. Atmospheric Chem. Phys. 12, 4723–4742. doi:10.5194/acp-12-4723-2012

Murphy, B.N., Donahue, N.M., Fountoukis, C., Dall'Osto, M., O'Dowd, C., Kiendler-Scharr, A., Pandis, S.N., 2012. Functionalization and fragmentation during ambient organic aerosol aging: application of the 2-D volatility basis set to field studies. Atmospheric Chem. Phys. 12, 10797–10816. doi:10.5194/acp-12-10797-2012

Murphy, B.N., Donahue, N.M., Fountoukis, C., Pandis, S.N., 2011. Simulating the oxygen content of ambient organic aerosol with the 2D volatility basis set. Atmos Chem Phys 11, 7859–7873. doi:10.5194/acp-11-7859-2011

Murphy and B.N., Pandis, S.N., 2009. Simulating the Formation of Semivolatile Primary and Secondary Organic Aerosol in a Regional Chemical Transport Model. Environ. Sci. Technol. 43, 4722–4728. doi:10.1021/es803168a

NASA/GSFC, 2005. Total ozone mapping spectrometer: http://toms.gsfc. nasa.gov/ozone/ozone.html.

Nenes, A., Pandis, S.N., Pilinis, C., 1998. ISORROPIA: a new thermodynamic equilibrium model for multiphase multicomponent inorganic aerosols, Aquat. Geochem., 4, 123–152, 1998. Aquat. Geochem. 4, 123–152.

Ng, N.L., Herndon, S.C., Trimborn, A., Canagaratna, M.R., Croteau, P.L., Onasch, T.B., Sueper, D., Worsnop, D.R., Zhang, Q., Sun, Y.L., Jayne, J.T., 2011. An Aerosol Chemical Speciation Monitor (ACSM) for Routine Monitoring of the Composition and Mass Concentrations of Ambient Aerosol. Aerosol Sci. Technol. 45, 780–794. doi:10.1080/02786826.2011.560211

Nussbaumer, T., Czasch, C., Klippel, N., Johansson, L., Tullin, C., 2008a. Particulate Emissions from Biomass Combustion in IEA Countries, Survey on Measurements and Emission Factors, International Energy Agency (IEA) Bioenergy Task 32, Zurich.

Nussbaumer, T., Klippel, N., Johansson, L., 2008b. Survey on Measurements and Emission Factors on Particulate Matter from Biomass Combustion in IEA Countries, 16th European Biomass Conference and Exhibition, Valencia, Spain, 2–6 June 2008, Oral Presentation OA 9.2.

O'Brien, J.J., 1970. A Note on the Vertical Structure of the Eddy Exchange Coefficient in the Planetary Boundary Layer. J. Atmospheric Sci. 27, 1213–1215. doi:10.1175/1520-0469(1970)027<1213:ANOTVS>2.0.CO;2

Ots, R., Young, D.E., Vieno, M., Xu, L., Dunmore, R.E., Allan, J.D., Coe, H., Williams, L.R., Herndon, S.C., Ng, N.L., Hamilton, J.F., Bergström, R., Di Marco, C., Nemitz, E., Mackenzie, I.A., Kuenen, J.J.P., Green, D.C., Reis, S., Heal, M.R., 2016. Simulating secondary organic aerosol from missing diesel-related intermediate-volatility organic compound emissions during the Clean Air for London (ClearfLo) campaign. Atmospheric Chem. Phys. 16, 6453–6473. doi:10.5194/acp-16-6453-2016

Paatero, P., 1999. The Multilinear Engine: A Table-Driven, Least Squares Program for Solving Multilinear Problems, including the n-Way Parallel Factor Analysis Model. J. Comput. Graph. Stat. 8, 854. doi:10.2307/1390831

Paatero, P. and Tapper, U., 1994. Positive matrix factorization: A non-negative factor model with optimal utilization of error estimates of data values. Environmetrics 5, 111–126. doi:10.1002/env.3170050203

Pandolfi, M., Querol, X., Alastuey, A., Jimenez, J.L., Jorba, O., Day, D., Ortega, A., Cubison, M.J., Comerón, A., Sicard, M., Mohr, C., Prévôt, A.S.H., Minguillón, M.C., Pey, J., Baldasano, J.M., Burkhart, J.F., Seco, R., Peñuelas, J., van Drooge, B.L., Artiñano, B., Di Marco, C., Nemitz, E., Schallhart, S., Metzger, A., Hansel, A., Lorente, J., Ng, S., Jayne, J., Szidat, S., 2014. Effects of sources and meteorology on particulate matter in the Western Mediterranean Basin: An overview of the DAURE campaign: An overview of the DAURE campaign. J. Geophys. Res. Atmospheres 119, 4978–5010. doi:10.1002/2013JD021079

Pankow, J.F., 1994. An absorption model of gas/particle partitioning of organic compounds in the atmosphere. Atmos. Environ.

Pankow, J.F. and Asher, W.E., 2008. SIMPOL.1: a simple group contribution method for predicting vapor pressures and enthalpies of vaporization of multifunctional organic compounds. Atmospheric Chem. Phys. 8, 2773–2796. doi:10.5194/acp-8-2773-2008

Passant, N.R., 2002. Speciation of UK emissions of non-methane volatile organic compounds, AEA Technology, Culham, 289.

Platt, S.M., El Haddad, I., Zardini, A.A., Clairotte, M., Astorga, C., Wolf, R., Slowik, J.G., Temime-Roussel, B., Marchand, N., Ježek, I., Drinovec, L., Močnik, G., Möhler, O., Richter, R., Barmet, P., Bianchi, F., Baltensperger, U., Prévôt, A.S.H., 2013. Secondary organic aerosol formation from gasoline vehicle

emissions in a new mobile environmental reaction chamber. Atmospheric Chem. Phys. 13, 9141–9158. doi:10.5194/acp-13-9141-2013

Pope, C.A. and Dockery, D.W., 2006. Health effects of fine particulate air pollution: lines that connect. J. Air Waste Manag. Assoc. 1995 56, 709–742.

Robinson, A.L., Donahue, N.M., Shrivastava, M.K., Weitkamp, E.A., Sage, A.M., Grieshop, A.P., Lane, T.E., Pierce, J.R., Pandis, S.N., 2007. Rethinking Organic Aerosols: Semivolatile Emissions and Photochemical Aging. Science 315, 1259–1262. doi:10.1126/science.1133061

SCG, L., 2004. Port-Wide Baseline Air Emissions Inventory, Prepared for the Port of Los Angeles.

Seinfeld, J.H. and Pandis, S.N., 1998. Atmospheric chemistry and physics: from air pollution to climate change, A Wiley-Interscience publication. Wiley, New York.

Shrivastava, M., Fast, J., Easter, R., Gustafson Jr., W.I., Zaveri, R.A., Jimenez, J.L., Saide, P., Hodzic, A., 2011. Modeling organic aerosols in a megacity: comparison of simple and complex representations of the volatility basis set approach. Atmospheric Chem. Phys. 11, 6639–6662.

Solazzo, E., Bianconi, R., Pirovano, G., Matthias, V., Vautard, R., Moran, M.D., Wyat Appel, K., Bessagnet, B., Brandt, J., Christensen, J.H., Chemel, C., Coll, I., Ferreira, J., Forkel, R., Francis, X.V., Grell, G., Grossi, P., Hansen, A.B., Miranda, A.I., Nopmongcol, U., Prank, M., Sartelet, K.N., Schaap, M., Silver, J.D., Sokhi, R.S., Vira, J., Werhahn, J., Wolke, R., Yarwood, G., Zhang, J., Rao, S.T., Galmarini, S., 2012. Operational model evaluation for particulate matter in Europe and North America in the context of AQMEII. Atmos. Environ. 53, 75–92. doi:10.1016/j.atmosenv.2012.02.045

Steinbacher, M., Zellweger, C., Schwarzenbach, B., Bugmann, S., Buchmann, B., Ordóñez, C., Prevot, A.S.H., Hueglin, C., 2007. Nitrogen oxide measurements at rural sites in Switzerland: Bias of conventional measurement techniques. J. Geophys. Res. 112. doi:10.1029/2006JD007971

Strader, R., Lurmann, F., Pandis, S.N., 1999. Evaluation of secondary organic aerosol formation in winter. Atmos. Environ. 33, 4849–4863. doi:10.1016/S1352-2310(99)00310-6

Tørseth, K., Aas, W., Breivik, K., Fjæraa, A.M., Fiebig, M., Hjellbrekke, A.G., Lund Myhre, C., Solberg, S., Yttri, K.E., 2012. Introduction to the European Monitoring and Evaluation Programme (EMEP) and observed atmospheric composition change during 1972–2009. Atmos Chem Phys 12, 5447–5481. doi:10.5194/acp-12-5447-2012

Tsigaridis, K., Daskalakis, N., Kanakidou, M., Adams, P.J., Artaxo, P., Bahadur, R., Balkanski, Y., Bauer, S.E., Bellouin, N., Benedetti, A., Bergman, T., Berntsen, T.K., Beukes, J.P., Bian, H., Carslaw, K.S., Chin, M., Curci, G., Diehl, T., Easter, R.C., Ghan, S.J., Gong, S.L., Hodzic, A., Hoyle, C.R., Iversen, T., Jathar, S., Jimenez, J.L., Kaiser, J.W., Kirkevåg, A., Koch, D., Kokkola, H., Lee, Y.H., Lin, G., Liu, X., Luo, G., Ma, X., Mann, G.W., Mihalopoulos, N., Morcrette, J.-J., Müller, J.-F., Myhre, G., Myriokefalitakis, S., Ng, N.L., O'Donnell, D., Penner, J.E., Pozzoli, L., Pringle, K.J., Russell, L.M., Schulz, M., Sciare, J., Seland, Ø., Shindell, D.T., Sillman, S., Skeie, R.B., Spracklen, D., Stavrakou, T., Steenrod, S.D., Takemura, T., Tiitta, P., Tilmes, S., Tost, H., van Noije, T., van Zyl, P.G., von Salzen, K., Yu, F., Wang, Z., Wang, Z., Zaveri, R.A., Zhang, H., Zhang, K., Zhang, Q., Zhang, X., 2014. The AeroCom evaluation and intercomparison of organic aerosol in global models. Atmos Chem Phys 14, 10845–10895. doi:10.5194/acp-14-10845-2014

Tsimpidi, A.P., Karydis, V.A., Zavala, M., Lei, W., Molina, L., Ulbrich, I.M., Jimenez, J.L., Pandis, S.N., 2010. Evaluation of the volatility basis-set approach for the simulation of organic aerosol formation in the Mexico City metropolitan area. Atmospheric Chem. Phys. 10, 525–546.

Twomey, S., 1977. Influence of pollution on shortwave albedo of clouds. J. Atmospheric Sci. 34, 1149–1152. doi:10.1175/1520-0469(1977)

UGZ, 2004. Umwelt- und Gesundheitsschutz Zürich: Vordringen von PM10 in den Atemtrakt. Umwelt- und Gesundheitsschutz Zurich.

Vaughan, A.R., Lee, J.D., Misztal, P.K., Metzger, S., Shaw, M.D., Lewis, A.C., Purvis, R.M., Carslaw, D.C., Goldstein, A.H., Hewitt, C.N., Davison, B., Beevers, S.D., Karl, T.G., 2016. Spatially resolved flux measurements of NO_x from London suggest significantly higher emissions than predicted by inventories. Faraday Discuss. doi:10.1039/C5FD00170F

Vestreng, V., Myhre, G., Fagerli, H., Reis, S., Tarrasón, L., 2007. Twenty-five years of continuous sulphur dioxide emission reduction in Europe. Atmospheric Chem. Phys. 7, 3663–3681. doi:10.5194/acp-7-3663-2007

Villena, G., Bejan, I., Kurtenbach, R., Wiesen, P., Kleffmann, J., 2012. Interferences of commercial NO2 instruments in the urban atmosphere and in a smog chamber. Atmospheric Meas. Tech. 5, 149–159. doi:10.5194/amt-5-149-2012

Waked, A., Favez, O., Alleman, L.Y., Piot, C., Petit, J.-E., Delaunay, T., Verlinden, E., Golly, B., Besombes, J.-L., Jaffrezo, J.-L., Leoz-Garziandia, E., 2014. Source apportionment of PM10 in a north-western Europe regional urban background site (Lens, France) using positive matrix factorization and including primary

biogenic emissions. Atmos Chem Phys 14, 3325–3346. doi:10.5194/acp-14-3325-2014

Wesely, M.L., 1989. Parameterization of surface resistances to gaseous dry deposition in regional-scale numerical models. Atmospheric Environ. 1967 23, 1293–1304. doi:10.1016/0004-6981(89)90153-4

WHO: Burden of disease from Ambient Air Pollution for 2012 – Summary of Results, available at: http://www.who.int/phe/health_topics/outdoorair/databases/AAP_BoD_results_March2014.pdf, 2014.

Woody, M.C., Baker, K.R., Hayes, P.L., Jimenez, J.L., Koo, B., Pye, H.O.T., 2016. Understanding sources of organic aerosol during CalNex-2010 using the CMAQ-VBS. Atmos Chem Phys 16, 4081–4100. doi:10.5194/acp-16-4081-2016

Yarwood, G., Rao, S., Yocke, M., and Whitten, G. Z.: Updates to the Carbon Bond Chemical Mechanism: CB05 Yocke & Company, Novato, CA 94945RT-04-00675, 2005.

Young, D.E., Allan, J.D., Williams, P.I., Green, D.C., Flynn, M.J., Harrison, R.M., Yin, J., Gallagher, M.W., Coe, H., 2015. Investigating the annual behaviour of submicron secondary inorganic and organic aerosols in London. Atmos Chem Phys 15, 6351–6366. doi:10.5194/acp-15-6351-2015

Zhang, L., Brook, J.R., Vet, R., 2003. A revised parameterization for gaseous dry deposition in air-quality models. Atmospheric Chem. Phys. 3, 2067–2082. doi:10.5194/acp-3-2067-2003

Zhang, Q.J., Beekmann, M., Drewnick, F., Freutel, F., Schneider, J., Crippa, M., Prevot, A.S.H., Baltensperger, U., Poulain, L., Wiedensohler, A., Sciare, J., Gros, V., Borbon, A., Colomb, A., Michoud, V., Doussin, J.-F., Denier van der Gon, H.A.C., Haeffelin, M., Dupont, J.-C., Siour, G., Petetin, H., Bessagnet, B., Pandis, S.N., Hodzic, A., Sanchez, O., Honoré, C., Perrussel, O., 2013. Formation of organic aerosol in the Paris region during the MEGAPOLI summer campaign: evaluation of the volatility-basis-set approach within the CHIMERE model. Atmos Chem Phys 13, 5767–5790. doi:10.5194/acp-13-5767-2013

Zuend, A. and Seinfeld, J.H., 2012. Modeling the gas-particle partitioning of secondary organic aerosol: the importance of liquid-liquid phase separation. Atmos Chem Phys 12, 3857–3882. doi:10.5194/acp-12-3857-2012

List of Figures

List of Tables

A.

Supplementary Material

A.1 Supporting Information Chapter 4

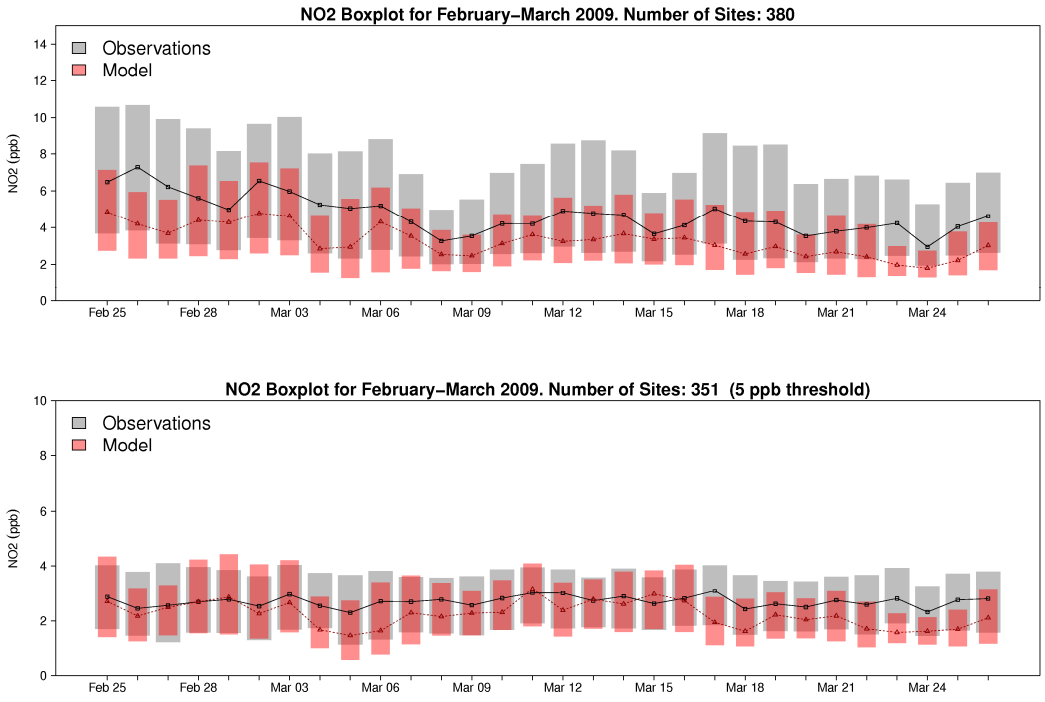

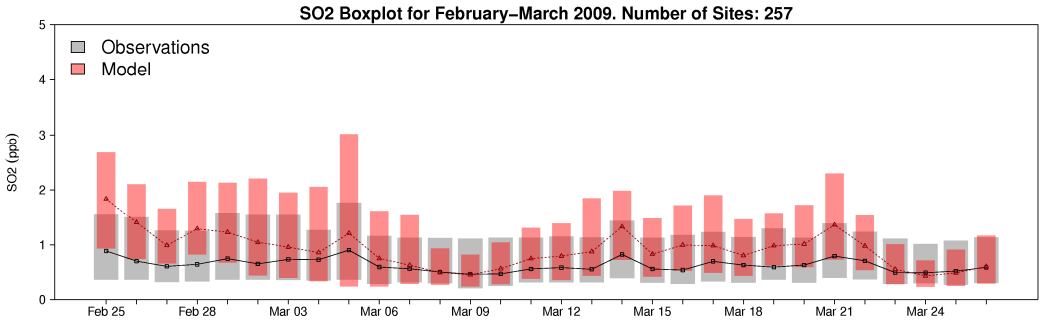

Figure A.1 1 *Comparison of modelled (VBS_BC) (red) and measured (grey) NO_2 (upper panel) and SO_2 (lower panel) concentrations at AirBase rural background sites (as in Table 4.2). The middle panel shows the comparison at stations where NO_2 concentrations do not exceed 5ppb. The extent of the bars indicates the 25th and 75th percentiles. The black and red lines represent measured and modelled medians, respectively.*

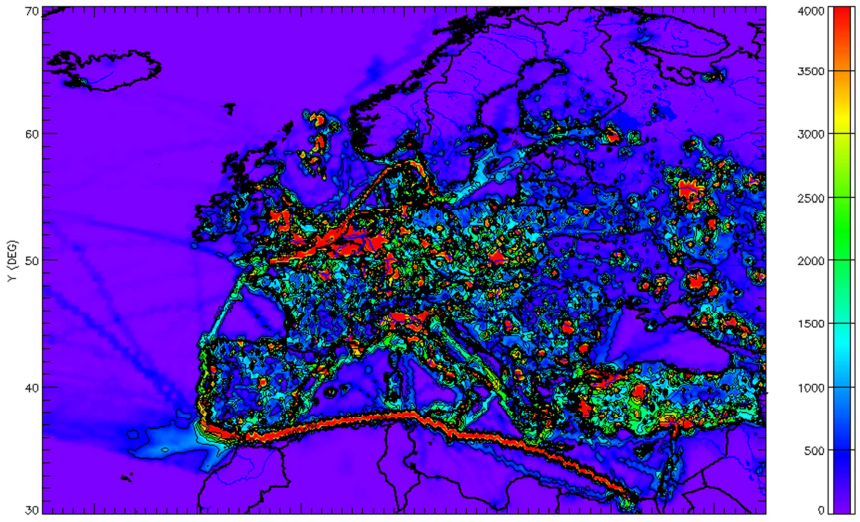

Figure A.1 2 *NO emissions in [mol / (h cell)] for 1 March 2009, at 6:00 AM.*

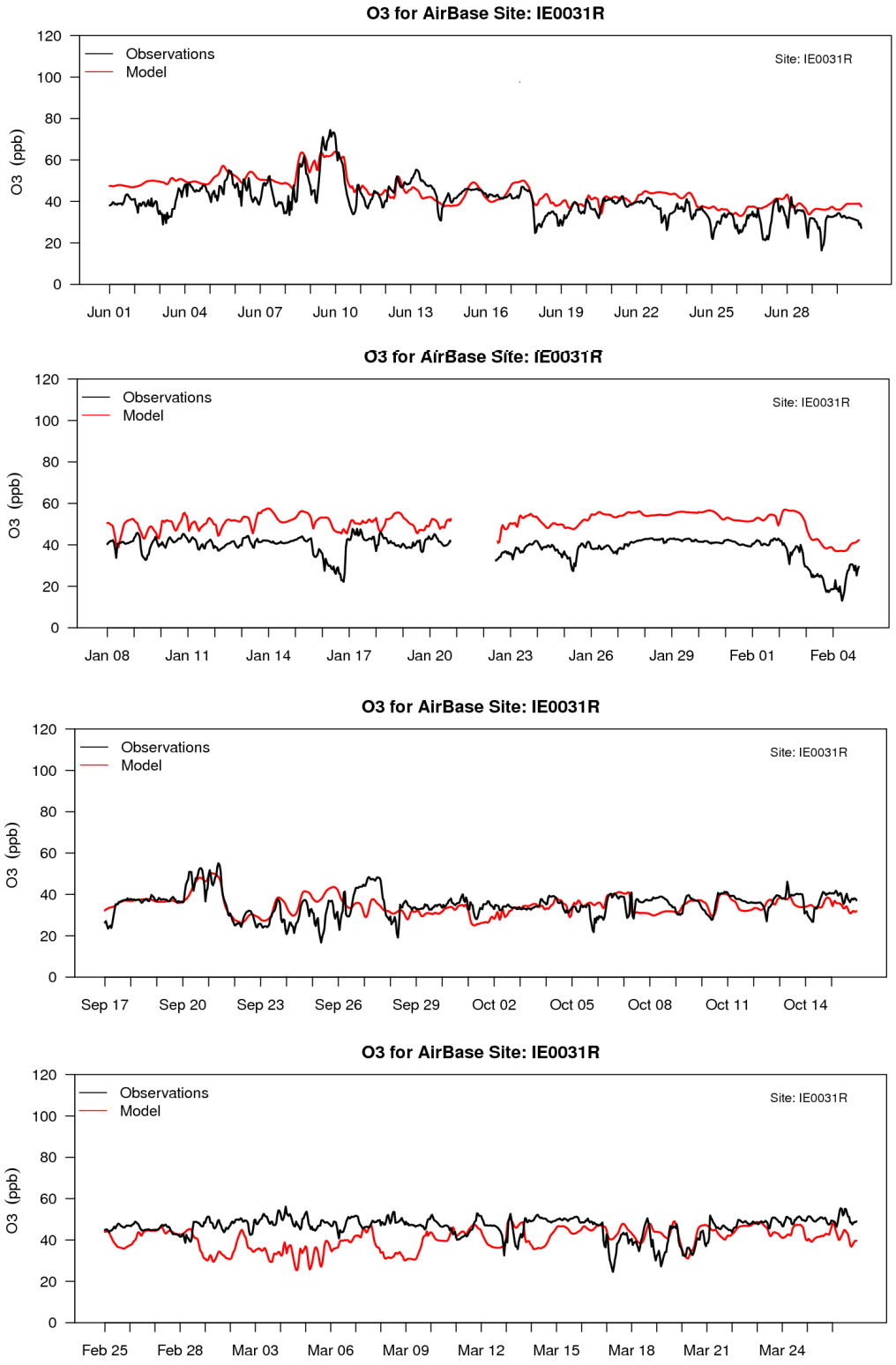

Figure A.1 3 *Comparison of modelled (base case, S3) and measured O_3 mixing ratios at Mace Head (IE0031R) for the four simulated periods: from top to bottom: June 2006, January-February 2007, September-October 2008, February-March 2009.*

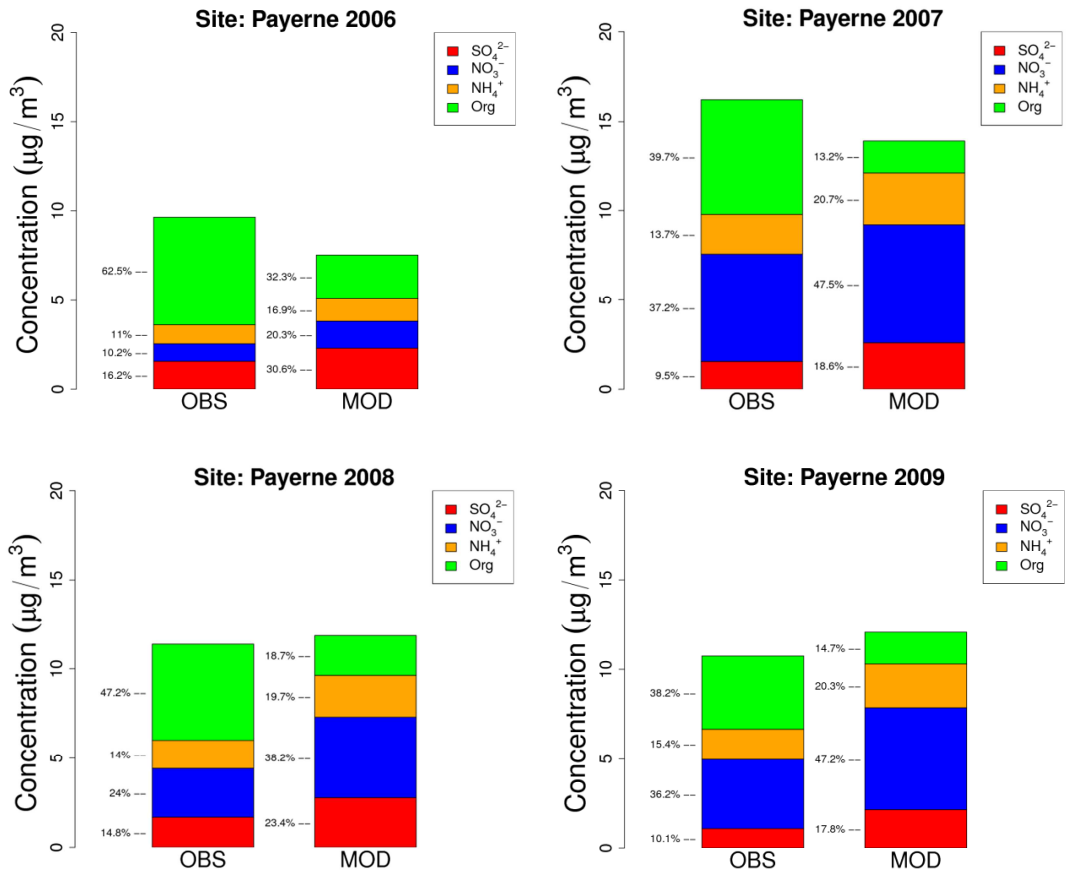

Figure A.1 4 *Comparison of observed (OBS) non-refractory PM_1 and modelled (MOD) $PM_{2.5}$ components at Payerne for all the investigated periods.*

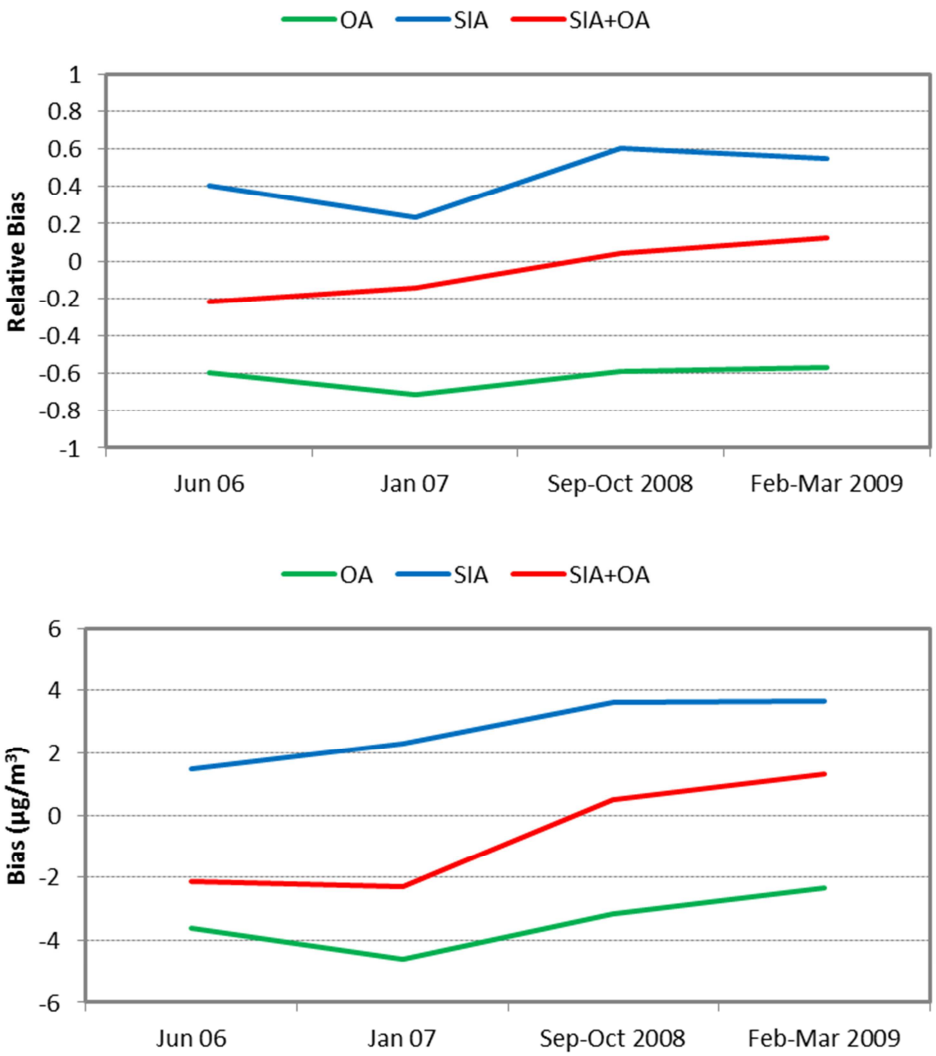

Figure A.1 5 *Absolute and relative biases for organic aerosol (OA), secondary organic aerosol (SIA) and OA+SIA in Payerne for all the investigated periods.*

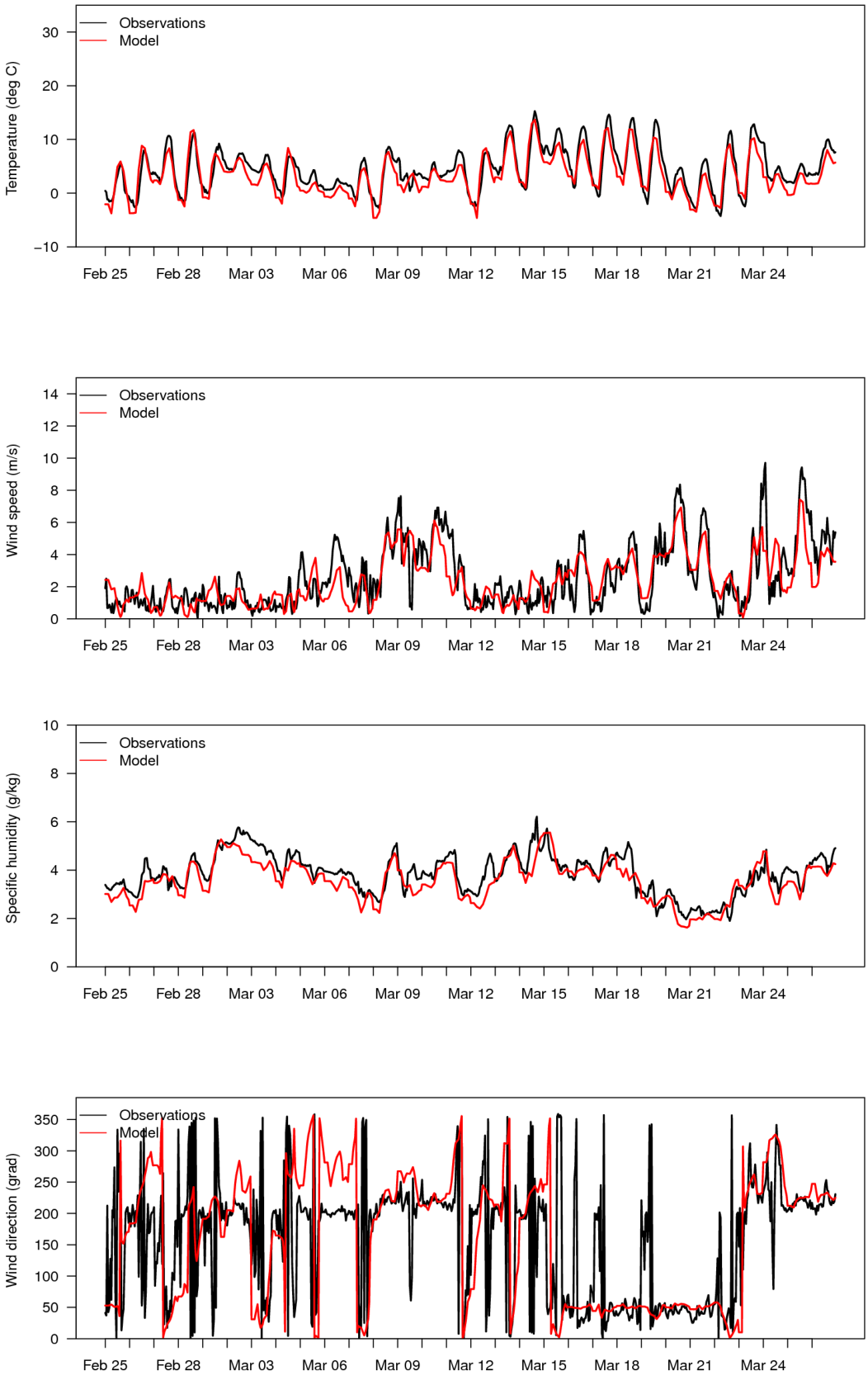

Figure A.1 6 *Comparison of observed and modelled temperature (°C), wind speed (m s^{-1}), specific humidity (g/kg) and wind direction (°C) comparisons at Payerne in February-March 2009.*

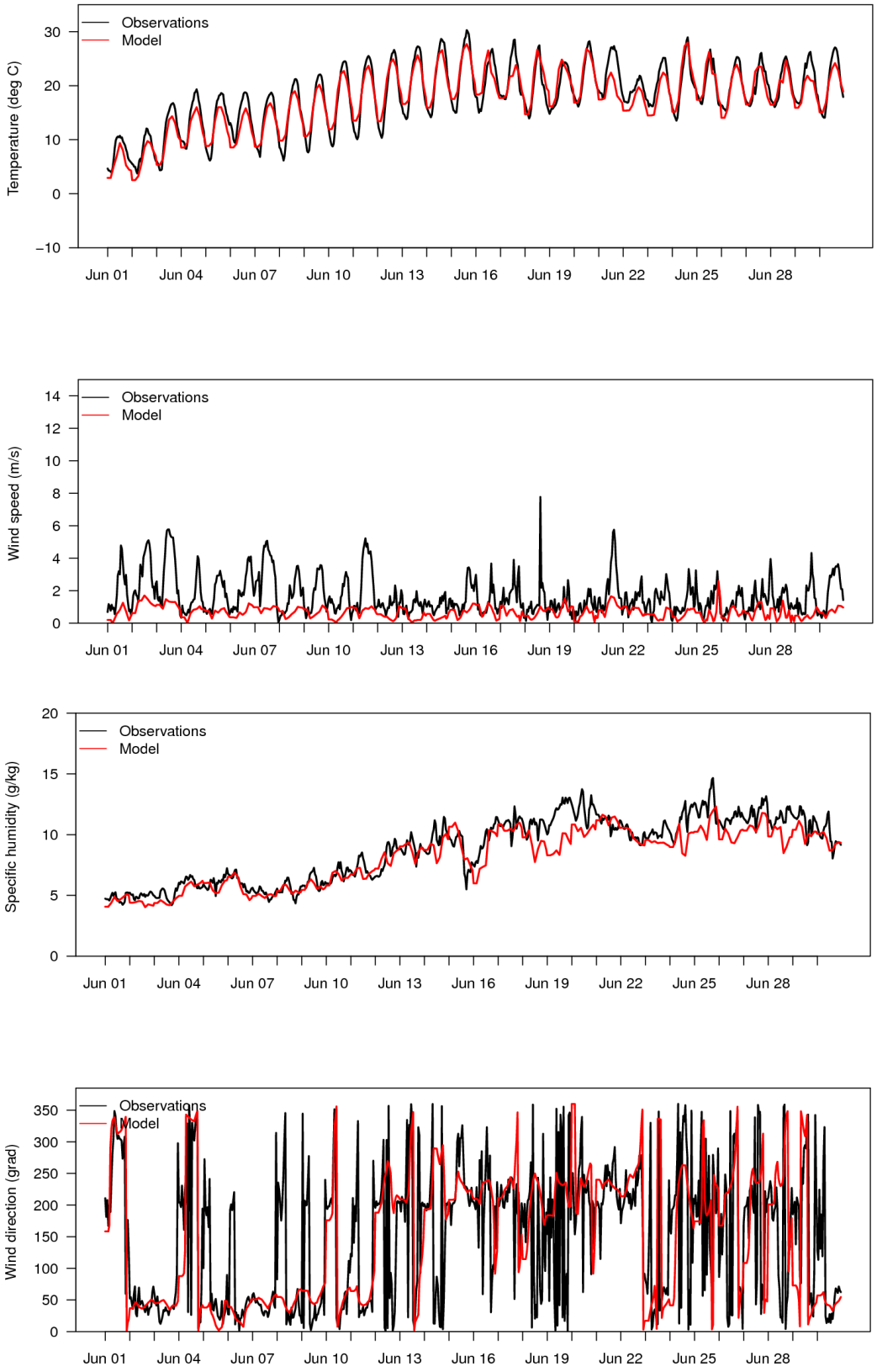

Figure A.1 7 *Comparison of observed and modelled temperature (°C), wind speed (m s^{-1}), specific humidity (g/kg) and wind direction (°C) comparisons at Payerne in June 2006.*

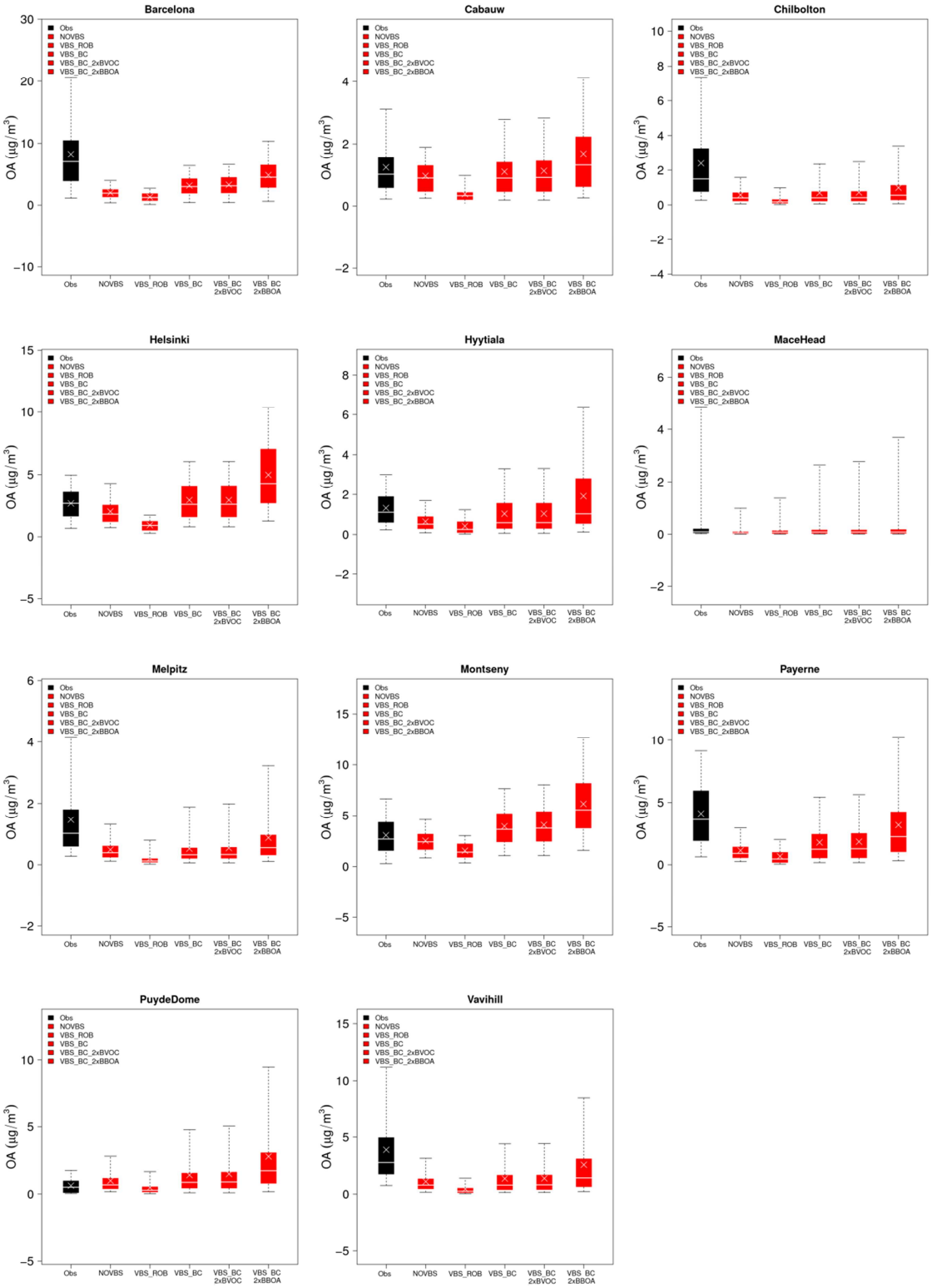

Figure A.1 8 *Observed and modelled OA concentrations using 5 scenarios at AMS sites for the period February-March 2009: Boxplots indicate medians, 5th, 25th, 75th and 95th quantiles for observations (black) and sensitivity tests (red). The crosses represent the arithmetic means.*

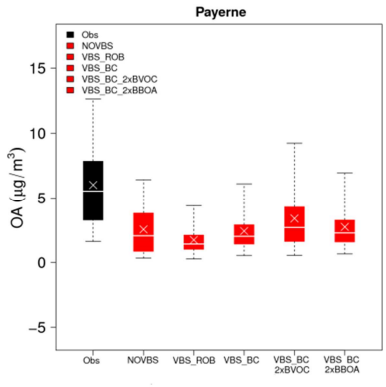

Figure A.1 9 *Observed and modelled OA using 5 scenarios at Payerne sites for the period June 2006: Boxplots indicate median, 5th, 25th, 75th and 95th quantile for observations (black) and sensitivity tests (red). The crosses represent the arithmetic means.*

Table A.1 1 *Properties of the VBS space (adapted from Koo et al., 2014). Carbon numbers for each volatility bin are calculated using the group-contribution of Donahue et al. (2011).*

Basis sets	C* ($\mu g\ m^{-3}$)	Carbon oxidation state	Carbon Number	Oxygen Number	Hydrogen number	Molecular weight	OA/OC
SV-OOA	0	0.102	7	4.90	9.10	172	2.05
	1	−0.188	7.25	4.38	10.1	167	1.92
	10	−0.463	7.5	3.84	11.2	163	1.81
	100	−0.724	7.75	3.30	12.2	158	1.70
	1000	−0.973	8	2.74	13.3	153	1.59
HOA-like	0	−1.52	17	2.69	31.3	278	1.36
	1	−1.65	17.5	2.02	33.0	275	1.31
	10	−1.78	18	1.34	34.7	272	1.26
	100	−1.90	18.5	0.632	36.4	268	1.21
	1000	−2.00	19	0.0	38.0	266	1.17
BBOA-like	0	−0.704	10	4.32	15.7	205	1.71
	1	−1.02	11	3.60	18.4	208	1.58
	10	−1.29	12	2.85	21.1	211	1.47
	100	−1.52	13	2.08	23.9	213	1.37
	1000	−1.73	14	1.27	26.7	215	1.28

* Properties of the lowest volatility bins refer to all OA with $C^* \leq 0.1\ \mu g\ m^{-3}$ (non-volatile OA).

Table A.1 2 *Statistical analysis for nitrate for February-March 2009 at different AMS sites with 50% reduction of ammonia scenario.*

Site	Mean observed NO_3^- (μg m^{-3})	Mean modelled NO_3^- Base case (S3) (μg m^{-3})	Mean modelled NO_3^- 50% red. NH_3 (μg m^{-3})	MB Base case (S3) (μg m^{-3})	MB 50% red. NH_3 (μg m^{-3})
Barcelona	3.6	5.8	3.6	2.19	< 0.1
Cabauw	2.2	6.7	5.3	4.49	3.08
Chilbolton	2.7	4.0	2.7	1.33	< 0.1
Helsinki	1.0	1.9	0.7	0.93	-0.28
Hyytiälä	0.2	1.0	0.3	0.75	< 0.1
Mace Head	0.6	1.7	0.8	1.11	0.17
Melpitz	3.1	4.3	3.1	1.25	< 0.1
Montseny	3.1	5.9	3.2	2.83	< 0.1
Payerne	3.9	5.7	5.0	1.81	1.11
Puy de Dôme	0.9	2.7	2.0	1.81	1.15
Vavihill	2.8	3.7	2.3	0.89	-0.56

Table A.1 3 *Statistical analysis for the OA concentration and different sensitivity scenarios for February-March 2009 periods at 11 AMS sites.*

Site	Mean observed OA (μg/m3)	Mean modelled OA (μg/m^3)	MB (μg/m^3)	ME (μg/m^3)	MFB [-]	MFE [-]
		NOVBS				
Barcelona	8.2	2.0	-6.25	6.27	-1.08	1.10
Cabauw	1.2	1.0	-0.27	0.52	-0.18	0.49
Chilbolton	2.4	0.6	-1.82	1.82	-1.14	1.15
Helsinki	2.7	2.0	-0.64	1.46	-0.21	0.64
Hyytiälä	1.3	0.6	-0.67	0.69	-0.69	0.72
Mace Head	0.8	0.2	-0.61	0.62	-0.71	0.90
Melpitz	1.5	0.5	-0.98	0.99	-0.86	0.88
Montseny	3.1	2.5	-0.53	1.69	-0.05	0.62
Payerne	4.1	1.1	-2.97	2.99	-1.03	1.07
Puy de Dôme	0.6	1.0	0.36	0.68	0.56	0.92

Vavihill	3.9	1.1	-2.79	2.79	-1.06	1.07
		VBS_ROB				
Barcelona	8.2	1.3	-6.96	6.96	-1.39	1.39
Cabauw	1.2	0.4	-0.85	0.87	-0.96	1.01
Chilbolton	2.4	0.3	-2.10	2.10	-1.50	1.50
Helsinki	2.7	0.9	-1.73	1.76	-0.88	0.92
Hyytiälä	1.3	0.4	-0.90	0.90	-1.18	1.18
Mace Head	0.8	0.2	-0.54	0.57	-0.43	0.77
Melpitz	1.5	0.2	-1.26	1.26	-1.48	1.48
Montseny	3.1	1.6	-1.51	1.87	-0.51	0.78
Payerne	4.1	0.7	-3.44	3.44	-1.45	1.46
Puy de Dôme	0.6	0.5	-0.15	0.46	-0.14	0.81
Vavihill	3.9	0.4	-3.44	3.44	-1.61	1.61
		VBS_BC				
Barcelona	8.2	3.1	-5.11	5.15	-0.80	0.82
Cabauw	1.2	1.1	-0.14	0.53	-0.13	0.50
Chilbolton	2.4	0.7	-1.70	1.70	-1.09	1.10
Helsinki	2.7	2.9	0.26	1.64	0.08	0.62
Hyytiälä	1.3	1.0	-0.28	0.52	-0.48	0.60
Mace Head	0.8	0.4	-0.38	0.43	-0.29	0.70
Melpitz	1.5	0.5	-0.95	0.98	-0.94	0.97
Montseny	3.1	3.9	0.88	1.88	0.31	0.57
Payerne	4.1	1.8	-2.33	2.43	-0.85	0.90
Puy de Dôme	0.6	1.4	0.78	0.96	0.68	0.91
Vavihill	3.9	1.4	-2.53	2.53	-1.04	1.04
		VBS_BC_2xBVOC				
Barcelona	8.2	3.3	-4.98	5.03	-0.77	0.80
Cabauw	1.2	1.1	-0.11	0.54	-0.12	0.50
Chilbolton	2.4	0.7	-1.67	1.68	-1.08	1.09
Helsinki	2.7	2.9	0.26	1.64	0.08	0.62

Hyytiälä	1.3	1.0	-0.28	0.52	-0.48	0.60
Mace Head	0.8	0.4	-0.37	0.42	-0.29	0.70
Melpitz	1.5	0.5	-0.92	0.97	-0.92	0.96
Montseny	3.1	4.1	1.02	1.96	0.33	0.58
Payerne	4.1	1.8	-2.27	2.39	-0.83	0.88
Puy de Dôme	0.6	1.5	0.86	1.04	0.70	0.93
Vavihill	3.9	1.4	-2.51	2.51	-1.03	1.03
VBS_BC_2xBBOA						
Barcelona	8.2	4.8	-3.43	3.91	-0.45	0.56
Cabauw	1.2	1.7	0.45	0.81	0.20	0.55
Chilbolton	2.4	1.0	-1.40	1.42	-0.87	0.89
Helsinki	2.7	5.0	2.32	2.93	0.50	0.75
Hyytiälä	1.3	1.9	0.59	0.96	0.07	0.54
Mace Head	0.8	0.5	-0.26	0.36	-0.23	0.68
Melpitz	1.5	0.9	-0.59	0.85	-0.55	0.70
Montseny	3.1	6.2	3.11	3.37	0.67	0.73
Payerne	4.1	3.2	-0.94	1.90	-0.37	0.57
Puy de Dôme	0.6	2.8	2.16	2.24	1.11	1.18
Vavihill	3.9	2.6	-1.31	1.93	-0.60	0.72

Table A.1 4 *Statistical analysis for the OA concentration and different sensitivity scenarios for June 2006 period at Payerne site.*

Scenario	Mean observed OA (µg/m3)	Mean modelled OA (µg/m^3)	MB (µg/m^3)	ME (µg/m^3)	MFB [-]	MFE [-]
NOVBS	6.03	2.56	-3.47	3.54	-0.91	0.93
VBS_ROB	6.03	1.74	-4.29	4.29	-1.11	1.11
VBS_BC	6.03	2.43	-3.6	3.62	-0.85	0.86
VBS_BC_2xBVOC	6.03	3.4	-2.63	2.78	-0.63	0.66
VBS_BC_2xBBOA	6.03	2.75	-3.28	3.32	-0.75	0.76

A.2 Supporting Information Chapter 5

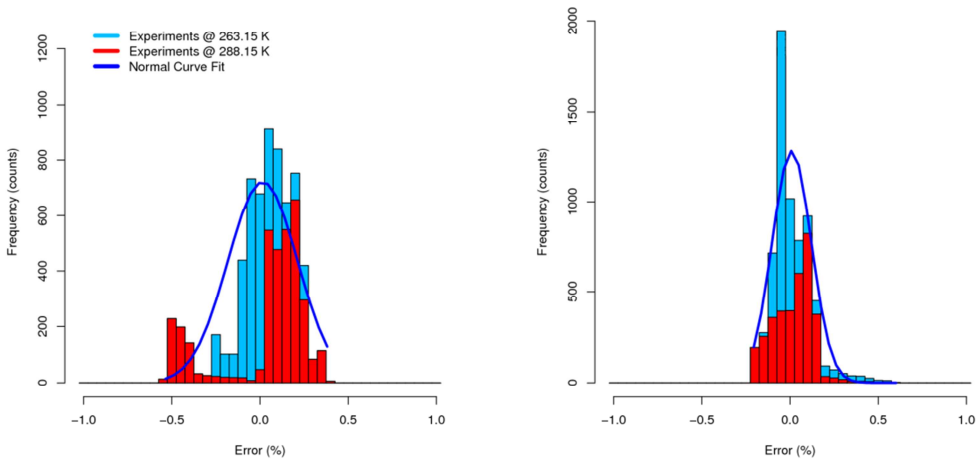

Figure A.2 1 *Best fitting solution error frequency distributions (counts per bin) for low (blue) and high temperature (red) experiments. Right side is the OA mass. Left side for the O:C ratio. Gaussian normal curve fit is reported in dark blue.*

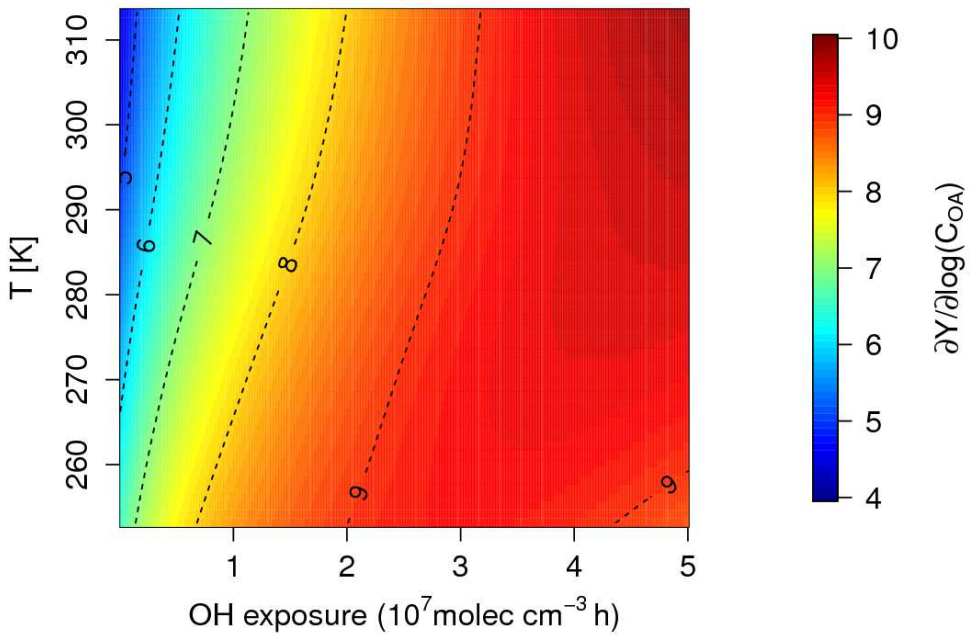

Figure A.2 2 *Variation of SOA yields with log(C_{OA}) (at 6, 60, 600 µg/m^3) as a function of T and OH exposure (from Figure 5.8, bottom panel).*

Table A.2 1 *List of NTVOCs compounds considered for the average mixture*

Compounds
Phenol
m-, o-, p-cresol
m-, o-, p-benzenediol /2-methylfuraldehyde
Dimethylphenols
guaiacol/methylbenzenediols
Naphthalene
2-methylnaphthalene/1-methylnaphthalene
Acenaphthylene
Syringol
biphenyl/acenaphthene
Dimethylnaphthalene

A.3 Supporting Information Chapter 6

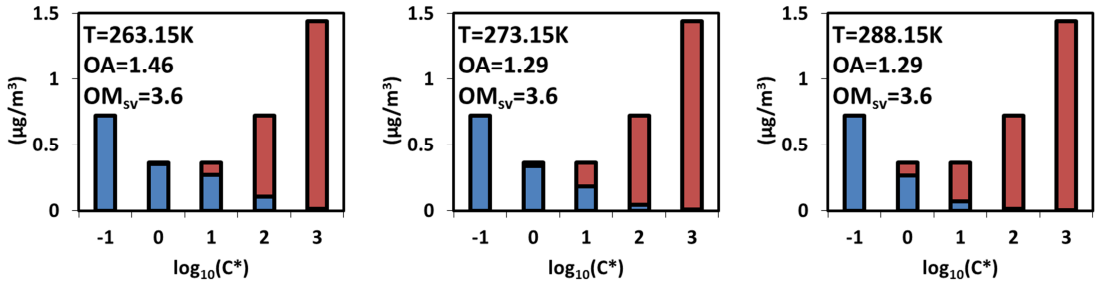

Figure A.3 1 *Box-model partitioning of biomass burning POA at c.a. 1 µg/m^3 OA at different temperatures (263.15, 273.15 and 288.15 K) using volatility distributions proposed by May et al. 2013.Particle phase in blue and gas phase in red.*

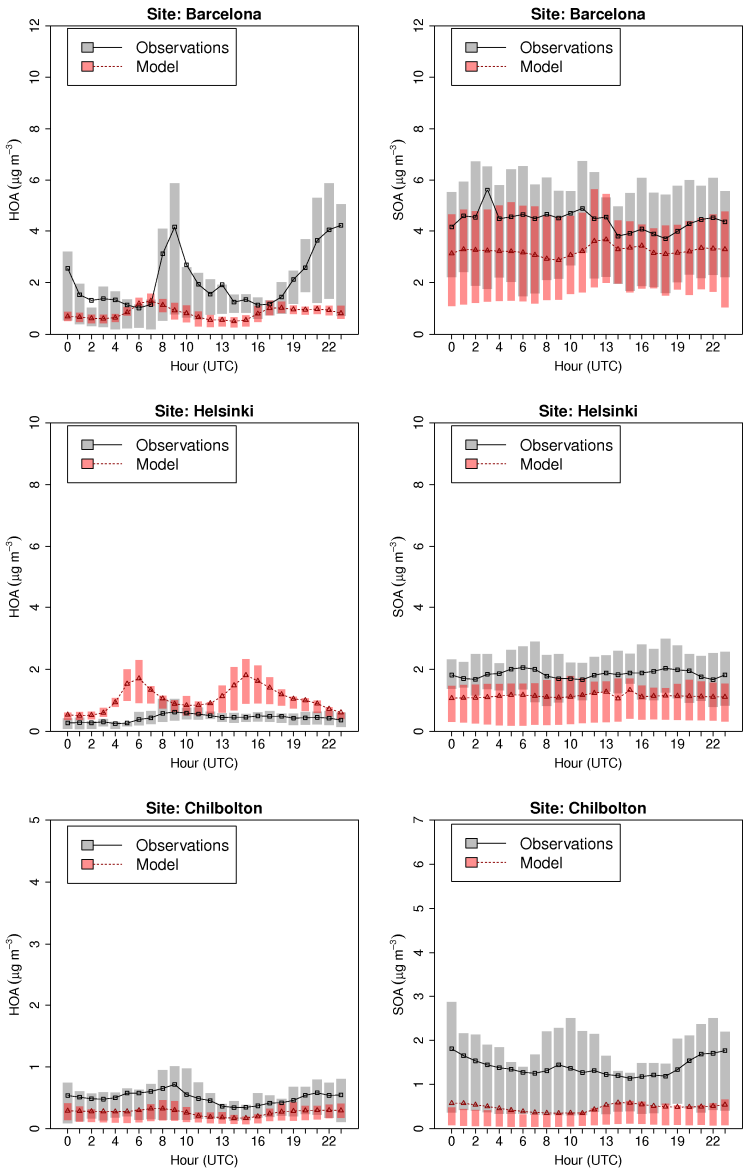

Figure A.3 2 *Comparison of modelled (red) and measured (grey) HOA and SOA diurnal profiles at the sites of Barcelona, Helsinki and Chilbolton. The extent of the bars indicates the 25th and 75th percentiles.*

Table A.3 1 *Statistics for model evaluation.* M_i *represents the modelled value,* O_i *the observations,* $\overline{O}$ *the mean of the observations and* n *the total number of data points.*

Mean Bias (MB)	$MB = \frac{1}{n}\sum_{i=1}^{n}(M_i - O_i)$
Mean Error (ME)	$ME = \frac{1}{n}\sum_{i=1}^{n}(\lvert M_i - O_i \rvert)$
Mean Fractional Bias (ME)	$MFB = \frac{2}{n}\sum_{i=1}^{n}(\frac{M_i - O_i}{M_i + O_i})$
Mean Fractional Bias (ME)	$MFE = \frac{2}{n}\sum_{i=1}^{n}(\frac{\lvert M_i - O_i \rvert}{M_i + O_i})$
Coefficient of determination (R2)	$R2 = 1 - \frac{\sum_{i}^{n}(O_i - M_i)^2}{\sum_{i}^{n}(O_i - \overline{O})^2}$

Table A.3 2 *Statistical analysis for HOA during February-March 2009 periods at 11 AMS sites.*

Site	Mean observed HOA ($\mu g\ m^{-3}$)	Mean modelled HOA ($\mu g\ m^{-3}$)	MB ($\mu g\ m^{-3}$)	ME ($\mu g\ m^{-3}$)	MFB [-]	MFE [-]	r	R^2
Barcelona	2.1	0.8	-1.3	1.5	-0.4	0.8	0.4	0.1
Cabauw	0.3	0.4	0.2	0.2	0.6	0.8	0.5	0.2
Chilbolton	0.5	0.3	-0.2	0.3	-0.5	0.7	0.8	0.6
Helsinki	0.4	1.0	0.6	0.7	0.8	0.9	0.2	0.1
Hyytiälä	0.0	0.1	0.1	0.1	0.7	0.8	0.6	0.3
Mace Head	0.1	0.1	-0.1	0.1	0.5	1.1	0.6	0.3
Melpitz	0.1	0.1	0.0	0.1	-0.1	0.6	0.6	0.3
Montseny	0.2	0.1	-0.1	0.2	-0.3	0.8	0.4	0.1
Payerne	0.3	0.3	-0.1	0.2	0.0	0.6	0.4	0.1
Puy de Dôme	0.0	0.1	0.0	0.0	0.3	0.8	0.1	0.0
Vavihill	0.4	0.2	-0.2	0.2	-0.4	0.7	0.5	0.2

Table A.3 3 *Statistical analysis for BBOA during February-March 2009 periods at 11 AMS sites.*

Site	Mean observed BBOA ($\mu g\ m^{-3}$)	Mean modelled BBOA ($\mu g\ m^{-3}$)	MB ($\mu g\ m^{-3}$)	ME ($\mu g\ m^{-3}$)	MFB [-]	MFE [-]	r	R^2
Barcelona	0.7	1.1	0.5	0.7	0.6	0.8	0.4	0.2
Cabauw	0.1	0.5	0.3	0.3	1.0	1.1	0.5	0.3
Chilbolton	0.5	0.2	-0.3	0.3	-0.6	0.8	0.6	0.4
Helsinki	0.4	1.4	1.0	1.1	1.1	1.1	0.1	0.0
Hyytiälä	0.1	0.5	0.4	0.4	1.5	1.5	0.7	0.5
Mace Head	0.3	0.0	-0.3	0.3	-0.9	1.4	-0.1	0.0
Melpitz	0.2	0.3	0.1	0.2	0.7	0.9	0.4	0.2
Montseny	0.2	0.3	0.1	0.2	0.5	0.8	0.2	0.1
Payerne	0.4	0.8	0.4	0.5	0.8	0.9	0.6	0.3
Puy de Dôme	0.1	0.2	0.1	0.2	0.5	1.0	0.3	0.1
Vavihill	0.7	0.7	0.1	0.5	-0.1	0.7	0.5	0.2

Acknowledgement

Many people have contributed to this work over the last years and I'm much obliged to them for different reasons:

Prof. Dr. Thomas Peter for accepting me as a PhD student and the useful discussions during the ETH interviews.

Dr. Matthias Beekmann for being my external supervisors and the time invested in reading this work.

Prof. Dr. Urs Baltensperger for given me the opportunity to work at the Laboratory of Atmospheric chemistry (LAC) of Paul Scherrer Institute and for the precious and stimulating discussions during interviews and seminars.

Dr. Sebnem Aksoyoglu and Dr. Andre Prévôt for their advice on air quality modelling, helpful discussions and continuous encouragement. They were always available and open to new ideas.

Dr. Imad El Haddad for helping with the development of the VBS box-model. His vast knowledge and capacity of transmit complex aspects in the field of atmospheric chemistry makes him a complete scientist. I wish him all the best for his professional and private life.

Dr. Johannes Keller, Tinguely Michel and Dr. Daniel Oderbolz for the technical assistance with the modelling system in use at the LAC.

All the EURODELTA-III community, in particular Guido Pirovano, Kees Cuvelier and Bertrand Bessagnet.

All the LAC PhD students for the nice and intense time spent together.

Hannelore Krueger for helping with all the bureaucratic procedures during my stay at PSI.

My mother and my brother for all their love.

Curriculum vitae

Giancarlo Ciarelli

born on February 12, 1985
in Lanciano (CH), Abruzzo, Italy.

Working Experience

04/2016–Current	**Scientific Officer** at Paul Scherrer Institute (PSI). Energy and Environment Research (ENE), Villigen PSI OST.
02/2012– 01/2016	**PhD** researcher at Paul Scherrer Institute (PSI). Energy and Environment Research (ENE), Villigen PSI OST. In the framework of the European project EURODELTA3 (EDIII) initiated by the Task Force on Measurements and Modelling (TFMM), a modular air quality modelling system (WRF-CAMx) was applied over Europe in order to investigate its performance and air pollution control strategies. The main duties involved gathering and manipulation of large environmental data sets i.e. anthropogenic emissions and meteorological data and high performance computing on dedicated facilities (CSCS and PSI clusters).
09/2013–08/2014	**Tutor at the** Swiss Federal Institute of Technology (ETHZ) Institute for Atmospheric and Climate Science (USYS), Zürich. Explaining and grading exercises for Aerosol I: Physical and Chemical Principles and Aerosol II: Applications in Environment and Technology.
09/2013–08/2014	**Trainee Researcher** at Paul Scherrer Institute (PSI). Energy and Environment Research (ENE), Villigen PSI OST.
09/2009–03/2010	**IT User Support** at Marche Polytechnic University, Ancona. Provide technical support and assistance to under-graduate and graduate students.
09/2006–03/2007	**Administrative assistant** at Marche Polytechnic University, Ancona Managing and archiving confidential documents and records.

Education

02/2012– 03/2016	PhD studies at the Swiss Federal Institute of Technology (ETHZ), Zürich, Switzerland. Focus on air quality modelling development and its application at European scale.
02/2011	Granted access to the Italian Engineer's Council Section A, Civil and Environmental Engineering N° 2044, Cheti, Italy.
2008–2010	Master of Science (MSc), Environmental Engineering Marche Polytechnic University, Ancona, Italy.
2004–2008	Bachelor of Science (BSc), Civil and Environmental Engineering Marche Polytechnic University, Ancona, Italy.
1999-2004	High School Science Liceo Scientifico Galileo Galiei, Lanciano, Italy.

Conferences and meetings

05/2015 Montpellier, France. 34th International Technical Meeting on Air Pollution Modelling and its Application. **Title:** "*Modelling Organic Aerosol in Europe: Application of the CAMx Model with a Volatility Basis Set Within the Eurodelta III Exercise*". Oral presentation.

09/2014 Natal, Brasil. 13th IGAC Science Conference on Atmospheric Chemistry. **Title:** "*Application of a model based source apportionment technique to track fine organic aerosol particles in Europe*". Poster presentation.

09/2014 Varna, Bulgaria. 16th International Conference on Harmonisation within Atmospheric Dispersion Modelling for Regulatory Purposes. **Title:** "*Intercomparison of the wet deposition of $NH4^+$, $NO3^-$ and $SO4^{2-}$ estimated by several air quality models for one of the EURODELTA3 campaigns*". EDIII team oral presentation.

06/2013 Anglet, France. MACC-II Summer School. *Modelling and forecasting of atmospheric composition at different scales.*

05/2013 Zagreb, Croatia 14th annual TFMM meeting. **Title:** "*Overview of the first results of the EURODELTA3 model intercomparison project*". EDIII team oral presentation.

09/2012 Granada, Spain European Aerosol Conference (EAC). **Title:** "*Application of process analysis in the CAMx model for evaluating physical and chemical processes affecting PM in Switzerland"*. Oral presentation.

Publications

7. **Ciarelli, G.**, Aksoyoglu, S., El Hadded, I., Bruns, E., Crippa, M., Jimenez, J.-L., Nemitz, E., Sellegri, K., Äijälä, M., Carbone, S., Mohr, C., O'Dowd, C., Poulain, L., Baltensperger, U., and Prévôt, A. S. H.: Modelling winter organic aerosol at the European scale with CAMx: evaluation and source apportionment with a VBS parameterization based on novel wood burning smog chamber experiments, Submitted to Atmospheric Chemistry and Physics.

6. Aksoyoglu, S., **Ciarelli, G.**, I. El Haddad, I., U. Baltensperger, U., and Prévôt, A. S. H.: Secondary inorganic aerosols in Europe: sources and the significant influence of biogenic VOC emissions especially on ammonium nitrate, Atmos. Chem. Phys. Discuss., doi:10.5194/acp-2016-739, 2016.

5. **Ciarelli, G.**, Aksoyoglu, S., Crippa, M., Jimenez, J.-L., Nemitz, E., Sellegri, K., Äijälä, M., Carbone, S., Mohr, C., O'Dowd, C., Poulain, L., Baltensperger, U., and Prévôt, A. S. H.: Evaluation of European air quality modelled by CAMx including the volatility basis set scheme, Atmos. Chem. Phys., 16, 10313-10332, doi:10.5194/acp-16-10313-2016, 2016.

4. **Ciarelli, G.**, El Haddad, I., Bruns, E., Aksoyoglu, S., Möhler, O., Baltensperger, U., and Prévôt, A. S. H.: Constraining a hybrid volatility basis set model for aging of wood burning emissions using smog chamber experiments, Geosci. Model Dev. Discuss., doi:10.5194/gmd-2016-163, 2016.

3. Bessagnet, B., Pirovano, G., Mircea, M., Cuvelier, C., Aulinger, A., Calori, G., **Ciarelli, G.**, Manders, A., Stern, R., Tsyro, S., García Vivanco, M., Thunis, P., Pay, M.-T., Colette, A., Couvidat, F., Meleux, F., Rouïl, L., Ung, A., Aksoyoglu, S., Baldasano, J. M., Bieser, J., Briganti, G., Cappelletti, A., D'Isodoro, M., Finardi, S., Kranenburg, R., Silibello, C., Carnevale, C., Aas, W., Dupont, J.-C., Fagerli, H., Gonzalez, L., Menut, L., Prévôt, A. S. H., Roberts, P., and White, L.: Presentation of the EURODELTA III inter-comparison exercise – Evaluation of the chemistry transport models performance on criteria pollutants and joint analysis with meteorology, Atmos. Chem. Phys. Discuss., doi:10.5194/acp-2015-736, 2016.

2. Aksoyoglu, S., Keller, J., **Ciarelli, G.**, Prévôt, A. S. H., and Baltensperger, U.: A model study on changes of European and Swiss particulate matter, ozone and nitrogen deposition between 1990 and 2020 due to the revised Gothenburg protocol, Atmos. Chem. Phys., 14, 13081-13095, doi:10.5194/acp-14-13081-2014, 2014.

1. Huang, R.-J., Zhang, Y., Bozzetti, C., Ho, K.-F., Cao, J.-J., Han, Y., Daellenbach, K. R., Slowik, J. G., Platt, S. M., Canonaco, F., Zotter, P., Wolf, R., Pieber, S. M., Bruns, E. A., Crippa, M., **Ciarelli, G.**, Piazzalunga, A., Schwikowski, M., Abbaszade, G., Schnelle-Kreis, J., Zimmermann, R., An, Z., Szidat, S., Baltensperger, U., Haddad, I. E. and Prévôt, A. S. H.: High secondary aerosol contribution to particulate pollution during haze events in China, Nature, 514(7521), 218–222, doi:10.1038/nature13774, 2014.